NASA Technical Memorandum 106944

Static Stability of a Three-Dimensional Space Truss

John F. Shaker
Lewis Research Center
Cleveland, Ohio

May 1995

National Aeronautics and
Space Administration

CONTENTS

LIST OF ILLUSTRATIONS

LIST OF TABLES

INTRODUCTION

In order to deploy large flexible space structures it is necessary to develop support systems that are strong and lightweight. The most recent example of this aerospace design need is vividly evident in the Space Station solar array assembly. In order to accommodate both weight limitations and strength performance criteria, ABLE Engineering has developed the **F**olding **A**rticulating **S**quare **T**russ (FASTMast) support structure. The FASTMast is a space truss/mechanism hybrid that can provide system support while adhering to stringent packaging demands. However, due to its slender nature and anticipated loading, stability characterization is a critical part of the design process. Furthermore, the dire consequences surely to result from a catastrophic instability quickly provide the motivation for careful examination of this problem.

Shown in figure (1) is the solar array assembly of the Space Station Freedom. The fundamental components of this system are the (1) solar array blanket system, (2) FASTMast support structure, and (3) mast canister assembly. The FASTMast once fully deployed from the canister will provide support to the solar array blankets. A unique feature of this structure is that the system responds linearly within a certain range of operating loads and nonlinearly when that range is exceeded. The source of nonlinear behavior in this case is due to a changing stiffness state resulting from an inability of diagonal members to resist

applied loads. The principal objective of this study was to establish the failure modes involving instability of the FASTMast structure. Also of great interest during this effort was to establish a reliable analytical approach capable of effectively predicting critical values at which the mast becomes unstable.

Due to the dual nature of structural response inherent to this problem, both linear and nonlinear analyses are required to characterize the mast in terms of stability. The approach employed herein is one that can be considered systematic in nature. The analysis begins with one and two-dimensional failure models of the system and its important components. From knowledge gained through preliminary analyses a foundation is developed for three-dimensional analyses of the FASTMast structure. The three-dimensional finite element (FE) analysis presented here involves a FASTMast system one-tenth the size of the actual flight unit. Although this study does not yield failure analysis results that apply directly to the flight article, it does establish a method by which the full-scale mast can be evaluated.

HARDWARE DESCRIPTION

Due to electric power demands of the Space Station user community it was necessary to provide solar array assemblies much larger than normally used for space flight. Limited by the modest payload volume of the Space Shuttle, designers were immediately driven to a deployable concept that could accommodate packaging and weight constraints. In order to support the solar array blanket it was necessary to design a support structure that possessed the strength characteristics of a space truss with the mechanistic features of a deployable structure. The answer to this problem was provided by ABLE Engineering with the FASTMast deployable mast assembly.

The FASTMast structure is comprised of thirty-two interconnected **bays** of mast. A complete flight unit will stand approximately 104 feet in length and supports two solar arrays which are a total of 40 feet in width. The principal structural components of this system include: (1) two solar array blankets (780 lbs), (2) mast canister (450 lbs), (3) two array blanket boxes (760 lbs), and (4) FASTMast (450 lbs). The total weight of the solar array assembly is approximately 2440 lbs. It is designed to provide 18 kilowatts (KW) of electrical power to the Space Station user community. Shown in figure (2) is a detailed description of the primary components that make up a single bay of mast structure. The longerons are the primary axial and moment load carrying elements of the structure. In order to

provide additional buckling resistance the lower twenty bays contain a tapered longeron that is shown in figure (3). The tapered longeron has a central cross-sectional area of 0.348 in^2 which decreases to 0.25 in^2 at each end. Longerons present in the upper twelve bays of the mast possess a constant cross-sectional area of 0.25 in^2.

The principal elements providing resistance to shear and torsional loading are the prestrained stainless steel 7X7 wire rope diagonals. In addition to the shear resistance provided by this structural member it also provides flexibility that is required of a deployable structure. The current design preload level in this element is 31 lbs. Supplying the load required for diagonal prestrain is a 0.375 in by 0.275 in rectangular cross-section fiberglass flex batten. In order to create the necessary force the flex batten is installed in a post-buckled state. The buckled shape of this element is clearly visible from the top view of the mast given in figure (4). A direct analogy to this design concept is the energy transmitted to a string from a buckled bow. This type of force inducing action is illustrated in figure (5). The flex batten is a key feature of the mast in terms of its deployability.

In addition to reacting the preload of the flex batten, the elbow joints provide a pivot point required for mast stowage and deployment. Therefore, it was necessary to design this joint with a dual-function end fixity. In order to facilitate the

folding action of the mast the elbow joints act as a hinge in the direction of rotation required for stowage. The deployment operation sequence will be described later in this report. Shown in figure (6) is a schematic of the elbow joint, flex batten, and diagonal element connection to the mast. Figure (7) shows the diagonal to longeron connection which is made with a bracket and two 4-40 socket-head cap screws. Also given in this drawing is a clear view of the folding direction of the longeron/flex batten interface. The pinned and hinged boundary conditions at this joint are associated with the Euler (linear) buckling and large displacement (nonlinear) failure modes respectively. The pinned condition exists at this interface when hinge action is not taking place. In figure (8) the connection between the flex batten and elbow fitting is given thus completing the description of this interface.

At the top and bottom of each bay of FASTMast are the rigid batten frames consisting of the corner fittings rigid batten tubes. This component is shown in figure (9). The corner fittings provide a pivot point for the longeron at the top of the bay and anchor the rigid battens to the space lattice. Engineering properties of these components are given in table (1). Rigid battens provide shear and torsion load resistance by restraining corner fitting motion. The taper feature of the rigid batten was incorporated in order to reduce weight and increase strength of the element.

Although the individual elements of the FASTMast structure do not possess large strength capability the integrated unit appears capable of withstanding service loads. However, in order to achieve the required strength to weight ratio this type of structure presents an obvious stability problem. Further complicating this problem is the fact that there exists both local (linear) and global (nonlinear) instability modes which are affected by deformed mast geometries and applied loading conditions. Therefore, in order to characterize FASTMast instability states the effects of changing geometry and applied-load interactions must be evaluated.

MAST OPERATIONS

The FASTMast was designed with the intent to support deployable structures such as antennas and solar arrays. For the Space Station solar array application this structure completely stowed will reside in the mast canister as shown in figure (10). A total of 32 bays make up the flight structure of which 31 are folded during stowage.

Once the command to initiate deployment has been given the mast canisters top moves upward with the first bay upward as shown in figure (11). Bays 3 through 32 remain in the folded position while bay 2 unfolds into its deployed state [figure (12)]. Shown in figure (13) is the kinematics of a single bay as it deploys and retracts. From this diagram the movement of the longerons and flex battens is very clear. The longerons will unfold and the flex batten swings around to its deployed position. This action is repeated in a counterclockwise manner about the four sides of the mast until bay 2 has fully extended. Full deployment of the mast is achieved when the procedure described above is repeated for each bay of space truss. Once fully deployed, the mast is locked into position giving it the required mechanical properties necessary to support the solar array blankets as shown in figure (1). Retraction of the mast into a stowed position is the reverse of the actions describe above.

One final point worth mentioning is that in the stowed state the flex batten strain state is 120% of yield. The manner in which the stowed flex batten is deformed is shown in figure (13). A mast unit could be stowed for as long as 4 years so creep must be considered when determining the final preload this element provides to the diagonals. From creep test data the reduction in flex batten stiffness over a four year period is approximately 20%. This fact obviously must be taken into account during analyses involving the flex batten.

DEFINITION OF STRUCTURAL LOADS

Ultimate viability of a structural system in its most succinct form can be expressed as the margin of safety (MS). Mathematically this quantity is represented by:

$$MS = \frac{\text{Allowable Load}}{(FS) \times \text{Limit Load}} - 1 \qquad (1)$$

where (FS) is the required factor of safety. The allowable load of the structure is the maximum load the structure can withstand before failure occurs. This characteristic of the structure is a function of the design and failure mode type. Limit load represents the maximum load level the structure will be subjected to during service. If the (FS) is a given quantity the structures problem is reduced to finding values of allowable and limit load. Limit load is developed from a combination of prior design experience and detailed test and analysis of the structure. Determination of the allowable load of a structure requires a clear understanding of structural behavior to include how the structure will fail under expected service loads. If allowable or limit loads are developed using inappropriate procedures the resulting (MS) determinations cannot be reliable.

DETERMINATION OF LIMIT LOAD

In order to generate the required limit load value for (MS) calculation the following must be addressed: (1) load source, (2) methods of predicting loads, and (3) analytical accuracy. What follows below is an explanation of (1) and (2), with (3) being beyond the scope of this effort. A complete description of limit load development for Space Station on orbit loading of the solar array assembly can be found in references [1] and [2].

The structural design problems being faced today by the Space Station solar array engineers are due to a great extent on accommodating the role of the Shuttle during Space Station buildup. Never before has the Shuttle had to maneuver around, and dock to a structure with the characteristics of the Space Station. In general the load levels during the early flights are those that drive structural design because there is little Space Station structure to absorb energy imparted to it by the Shuttle. This is clear from figure (14) which shows the relative sizes of the two vehicles at both the initial and final Space Station configuration. From this figure it can be seen that the Shuttle is very close to the solar array assembly during the early construction phase of the Station. By the end of Space Station construction the docking port is approximately 150 feet from the array while during the second mission build the two are separated by only 40 feet. This fact alone greatly increases the level of load transmitted to the solar array assembly during Shuttle

operations. What makes this particular problem unique is the fact that there are many spacecraft configurations (stage configurations) during the build process each requiring examination in order to determine if it harbors a worst case limit load.

DESCRIPTION OF ROCKET THRUSTER PLUME INDUCED LOADING

The principal source of mast loading is imparted to the structure during Shuttle/Space Station docking and approach maneuvers. These loads are due to docking impact, and Shuttle Reaction Control System (RCS) and/or Altitude Control System (ACS) jet exhaust plume impingement on the solar array panels. The loads due to exhaust plumes can be considered either dynamic or quasi-static surface pressure loads acting on the solar array blankets. Typical surface pressures are on the order of 0.01 lb/in^2. On the other hand, docking loads are an impulsive excitation transmitted down the truss of the Space Station to the base of the solar array assembly. Applied loads from plume and docking events result in shear, torsion, axial, and moment loads on the mast structure. In order to better understand the manner in which the solar array mast is externally loaded, it is important to clearly understand these two events.

One of the most dramatic loading events associated with Shuttle operations is the action of RCS and ACS jet plume impinging on

the solar array. Shown in figure (15) is the Shuttle position during the last stages of approach to the space Station. In order to engage the docking port the astronauts must guide the vehicle through an approach cone whose apex is the docking port. Control of vehicle position is maintained manually by firing RCS jets as shown in figure (16). There are a total of 44 ACS and RCS jets located throughout the Shuttle and they are given pictorially in figure (17). The ACS jets fire at a 25 lb_f rate and the RCS jets emit a thrust of 55 lb_f. Although their use is restricted to circumstances of great need, the Primary Reaction Control System (PRCS) jets can be used during maneuvers and are rated at 870 lb_f of thrust. Real-time simulations of Shuttle/Space Station docking maneuvers indicate several large solar array loading conditions result from the thruster plume event.

As was stated earlier plume loading can be either quasi-static or dynamic in nature. Shuttle approach to Space Station is generally slow and deliberate. The pilot will continually fire the control jets in order to guide the craft into the docking mechanism capture device as is shown in figure (18). Therefore, the actual thrust pulses emitted from the rockets will occur in small bursts whose duration will generally be on the order of milliseconds. Depending on the forcing amplitude and frequency, pulse loading of this type could cause dynamic amplification of solar array responses. This is in contrast to a maneuver that requires the Orbiter to execute a long duration thruster firing

which would result in a quasi-static pressure load. An example of quasi-static loading could include a maneuver requiring the Shuttle to quickly move away from the Space Station to avoid an undesirable alignment or collision. This would require a long duration fire resulting in a quasi-static loading. The net result of this action is very similar to that of a sailboat mast under conditions of wind loading. Although a detailed description of Shuttle maneuvers and thruster firing profiles have been omitted here, it should be clear that both static and dynamic thruster plume events must be included in the loads definition.

DESCRIPTION OF DOCKING LOADS

The second dynamic loading event considered herein is the docking event. Docking loads are defined as loads that result from impact between the Shuttle and Space Station docking mechanisms. The impulsive load transmitted to the truss structure results in a lateral base excitation of the solar array assembly. Solar array load levels induced during this event have also pushed the hardware to its design limit. Again, the magnitude of the applied load transmitted to the structure will depend to a large degree on the manner in which the pilot executes Shuttle approach. Large array responses are associated with high impact velocities. Another factor affecting force transmission during this loading event is the stiffness of the docking mechanism

capture devices. Once the approach route and docking stiffnesses have been defined the profile of the forcing function can be developed.

GENERATION OF LIMIT LOAD LEVELS

Once the source(s) of limit load has been identified the focus of the loads effort shifts to one of computational strategy. However, prior to conducting structural response analyses it is necessary to develop the appropriate applied force **F**(t) acting on the system. In the case of solar array assembly loads analyses **F**(t) will be comprised of forces due to plume and docking events. Of these two load types the most complicated to express as a function of time is that due to jet plume. The applied loading itself originates from the pressure effects of the gas plume impinging on the solar array panel. Due to the fact that the surface area of the array blanket is approximately 3500 ft^2, even a small surface pressure can have considerable loading consequences. The fluid-structure interaction software program utilized for generating plume impingement loads is called RCSFORCE [3]. This code was developed by the Johnson Space Center (JSC) in order to calculate loads due to surfaces immersed in a jet exhaust. RCSFORCE requires structural data in NASTRAN (**NAS**A **STR**uctural **AN**alysis) Program bulk data format. In addition to a definition of the structure, the code requires jet thruster firing time histories generated from real-time flight

simulations. Each simulation is based upon flight trajectories and solar array orientation of a particular mission. The Shuttle thruster dynamic pressure model contained in the code assumes a supersonic, adiabatic, non-viscous, non-conducting flow of ideal gas. Also, it is assumed that the transient nature of the jet thrust time history is negligible and therefore the impulsive loading can be modeled as a simple square wave. Not intuitively obvious is the fact that the plume gas dynamics itself is altered by variations of Shuttle flight trajectories and solar array orientation. Therefore, for each phase of Space Station construction [see figures (19) and (20)] analyzed the following variables must be examined in terms of its affect on plume loads: (1) location of the array on the truss structure, (2) orientation of the solar array relative to articulation angles alpha (α), beta (β), and gamma (γ), (3) Space Station flight operations, (4) Station/solar array dynamic coupling, and (5) plume flow field uncertainty. The variability in these flight conditions are treated using a Monte Carlo procedure which when input into RCSFORCE yields a 3-σ plume loading contribution to $\mathbf{F}(t)$.

The docking load forcing function although not as difficult to develop as that due to plume, it is necessary for complete characterization of $\mathbf{F}(t)$. Calculation of docking loads is performed using the Ring-Finger Docking Dynamic code also developed by JSC [4]. As was the case with plume load definition, Shuttle approach trajectories are supplied as input to the analysis. From a given approach scenario contact

conditions are specified for all appropriate docking mechanisms that will be used by the Space Station program. The analysis code assumes the two vehicles that are docking have a given separation and initial velocity. An important point to note is that the initial state variables are not changed during the analysis. At the point of contact integration of the equations of motion commences. Docking simulation continues until either structural latching occurs or maximum allowable time duration for the docking procedure is achieved. Again variability in parameters affecting load levels are treated using Monte Carlo techniques in an approach similar to that used for plume loading. Output from this analysis includes forces and moments imparted to the structure as a result of impact. This result when combined with that of the preceding plume loads assessment yields the final form of $\mathbf{F}(t)$.

Upon successful development of $\mathbf{F}(t)$, limit loads throughout the solar array structure are determined by performing a transient response analysis. Due to the large size of the FE models the analysis is performed using modal synthesis techniques common to the aerospace industry. Current Space Station on-orbit configuration FE models contain from 300,000 to 500,000 degrees of freedom. The analysis is performed in modal space in order to reduce the computational requirements to acceptable levels. The structural analysis code used to generate structural responses is MSC(MacNeal-Schwendler)/NASTRAN and the modal transformation is a Craig-Bampton [5] formulation. As was previously mentioned

derivation of the maximum limit load requires examination over the appropriate range of stage configurations. However, due to the large number of possible Space Station configurations and shuttle approaches, performing transient analyses with high-fidelity FE models becomes prohibitive in terms of time and cost. Therefore, prior to detailed response analyses required for design assessment, important flight configurations are identified by performing loads analyses with simpler models. These lower fidelity finite element models accurately reflect the dynamic characteristics needed to identify configurations containing design-driving response levels. Data recovery points located at important positions on the structure serve to characterize a given configuration in terms of analytical importance. If high loads are shown to exist in areas of concern during an analysis supported with low-fidelity FE models, that configuration is selected for more detailed analysis. Furthermore, because maximum loading events for different hardware items occur for different stage configurations, the total set of configurations requiring analysis can grow very quickly. At this time there are 300 stage configurations being considered for detailed loads assessments. Once critical configurations have been identified, high fidelity finite element models replace the simple dynamic models and the transient response analyses are repeated. Each contractor identifies critical locations on the structure and the maximum response levels achieved during analyses at those positions are by definition limit load.

Although the process by which limit loads are developed for the solar array assembly appears arduous and complicated its components are grounded in time-tested analytical techniques. The results from the transient analyses are most certainly accurate but validity still remains a question. Due to the large level of finite element model complexity, unknown dynamic coupling effects and non-rigorous treatment of random variables, validity of analysis results should be verified by appropriate test programs. Without test-verification of analysis results there is little hope of eliminating analytical uncertainties until after the structure is placed into service.

FAILURE MODE IDENTIFICATION

The allowable load of a structure is a function of its design and the anticipated failure mode. Determination of allowable load requires a clear understanding of structural behavior during loading events and identifying the appropriate mode of failure. Once these two goals have been achieved a valid analytical model can be constructed and the allowable load of the structure can be determined.

From the discussion of the loading environment it is clear that the solar array mast will be subjected to a combined state of moment (M), axial (A), shear (V), and torsion (T) load as graphically depicted in figure (21). This figure merely attempts to present a simplified representation of all possible applied loads at a system level. FASTMast design curves for the linear response regime are given in figure (22). In addition to material yield, the slender makeup of the mast implies instability as a possible failure mode. Therefore, load levels associated with stability and yield failure modes must be examined in order to identify which is more likely to occur. For this discussion it is assumed that applied loads act independently and therefore can be analyzed as such. This statement merely invokes the principle of superposition thus implying linear-elastic behavior.

Moment and axial loads on the structure will be reacted principally as tensile and compressive forces in the longerons. If it is assumed that longeron and rigid batten initial curvature is zero and diagonal preloads are equal throughout, the entire mast system can be modeled as a pinned-pinned column for preliminary failure mode analysis. The solar array mast has a test derived effective EI [6] of 16.5 x 10^8 lb-in^2, and length L=1296 in, which when input into the expression for Euler buckling given in equation (2) yields a critical buckling load of 9700 lbs. However, there are four longeron columns in the mast and therefore

$$P_{cr} = \frac{\pi^2 EI}{L^2} \qquad (2)$$

the critical axial load would be one-fourth this amount, or 2425 lbs. Although it appears that a more appropriate buckling model would be a cantilevered column, the blanket preload which acts downward serves to create a follower force loading condition. Referring to figure (23) it is clear that an axial load acting through point C at the base throughout deflection δ will eliminate the bending moment M that is present in the formulation of critical load for a cantilevered column. In terms of material yield the limiting failure load given a minimum longeron cross-section area of 0.26 in^2 and yield stress of 42 ksi, would be approximately 11,000 lb. for a single longeron column. Because the critical buckling load is less than the material yield

failure load, stability must be considered the primary failure mode for axial and moment loading on the mast.

In order to determine the primary failure mode associated with shear and torsion loads, a procedure similar to that above is carried out. As was previously stated shear and torsion loading is reacted internally by the diagonals and battens. An attempt to illustrate mast reaction to shear load is given in figure (24). Shown in this figure is the action of the flex batten and diagonals due to the action of preload P and shear load V. The shear and torsional stiffness of the mast is a result of the post-buckled flex batten force P inducing a tensile preload in the wire diagonals. The load state in figure (24a) is a result of only preload P while the manner in which the mast will react shear load V is illustrated in figure (24b). It is assumed that each diagonal is prestrained to the same level while resisting shear load equally. The flex batten reaction to the shear load is zero because it is in a post-buckled state and cannot take additional load. Although figure (24b) indicates that a set of diagonals would be in "compression", physically this equates to a reduction of the force P supplied by the flex batten. The limiting state is reached when the load in the "compressed" diagonal becomes zero (slack condition), at which time the flex batten begins to pick up additional compressive load and the mast begins to move into a folding mode indicative of mast retraction action (figure 25). The applied shear level at which unwanted mast stowage occurs is that required to overcome the preload in

the wire diagonals. A shear load of this magnitude is much lower than that required for material yield in either the diagonal or flex batten. Therefore the principal failure mode for shear and torsion loads is also one of structural instability. Furthermore, this particular failure mode involves nonlinear behavior due to the change in system stiffness that occurs as the diagonals become slack.

Based upon the preliminary failure mode assessment above it is clear that an evaluation of FASTMast stability should be undertaken. Upon acceptance of that determination two questions immediately present themselves: (1) Is the failure mode a global or local event [see figure (26)]?, and (2) is response of the structure linear or nonlinear? A global or system failure event would correspond to the folding mode that results from excessive shear load. The instability event involving mast folding is mechanistic in nature and is due in part to the hybrid nature of the space truss design. Furthermore, due to mast stiffness changes that occur during large deflections of the elbow joint, this form of instability appears to be nonlinear in nature. On the other hand, the local failure mode involves the classic general instability of a pinned-pinned column subjected to an axial load which would occur during excessive moment and axial loading on the mast. The local instability event involves Euler buckling of a single longeron as is shown in figures (26) and (27). The principal difference between these two failure modes is that the system event is kinematic in nature. Also, the local

event does not appear to be associated with nonlinear behavior indicative of the system type failure mode. Therefore, in order to characterize instability limits of this structure it will be necessary to employ several analytical techniques.

Assuming that the limit load and failure mode identification efforts have been properly performed, determination of the FASTMast (MS) has been reduced to determination of an instability load. It appears that there exists both a local (linear) and global (nonlinear) instability state that must be evaluated in order to determine the allowable load. Once each failure mode has been characterized, the smallest critical load will represent the maximum allowable load, and the (MS) can be determined using equation (1).

THEORETICAL DEVELOPMENT

During the preceding loads discussion two modes of instability for the FASTMast structure were presented. The first failure mode involved general instability of a column and the second was that due to premature mast folding into the stowed position. Both modes of failure are ultimately the result of an axial load P that exceeds the capability of the FASTMast longeron/flex batten assembly. The goal of this analytical effort is to investigate both failure modes and determine which will occur at the lowest level of applied load.

The approach employed here was to analyze the structure at increasingly complex levels of assembly and determine instability regimes for varying load states. In order to better understand applied load interaction effects on stability, singular load states were examined prior to more complicated combined states. The knowledge gained from analyses involving singular load states was used as a guide for studies involving boundary conditions with multiple applied loads.

ONE-DIMENSIONAL LINEAR STABILITY ANALYSES OF A LONGERON SYSTEM

As a starting point it seemed appropriate to investigate the stability of the smallest structural element that alone could affect the stability of the system. The rationale being that stability characterization of a three-dimensional space-truss/mechanism would be difficult to achieve without a clear mechanical understanding of its principal elements. Shown in figure (28) is one column of a one-bay longeron system modeled as a pinned link supported by a flexible foundation. Four identical columns are required for a three-dimensional space truss. The physical system that this model represents is given in figure (6). This model is used to analyze the load P at which the folding failure mode might occur. This is the system failure mode alluded to earlier in which the mast tends to the stowed position [see figures (26)and (27)]. The value of K for the spring is that due to the action of the flex batten and steel diagonals that meet at point O. The applied load P is an axial longeron load whose origin is that due to some system level loading event such as a compressive force or moment acting as described earlier. Furthermore, it is assumed that θ is small and the longeron is rigid. If the system remained in equilibrium in spite of some displacement δ, it would be in a state of neutral equilibrium. The magnitude of P associated with this condition is called the critical load and will be designated by P_{CR}. If $P < P_{CR}$ the displacement would develop forces tending to

restore the assembly to its original position and the equilibrium would be stable. On the other hand, if $P > P_{CR}$, the forces developed by the displacement would tend to cause increased displacement and equilibrium would be unstable. Therefore, the problem is to determine the critical load at which the system would be in equilibrium in spite of very small displacements.

The critical load for the configuration given in figure (28) can be developed from the equations of static equilibrium. Summing forces at point O yields the following:

$$\sum F_O = F_S - 2P\sin\theta \qquad (2)$$

where F_s is the force in the spring. However, if $F_s=K\delta$, and $\delta=L\theta$, equation (2) can be rewritten as

$$P_{CR} = \frac{KL}{2} \qquad (3)$$

This relation must be satisfied if the longeron assembly is to remain in neutral equilibrium. The chief apparent defect of this criterion is that the spring is assumed to be supported by a rigid base. It is clear that for this structure there is base flexibility and the actual value of stiffness K at joint O will be influenced by action of the support. However, the value of P_{CR}

derived from equation (2) will yield conservative critical load levels due to the assumption that the base is rigid.

The next obvious extension to the approach given above would appear to be a model consisting of a series of pinned links supported on elastic foundations as shown in figure (30). This configuration represents the longeron/batten arrangement of one column of three bays of FASTMast structure. Therefore K_1, K_3, and K_5 are stiffness at the flex batten/longeron interfaces, and K_2, K_4, are those at the rigid batten/longeron interfaces. Again the axial load P is a column load that results from some form of external loading. Following the same approach used with the one link system arbitrary deflections U_1 through U_7 are imparted to the structure the resulting equations are

$$\begin{bmatrix} 2-(K_1L/P) & -1 & 0 & 0 & 0 \\ -1 & 2-(K_2L/P) & -1 & 0 & 0 \\ 0 & -1 & 2-(K_3L/P) & -1 & 0 \\ 0 & 0 & -1 & 2-(K_4L/P) & -1 \\ 0 & 0 & 0 & -1 & 2-(K_5L/P) \end{bmatrix} \begin{Bmatrix} U_1 \\ U_2 \\ U_3 \\ U_4 \\ U_5 \end{Bmatrix} = [0] \quad (4)$$

In order to determine a nontrivial solution to the above set of equations the determinant of the coefficient matrix must be equal to zero. The solution of this eigensystem yields the critical buckling loads as eigenvalues and failure shapes as eigenvectors. Together, the eigenvalue and eigenvector represent valid states of equilibrium for this system under the assumed loading

configuration. However, it is important to understand the distinction between the results of this eigenvalue problem and the state of structural stability present in the system under consideration. The solution of this eigenvalue problem guarantees only that there exists a structural shape which satisfies the conditions of equilibrium under a critical load P_{CR}. This loading condition is referred to as the critical load because exceeding it results in indefinite displacements when substituted into the appropriate beam-column, or simple column equation for deflection. Although there exists other shapes which are valid equilibrium states they occur at load levels above P_{CR} and therefore physically unattainable. Verification of the existence of an instability at a specified P_{CR} can be achieved by structural testing or the application of energy arguments.

The second type of local mast failure identified earlier was Euler buckling of the one-bay longeron system. This failure is a linear stability problem that can be simply modeled as shown in figure (29). This failure involves Euler buckling of a single longeron with both ends possessing a pinned condition. The direction of this failure is also given in figure (27) and the critical buckling load for this configuration can be determined from equation (2). It is clear that the entire 32 bay column would fail under the same critical load if entire mast column was assumed to be straight and the load is uniform over the entire length.

From the simple models developed above it is possible to generate both failure load levels and shapes associated with a longeron system subjected to axial load. It is now possible to determine a first estimate of P_{CR} and associated failure shape for an axially loaded longeron system. Furthermore, the preliminary information provided by these one-dimensional models will provide valuable insight to the three-dimensional behavior of the FASTMast structure.

TWO-DIMENSIONAL PLANAR TRUSS WITH GEOMETRICAL NONLINEARITY

As was mentioned earlier during the failure mode identification discussion shear and/or torsion loading causes the diagonals to go slack at the onset of instability. Since the prestrain in the diagonals provide shear stiffness to the system, instability in this case induces an alter system state. It should be clear that a valid FE model must be able to account for this system change during a stability analysis. Therefore, prior to proceeding with a three-dimensional FE model it must be determined how to correctly model this effect.

Shown in figure (31) is a diagram of one bay of the FASTMast structure. The loading type of interest for this study was a transverse shear load (V) applied at the top of the space truss structure. The principal components which react this type of loading are the flex battens, diagonals, and rigid battens. A tensile preload is introduced into the diagonals by compressing the flex batten into the prestressed position shown in figure (5). As long as the preload in the diagonal remains greater than zero the structure behaves linearly and may be analyzed as such. However, if V is equal to, or greater than the preload induced by the flex batten the diagonals become slack as shown in figure (32). This results in a decrease of torsional stiffness and the overall mast stiffness becomes bilinear in nature. In order to account for this geometric nonlinear behavior, it is extremely important that the FE model accurately model diagonal behavior.

Therefore, prior to creating a detailed FASTMast FE model a study involving the behavior of the ANSYS cable element was undertaken.

Due to the symmetrical nature of the FASTMast a study of this type can be conducted with the two-dimensional planar truss shown in figure (33). This particular model represents one face of one-half of a bay of the FASTMast structure. A simple model consisting of four nodes and five elements was constructed and analyzed using the ANSYS finite element code. The element characteristics are given in table (2). These properties are similar to those of the FASTMast structure. The boundary conditions included all joints being pinned and restricted to planar motion. Cable preload was developed by applying a uniform temperature over all nodes thus causing the flex batten to expanded outward against the elbow joint assembly. This action resulted in a flex batten load at the elbow joint of approximately 47 lbs which created a diagonal tensile preload of 28 lb. In order to complete the preloading of the structure each cable element was assigned an initial prestrain of 0.000607 in/in that results from the tensile preload. Force balances performed at the nodes prior to large displacement analyses confirmed the structure was in static equilibrium.

With the above model a nonlinear large displacement analysis was performed using ANSYS version 5.0. A lateral load of V=100 lb was applied at the top of the mast in the x-direction at node 3. The loading was applied as a ramp function in ten equal loadsteps

of 10 lbs each. At the end of each load increment, successful equilibrium equation convergence was required before proceeding to the next substep. The effects of large displacements was invoked by utilizing the nonlinear geometry option offered by the ANSYS code. This option allows for large structural displacements under the condition strains remain small. Upon completion of the analysis nodal force balance data was reviewed and showed equilibrium was maintained throughout the analysis.

Examination of analysis results shows clearly that the ANSYS tension-only spar accurately models preload reduction under the influence of shear load. As a starting point in this discussion the deformed geometry is given in figure (34) at the final substep of the analysis. From this figure it is clear that the prescribed planar behavior was achieved and no bending moments were induced at the pinned connections. Given in figures (35) and (36) are components of element forces as a function of load step for element 5 recovered at node 3. Each 0.1 unit on the ordinate represents one substep in the analysis. It is evident from these figures that the cable preload was reduced to zero by substep six of the analysis. Again it is pointed out that the loss of cable tension is a result of FASTMast reaction to the shear load. As the shear force level increases to a magnitude equal to that of the flex batten preload the cable element goes slack and the ability of the truss to resist shear decreases. Figures (37) and (38) show that as the load of element 5 goes to zero element 4 begins to exhibit a much increased state of

tensile load. The x and y-loads in these figures are those of element 4 taken at node 2. Although not presented here, loads in elements 1, 2, and 3 were reviewed and found to have proper behavior over the entire loading regime.

Another clear indication of nonlinear behavior is shown in figures (39) through (42) which give nodal displacements at the top corners of the truss. Examination of all four plots reveals that system stiffness changes when element 5 goes slack. The increased slope of these curves beyond substep six indicates that for the same amount of load (recall that applied load is equal for all substeps) the structure achieves a greater displacement. Put another way, the system stiffness has decreased thereby allowing smaller loads to result in larger displacements. This is a representation of the bilinear phenomenon associated with this structure under conditions of shear/torsion loading as cables go slack. Closer examination of the y-displacements at node 2 and 3 in figures (40) and (42) give indications of expected cable preload and slackening behavior. These figures reveal a negative y-displacements at the first substep, albeit very small, due to cable tension pulling the truss corners downward. As the applied load is initiated and cable element 5 begins to lessen in tension, node 3 begins to move upward and to the right. Figures (39) and (40) show that at substep six node 3 begins to move rapidly to the right and downward indicating the diagonal element has gone slack. Furthermore, figures (41) and

(42) indicate that node 2 horizontal and vertical motion is greatly increased by the sixth substep.

The results given above verify two very important assumptions developed during the discussion of failure modes of the FASTMast structure. The first point verified by this effort was the existence of nonlinear behavior of this preloaded truss as the cable tension load goes to zero. The bilinear nature of this phenomenon is clearly shown in this very simple exercise. The second point of interest revealed here is the need to properly model the prestrained cable elements in order to develop viable failure loads. The dramatic affect on system response that accompanies loss of cable tension will undoubtedly have dramatic consequences in terms of system response. Therefore, the three-dimensional FE model of the FASTMast must possess a valid representation of the cable under influences of shear and torsion loads. Specifically the model must present an accurate accounting of system stiffness changes as diagonal members go slack.

THREE-DIMENSIONAL FINITE ELEMENT ANALYSIS

The final and most important step in this effort is the three-dimensional FE analysis of the FASTMast system. Although the one-and two dimensional analyses are very important to the development of first-order approximation of system behavior, physical reality can be best approximated with a three-dimensional FE model. Furthermore, analyses must span both the linear and nonlinear response regimes. Therefore, FE models and computational strategies were tailored to response regimes most likely to occur during service. The linear regime under consideration includes responses due to moment, axial, and shear load when the wire diagonals are in a state of tension. The nonlinear response analysis includes the same load types but are applied to a mast structure possessing slack diagonals. In addition to the development of realistic critical loads, FE techniques can also be used to study how hardware state variations affect response characteristics. The goal of this phase of the analytical effort is to develop a realistic model and properly employ computational techniques necessary to calculate viable critical loads.

THREE-DIMENSIONAL LINEAR STABILITY ANALYSIS

The model used to support this portion of the stability analysis was a MSC/NASTRAN format model that was used to support the early phases of the three-bay FASTMast test program. The most complete description of this model can be found in [7]. Shown in figure (43) is the undeformed MSC/NASTRAN linear FE model. It is comprised of 868 nodes, 824 elements and 4300 degrees of freedom. All physical properties included in this model were derived from the those associated with the FASTMast Development Unit Number 2 (Dev 2). The fidelity of Dev 2 hardware is very close to that of the FASTMast flight unit.

The longerons included in this model are the tapered variety found in the lower 20 bays of the flight unit. Tapered longerons were used in this model in order to reflect the construction of the test article. This part of the structure was modeled with the number of BAR elements required to effectively capture the increased bending stiffness provided by the longeron taper. Pin flags, which allow no transmitted moment between nodes, were inserted at each elbow joint to simulate pinned conditions. However, no attempt was made to model the rotational capability of the elbow joint between longerons. Jointed regions of the structure were modeled in all six degrees of freedom with RBE2 elements which provide equations of constraint necessary to simulate infinite stiffness. Each rigid batten frame leg was modeled with one BAR element and no attempt was made to include

the pronounced taper of this structural element. Due to the fact that during linear analyses the steel wire diagonals remain in a state of tension they are modeled with two-dimensional ROD elements.

The most complicated element in this model is that required for the flex batten. Each flex batten is modeled with a NASTRAN GENERAL element. This element allows direct user input of axial, bending and torsional stiffnesses. Stiffness matrix inputs were developed using Castiglianos theorem in conjunction with the energy and deflection state present in the post-buckled flex batten. Each GENERAL element was supplied with the required six-by-six element stiffness matrix.

In order to induce the required diagonal preload of 31 lbs the nodes at the flex batten/diagonal interface are loaded to 51 lbs. This is accomplished with the FORCE card. An exaggeration of the mast preload effect is given by figure (44). Finally, during all stability analyses the bottom of the mast was constrained in a pinned fashion using single-force-constraint (SPC) cards.

Prior to proceeding with linear stability analyses a simple deflection analysis was performed in order to determine if the gross behavior of the structure appeared reasonable. Given the appropriate equivalent beam properties the FASTMast structure can be modeled as such. For a cantilever beam under the influence of a tip load the deflection is given by

$$\delta = \frac{Vl^3}{3EI} + \frac{6Vl}{5GA} \qquad (6)$$

The second term in equation (6) is the deflection due to shear which must be included due to relative large depth of this beam. The factor 6/5 preceding the shear deflection term is that due to a rectangular section. Another point clearly evident is the nature in which a tip load will dominate the deflection response for small l. Able Engineering has developed test-derived values of EI=16.5x10^8 lb-in^2 and GA=10.3x10^4 which can be used in equation (6) in order to determine δ due to end load V. An end load of 100 lbs results in a maximum deflection of 0.1761 in. The same tip load of 100 lbs was applied to the linear NASTRAN model with a fixed end condition at the base. The deflected shape is shown in figure (45) and has a maximum displacement of 0.1471 inches. It is clear that the FE model of the structure is much stiffer than the ideal beam representation. The discrepancy in this case is most likely due to the fact that the test derived stiffnesses include elbow and corner joint flexibilities that the model does not. However, the higher model stiffness is consistent with the fact that elbow and corner joints possess no flexibility. This model will certainly require updating prior to final P_{CR} determinations necessary for design assessments.

This portion of the stability analysis included two different

applied loads. The values of P_{CR} determined at this stage of the analysis involved the load types shown in figures (46) and (47). Due to the fact that the model joints are rigid the structure critical loads from this study will represent a lower bound. Note that this implies a conservative determination for design assessment. However, it provides a basis for comparison during future linear and nonlinear response data evaluations. As structural test data and final design drawings become available all models should be updated and stability analyses repeated.

THREE-DIMENSIONAL NONLINEAR LARGE DISPLACEMENT ANALYSIS

The source of nonlinearity in this case is due to the changing system stiffness as the structure experiences large deflections. This particular large displacement problem includes the effects of large translations and rotations while strains remain small. However, due to the potential convergence problems associated with this type of analyses it is extremely important the FE model closely match the nonlinear elements of the hardware. Therefore, accurate modeling of the flex battens, wire diagonals, and mast joints was deemed critical for generation of accurate and valid data.

The model used for this analysis was based on the FASTMast Dev 2 design. ANSYS was selected as the nonlinear FE code due to its proven nonlinear capabilities. The entire model consisted of 300

elements, 292 nodes, and an estimated 1332 degrees of freedom. Shown in figure (48) is the undeformed preloaded ANSYS model. In order to define the entire model five element types and ten real constant sets were required. All mast structural properties were based on the most-up-to-date information available.

Instead of modeling the longeron taper as was done in the linear NASTRAN FE model, the ANSYS longerons were model as straight members with a square cross-section of 0.59 in by 0.59 in. This cross-sectional area represents the largest that occurs along the length of the tapered longeron. Modeling the longeron in this manner is a simplification deemed appropriate for the first model iteration. Twenty-four three-dimensional straight beams were used to model three bays of FASTMast structure. Each rigid batten frame required three-dimensional truss elements to model the batten tube and three-dimensional tapered beams to model the corner fittings. The wire diagonals were represented by two-dimensional tension only spar elements which included an initial prestrain equal to that prescribed by the required tensile preload. Finally, the fiberglass flex battens were also represented by three-dimensional beam elements.

In order to represent joint flexibilities at the elbow and corner fittings hinge elements were introduced to these parts of the structure. The ANSYS hinge joint provides translational and rotational stiffness in all six degrees of freedom at the point of application. At each elbow joint there are four hinge

elements and at each corner fitting there are two. A hinge element consists of a coincident node pair that are connected in all but one rotational degree of freedom. Shown in figure (49) is an example of an elbow joint modeled using hinge elements. In this example the coincident node pairs are (5,45), (5,35), (5,25), and (5,15). At each longeron end there is a hinge that allows for ninety-degree rotation plus a 0.6 degree back rotation required to model stopping action of the deploying mast. After engaging the stop the hinge is no longer free to rotate and instead behaves as a torsional spring with a rotational stiffness of $1x10^6$ in-lb/rad. Also included in this element is a test-derived translational stiffness of the two hinged nodes relative to each other of $4.3x10^5$ lb./in. The hinges on flex batten ends do not have rotational limits and possess very high translational stiffnesses. An identical connection process is carried out at the corner fittings without the inclusion of the flex batten.

The ability to identify instability points during a geometric nonlinear large displacement analysis is not straightforward. Unlike linear static analyses, the structure is loaded incrementally and the equations of motion are solved in a piecewise linear manner over subintervals of the response regime. Over each loading increment the equations of equilibrium are solved iteratively until the solution converges within some specified tolerance ban. During this analysis both force and moment convergence criteria were used to evaluate the adequacy of the solution before proceeding to the next load step. Solution

iterations continue until either convergence is achieved or the analysis is terminated by user request. Upon successfully satisfying the equations of equilibrium the stiffness matrix is updated and the analysis moves to the next interval of applied load. This process is repeated over the entire range of applied load. The fact that the solution is derived in a piecewise manner introduces the first analytical difficulty which involves bypassing the point of instability due to an interval selection that is too broad. This situation can occur for instabilities such as "snap through" buckling. Furthermore, even if the proper interval has been identified there still remains the question of at which point in the interval instability will actually occur. For example, if an instability occurred between 10 and 20 lbs the failure load level possibilities include 11, 12, ... , and 20 lbs. The only explicit conclusion presented by code output is that a failure occurred somewhere between the end points of the applied load interval. Identification of instability points from output data can be accomplished by identifying radical changes in output values at some predefined characteristic point. In this case large displacements at the top of the mast due to a load of smaller or equal magnitude than the preceding step was taken to infer a point of instability. An analytical consequence of such an event may result in a set of equilibrium equations that prove to be nonconvergent. This type of nonconvergence is due to the fact that the structure has undergone a shape change that will not satisfy conditions of equilibrium. However, convergence problems may also result from modeling errors that have no

relationship to a possible state of instability. Therefore, prior to reporting large displacements and nonconvergent behavior as indications of instability points structural response must be judged appropriate. The analyst must ensure that the FE model is accurately representing nonlinear behavior and results reflect problem physics. In general this is accomplished by utilizing engineering insight and structural test data during the data reduction process.

The nonlinear analysis presented here involves the following applied load regiment: (1) lateral load (V) as given in the linear stability analysis, (2) pure moment load a shown in figure (50), and (3) a combined lateral and moment load as given in figure (51). In each case loads will be gradually increased until an instability occurs or the range of expected applied loading has been completely analyzed. The objective of this analysis is three-fold: (1) demonstrate that an instability can be extracted using this process, (2) provide nonlinear critical load levels for comparison to the linear case, and (3) determine the effect on critical load levels due to applied load interactions. Clearly this analysis will not complete the nonlinear stability study for this structure. However, the procedure presented will provide the foundation for future advanced studies of the FASTMast structure.

RESULTS AND DISCUSSION

With the foregoing theoretical development serving as a basis, one and three-dimensional stability analyses were performed to evaluate the behavior of the FASTMast structure. Both linear stability and nonlinear large displacement analyses techniques were employed to determine critical loads. In the case of linear analyses the failure load was taken to be that at which bifurcation was evident. Large displacement instabilities were identified as unusually large mast tip displacements occurring during a small change in applied load. In all cases nonlinear instability resulted in a set of nonconvergent equations for equilibrium and the analysis was ended. Finally, the implication of each result is discussed in terms of overall structural stability of the system.

The first and simplest analysis involved the single longeron system modeled as a simple column with a pinned connection. This model represents the lowest level of the mast system at which instability will be examined for this study. The expression for linear instability is given by equation (2) and nonlinear response was determined using equation (3). Note that the utilization of equation (3) represents an attempt to cast the nonlinear stability problem as a linear eigenvalue problem. This approach should not be confused with the nonlinear FE analyses employed to characterize the nonlinear stability response of the mast. Results are presented in table (3). With a test-derived

joint stiffness of K=400 lb/in and L=20 in, equation (3) yields a P_{CR} of 4000 lbs. For the Euler buckling case represented by equation (2) the value of P_{CR} for a single pinned-pinned longeron column is 2492 lbs. This calculation included values of $E=10^7$ lb/in^2, $I=0.0101$ in^4, and L=20 in. In this case the linear buckling case represents the critical state of instability.

The single longeron models from above were then expanded to include longeron systems of a three bay FASTMast unit. From the symmetry of the loading it is clear that the critical Euler load will be identical to that of the one bay model. The system failure model was represented by the system of equations given in (4) with K_1, K_3, K_5 equal to 400 lb/in, and K_2 and K_4 equal to 35 kip/in. Solution of this eigenvalue problem was obtained using the commercial code *MATHEMATICA*. The smallest eigenvalue of this system was 4000 lbs which is identical to the result of the single longeron system. Given in figure (52) is the failure mode which depicts the shape of the folding action of the mast. Again due to the symmetric nature of the load the similarity between the one and three-bay model results was not surprising.

Next the linear FE analysis of the three-bay unit was performed for two independent cases which included axial and lateral loads states at the mast top. The results are given in table (4). For the case of the axially loaded columns P_{CR} was 1915.25 lb, and the laterally loaded column P_{CR} value was lower at 1298.28 lb. The failure shapes for both cases are given in figures (53) and (54).

In both cases the failed shapes were local buckling involving the longeron assembly. Another important point to be made here is that the failed shape in both loading cases is the Euler mode presented by the one-dimensional model. In order to compare the failure load levels between the one and three-dimensional cases the FE longeron load at instability is also presented in table (4). In terms of longeron axial load the FE analysis yields a P_{CR} value that is 23% less than that given by the one-dimensional model. Due to the fact the rigid battens are providing additional longeron support this result appears to indicate an error in the model. However, the FE model accounts for longeron taper and therefore the effective moment of inertia of an individual longeron is less than that of the simple one-dimensional model. Furthermore, the longeron end connections in the FE model are rigid interfaces which also decreases P_{CR}. Therefore, the lower FE P_{CR} value for this load case is consistent with the variation in models.

For the lateral load case the value of maximum longeron load given in table (2) is 2375.42 lbs. The maximum axial longeron load occurred at the base of the mast and is larger than the value of P_{CR} for the case of mast compressive loading given above. This result is due to the fact that the longerons above the base elements have less compressive load and therefore can offer additional support. The net result of this longeron interaction is an increase of longeron axial load at instability.

The nonlinear large displacement FE analysis results for independently applied loads are also presented in table (4). These loads types were used because together they represent a catalyst for nonlinear behavior. The first nonlinear analysis performed involved a lateral load applied at the mast top in a ramp fashion from 10 to 120 lbs. As was the case for all nonlinear analyses, the preload was developed during the first two load steps utilizing a temperature and shape formation load on the flex batten. Furthermore, the diagonal preload level was 31 lbs for all analyses. Shown in figure (55) is the y-deflection of the mast tip as a function of applied shear load. From 10 to 100 lbs the response is linear and the mast stiffness is approximately 661 lb/in. As the load increases beyond 100 lb the system stiffness is drastically reduced to a level of 31 lb/in. The dramatic stiffness reduction in this case occurs as the preloaded diagonals become slack as shown in figure (56). The plot of diagonal preload as a function of load step given in figure (57) is typical of cable action during shear loading. Also, from this figure it is clear that loadstep representing zero preload coincides with the dramatic decrease in mast stiffness given in figure (55). The maximum tip deflection was 0.740 inches and instability did not occur. The deformed shape for this load case is given in figure (58) and shows the folding action of the mast for this failure mode.

Although it is clear that system stiffness decreases as diagonals become slack the cause of this degradation requires further

explanation. The decrease in system stiffness for this structure can be illustrated with planar truss example. Given in figure (59a) is a planar truss subjected to a lateral load V. This particular truss structure possess FASTMast characteristics and contains 12 degrees of freedom, 10 truss elements (four diagonals, four longerons, one rigid batten, and one flex batten), and four unknown reactions at the base. In order to maintain a stable state of equilibrium the number of structural elements plus the number of restraints must be equal to or greater than the degrees of freedom. If the diagonals are fully effective the sum of restraints and structural members is 14 which is greater than the number of degrees of freedom. As the lateral load V increases to a level equal to the flex batten load F two diagonal members become ineffective as shown in figure (59b). In this case the sum of effective structural elements and restraints is 12 which equals the number of degrees of freedom and the system appears to be stable. However, closer examination of the effective structural elements reveals a flex batten element which is in a post-buckled state and therefore can offer no additional resistance to lateral load V. Therefore, when cables become slack the sum of restraints and structural elements is actually 11 and the truss configuration is unstable. The instability in this case is evidenced by a dramatic decrease in system stiffness. Note that in the case of zero slack cables an ineffective flex batten does not create a state of instability because there are still 13 elements of constraint. A second illustration of this phenomenon is shown in figure (60).

However, the structure in this case is a traditional truss with no flexible elements. The fully effective truss of figure (60a) can be assigned a stiffness K. If two of the diagonal elements are rendered ineffective as shown in figure (60b) truss stiffness is reduced to K/2. In this case the system stiffness is reduced by only 50% because the rigid battens provide structural stiffness the flex battens could not.

The next nonlinear case of interest involved a pure moment applied at the top of the mast as a ramp load from 10 to 160 kip-in. A plot of the lateral tip deflection as a function of load is given in figure (61). Under this type of loading the mast response remains linear and instability does not occur. The maximum tip deflection achieved during this loading event is 0.667 inches. Presented in figure (62) is the deformed geometry for this case.

The final nonlinear analysis presented here involves a combined lateral and moment load applied simultaneously at the mast top. Both loads were applied in a ramped manner identical to that of the independently applied load cases. From the response curve given in figure (63) it can be seen that the system stiffness begins to decrease as the lateral load achieves a 95 lb level. Instability in this case occurred at applied load levels of 100 lb lateral load and 100 kip-in moment. Associated with this failure state was a maximum tip deflection of 82.0 inches. Given in figures (64) and (65) are the deformed geometry plots for this

case. The most important result of this analysis is the fact that a combined load state of lateral and moment load caused large displacements whereas individually applied loads at higher levels did not. It appears that the unstable system stiffness resulting from high lateral loads when combined with large longeron axial loads precipitate FASTMast collapse. Therefore, careful consideration must be given to all credible combined load states before a final determination of instability load levels can be rendered. Also, nonlinear instability applied load levels are much lower than the linear buckling results and therefore represent the limiting case.

From the above results it is also evident that the ability to model this three-dimensional event utilizing one-dimensional models may leave something to be desired. In both the linear and nonlinear cases the one-dimensional models predicted instability levels much higher than resulted from the FE analysis. This is clear upon comparison of the values in tables (3) and (4). In table (3) the local failure mode (linear) represents Euler buckling of a longeron system and the system failure mode (nonlinear) is the folding failure mode. The corresponding three-dimensional values in table (4) are from the linear and nonlinear axial load cases respectively. The one-dimensional Euler buckling load is 2492 lbs and the corresponding three-dimensional value is 1915.25 lbs. In terms of nonlinear failure levels, the one-dimensional model indicates a critical level of 4000 lbs while the three-dimensional model exhibits no

instability at all. The source of these discrepancies can most likely be attributed to the three-dimensional load path of the FASTMast which cannot be modeled in one-dimension. For example, the assumption that the base of the elastic foundation supporting the one-dimensional system failure model was rigid is not accurate in this case. In reality the base support is actually the elbow joint on the opposite side of the longeron system under consideration and it is most certainly not rigid. Furthermore, the elbow joints and rigid battens form a three-dimensional support lattice not modeled easily in one-dimension. For these reasons the disparity between one-dimensional and three-dimensional results is not surprising.

Another important deficiency of the one-dimensional nonlinear model is its inability to identify changing system stiffness as shear loads reach a critical threshold. This fact severely limits the ability of a one-dimensional model to accurately predict failure load levels. However, the one-dimensional models do provide a valuable basis for comparison since differences in values of P_{CR} can be rationalized by sound engineering arguments. Furthermore, the one-dimensional models can provide valuable insight in terms of the failure mode type. In this instance the use of one-dimensional models provided valuable insight during FE model development and interpretation of FE method results.

CONCLUSIONS

From the results given above it is clear that the nonlinear response regime of the FASTMast structure represents the limiting state in terms of stability. Furthermore, an accurate assessment of stability can only be achieved if states of combined loading are properly addressed. From this study it is very clear that the limiting design feature in terms of structural stability is the flex batten. The flex batten provides preload to the diagonals which in turn impart shear and torsional stiffness to the structure. When applied shear load reaches a level equal to, or greater than, the preload generated by the flex batten, system stiffness is reduced by 95%. It is clear that this state represents a point of instability because the addition of moment load (which is reacted as longeron axial load) causes large structural displacements.

This work represents a foundation upon which future analyses can evolve. Three applied load types have been presented and linear and nonlinear failure modes have been identified. A method for nonlinear stability assessments has been presented and appears to have promising potential. However, there are issues involving modeling, convergence, and interpretation that must be resolved prior to undertaking the large amount of nonlinear analysis that remains. Furthermore, the nonconservative nature of FE instability predictions must also be considered before analytical results become part of the design assessment. In order to

achieve the level of understanding and confidence required for meaningful hardware evaluations, analyses and tests efforts must be integrated such that nonlinear results are adequately verified.

FUTURE WORK

It is clear that in order to characterize the FASTMast flight article in terms of stability much work remains. A principal accomplishment of this effort has been the identification of FASTMast stability failure modes associated with anticipated loading events. Furthermore, a methodology has been established that provides a basis for future linear and nonlinear assessments. Given below are several suggested efforts that together would provide a total stability assessment of the solar array assembly in the on-orbit configuration.

Prior to development of a full-scale FE model of the FASTMast flight article several modeling characteristics must undergo further refinement. In this respect the largest deficiency resides with the linear and nonlinear FE model joint stiffness definitions. Correct modeling of this structural element is essential for realistic predictions of mechanistic behavior. Hinge element stiffnesses should be derived by performing appropriate structural tests. Nonlinear characteristics of the wire ropes diagonals should be included in the cable elements. Longeron taper and elbow joint interface offset must be included in all FASTMast FE models. Linear FE model characteristics that require updating include modeling of the rigid batten frame, diagonals, and the flex battens. Also, all FE models should include design changes indicated by released flight drawings.

In order to verify the validity of model updates analyses results should be correlated with ongoing FASTMast testing. Once the models have been updated, stability analyses should be repeated and results compared to earlier failure levels. In order to complete the study of FASTMast stability analyses involving combinations of shear, torsion, and moment loading should be undertaken. The fact that shear and torsion loads are likely to interact nonlinearly during large displacements quickly provides motivation for this endeavor. Also, the development of meaningful failure interaction curves will clearly involve combinations of all possible service loads.

With an updated three-bay FE model additional parametric analyses should be performed to better understand mast behavior. These analyses should precede expensive and time-consuming analyses of thirty-two-bay flight unit. The analyses of interest in this case can be conveniently divided into two categories involving mast design deviations and applied load interaction studies. As shown during the nonlinear response assessment the diagonal prestrain level will have a profound effect on response to applied shear loads. However, the assumption of uniform diagonal preload invoked for the current analyses will not be practically realizable over the entire life of the mast. Therefore, the effects of varying diagonal preloads should be studied to ensure design specifications are adequate to prevent instabilities. Other important parameters that require evaluation include longeron misalignment and flex batten degradation. In addition

to decreasing shear load resistance, longeron misalignment will also degrade longeron axial load carrying capability.

Upon completion of three-bay parametric studies an evaluation of applied load interactions effects on stability should be performed. This should be carried out for both the linear and nonlinear response regimes. The product of this effort would be load interaction curves that show the relationship between shear, moment, and torsion loading at instability. Also, a better understanding of service loads must be developed in order to properly evaluate the implications of the failure interaction curves. This is due to the fact that certain applied load states possible in a sensitivity study may have no basis in reality. Extending this effort even further, the ideally preloaded structure would be degraded as described in preceding paragraph and interaction curve development repeated.

In terms of the nonlinear large displacement analysis a methodology must be developed that will allow accurate isolation of the failure interval. If the failure region can be isolated early in the analysis, smaller load steps can be used without compromising the overall cost of analysis. With smaller load steps easier identification of instability points should be a realizable goal. Also much thought must be given to how combinations of load are to be applied to the structure. The interaction state between applied loads must be well understood before realistic levels can be defined.

Once it has been established that the modeling technique is sound and mast behavior is well understood the stability analyses can proceed to include the thirty-two-bay flight unit. Care must be taken when incorporating three-bay derived model updates into the thirty-two bay model. In other words, updates used for the thirty-two bay FE model must not include behavior anomalies that may be inherent only to three-bay responses. Of primary concern are any test boundary effects not relevant to the flight design. Additional care during model updating is warranted in this case due to the fact that both units will likely behave differently in the nonlinear regime. With the updated thirty-two bay models the linear and nonlinear stability analyses should be repeated to establish critical loads of the flight article. In order to completely characterize mast stability important parameters identified during three-bay studies should be varied and critical loads determined for those states. The final product of this characterization effort would be a complete set of failure loads in both response regimes for the flight hardware. Also, given the appropriate limit load margins of safety must be determined for different load states.

Finally, in order to include the stochastic nature of both the loads and mast strength characteristics it may desirable to perform an in-depth reliability analysis of the solar array assembly. With the aid of loading and strength probability distribution functions it is possible to use reliability methods

to determine failure probabilities. In the case of the solar array assembly this would require additional work due to the lack of strength and loads data that would be required for a probabilistic study. However, this difficulty could be overcome by properly employing system simulation Monte Carlo methods. An example of this type of analysis is presented in reference [8].

ACKNOWLEDGEMENTS

As is generally the case with any worthwhile endeavor much support is required along the way and this effort has been no exception. I would like to extend special thanks to Dr. Francis J. Shaker for his many hours of patient guidance throughout this effort. His initial problem definition and mechanical insight provided the basis for this entire effort. I would also like to thank Dr. Dario A. Gasparini for his many valuable comments and encouragement over the course of this project. Finally, I reserve the largest thanks for my wife Sue. You see, without her never-ending support not only would this work never have been completed, there would have been no desire to do so.

REFERENCES

[1] "Space Station Program Structural Design Loads Data Book Volume 1:Structural Design Loads Analysis Criteria", Space Station Freedom Program Office, SSP 30800 Volume 1, May 1993.

[2] "Space Station Freedom Critical Design Review Plume Impingement Loads and Dynamics Analysis Criteria", LESC Report No. 30740, May 1993.

[3] Rayos, E. M., "Users Guide for the RCS Plume Force Program, "LESC Report No. LESC-24588, October 1987.

[4] Mount, G. O. Jr., Mikhalkin, B., Six Degrees of Freedom FORTRAN Program "ASTP Docking Dynamics" Users Guide, Rockwell International Space Division Report No. SD 74-CS-0023, June 1974.

[5] Craig, R. R. Jr., Bampton, C. C., "Coupling of Dynamic Substructures for Dynamic Analyses", AIAA J., v. 6, 1313-1319(1968).

[6] "Mast-Canister Stiffness and Strength", AEC-Able Engineering Report No. AEC92518R743, October 1992.

[7] "3-Bay FASTMast Axial Test and Analysis", Lewis Research Center Engineering Directorate Report No. SAB 93-002, February 1993.

[8] Yunis, I. S., Carney, K. S., "The Application of Structural Reliability Techniques to Plume Impingement Loading of the Space Station Freedom Photovoltaic Array", Structures, Structural Dynamics, and Materials Conference, 34th, AIAA, New York, 1993.

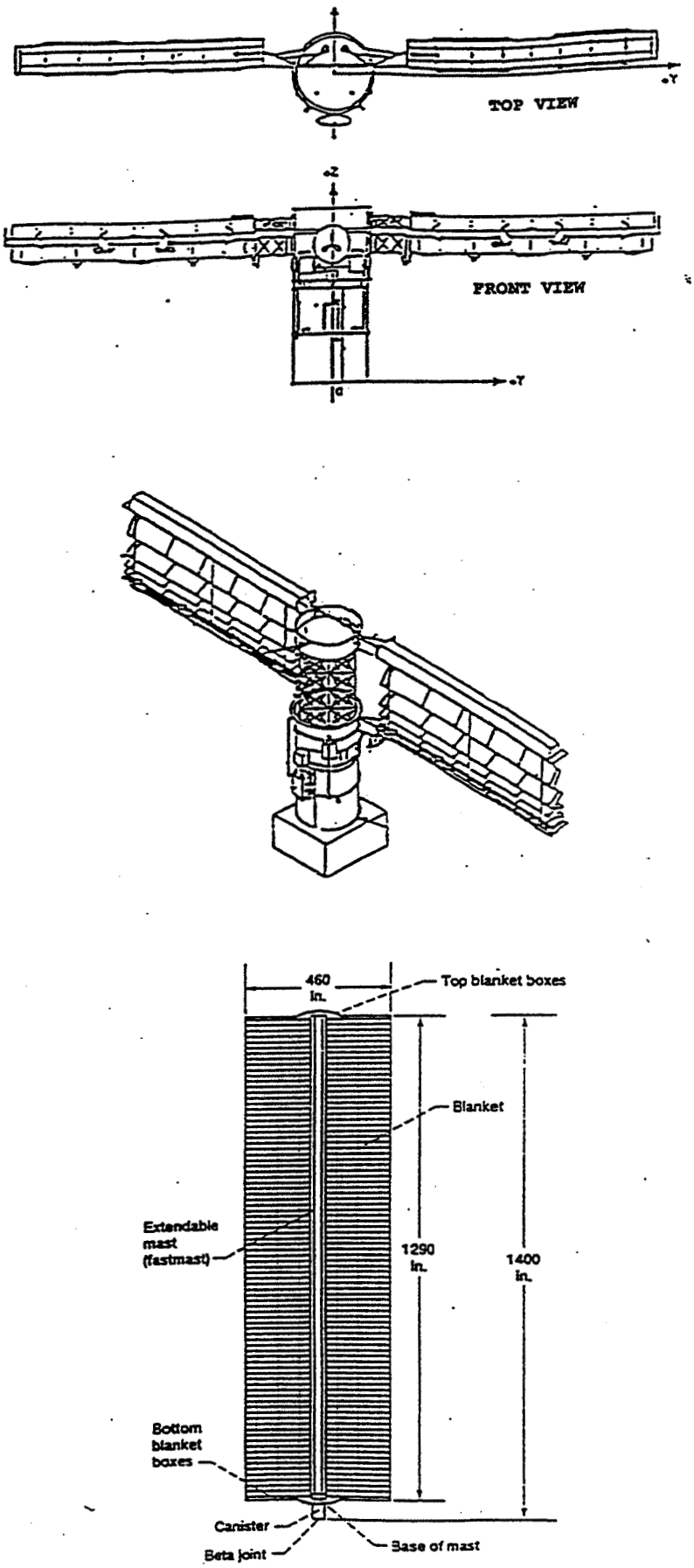

Figure 1 - Top to bottom : Stowed, partially deployed, fully deployed solar array assembly

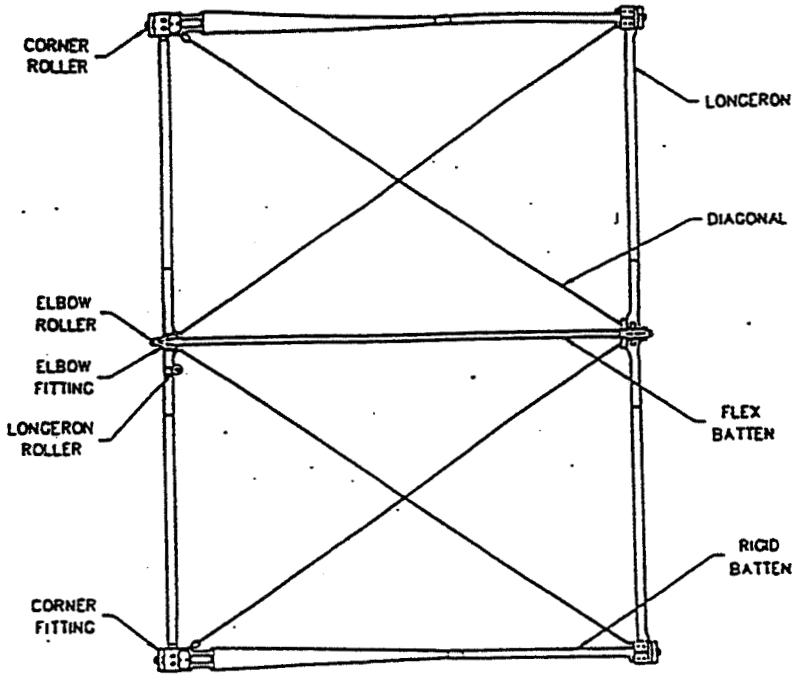

Figure 2 - FASTMast - One bay

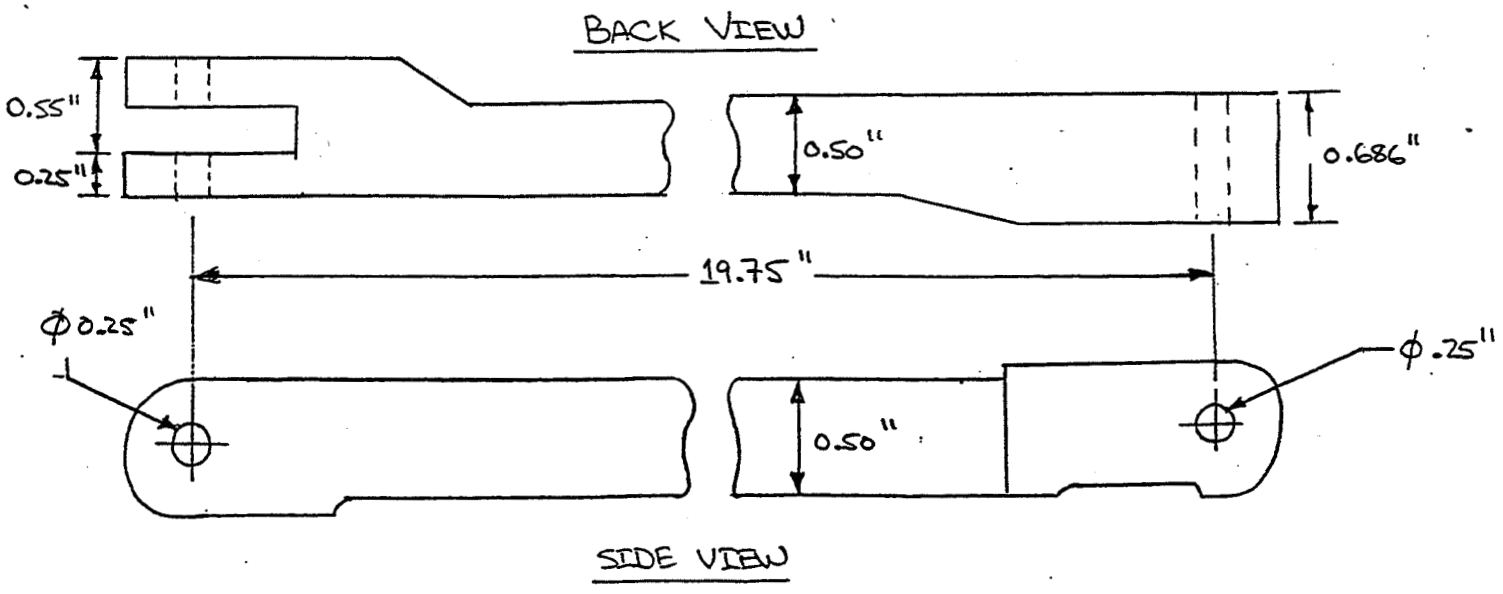

Figure 3 - Longeron

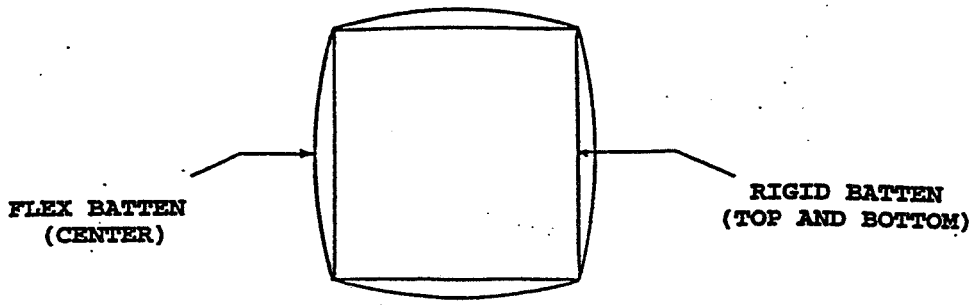

Figure 4 - FASTMast - Top View

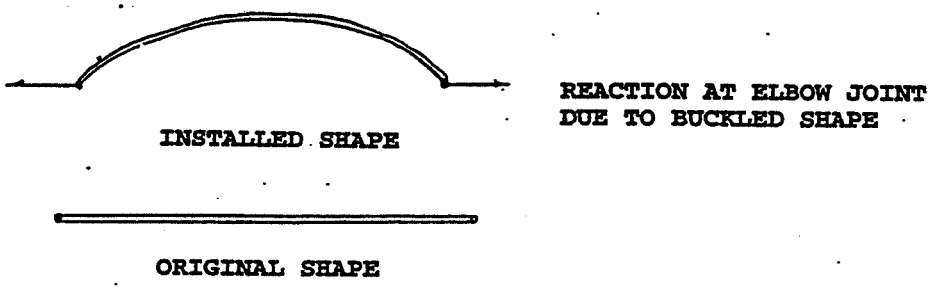

Figure 5 - Preload Flex Batten

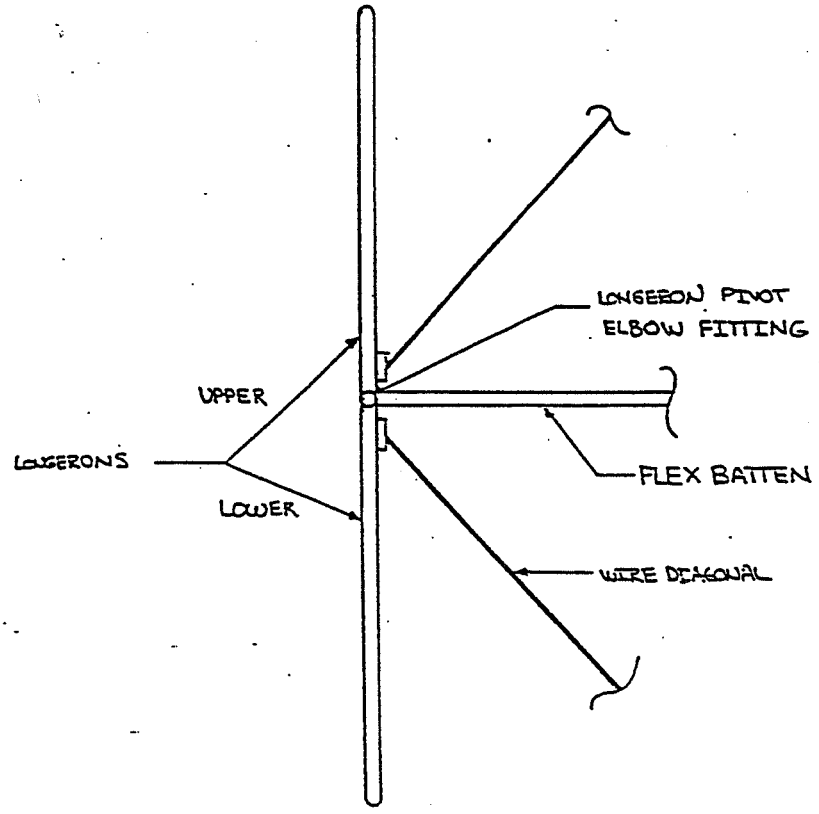

Figure 6 - Longeron/Flex Batten Interface

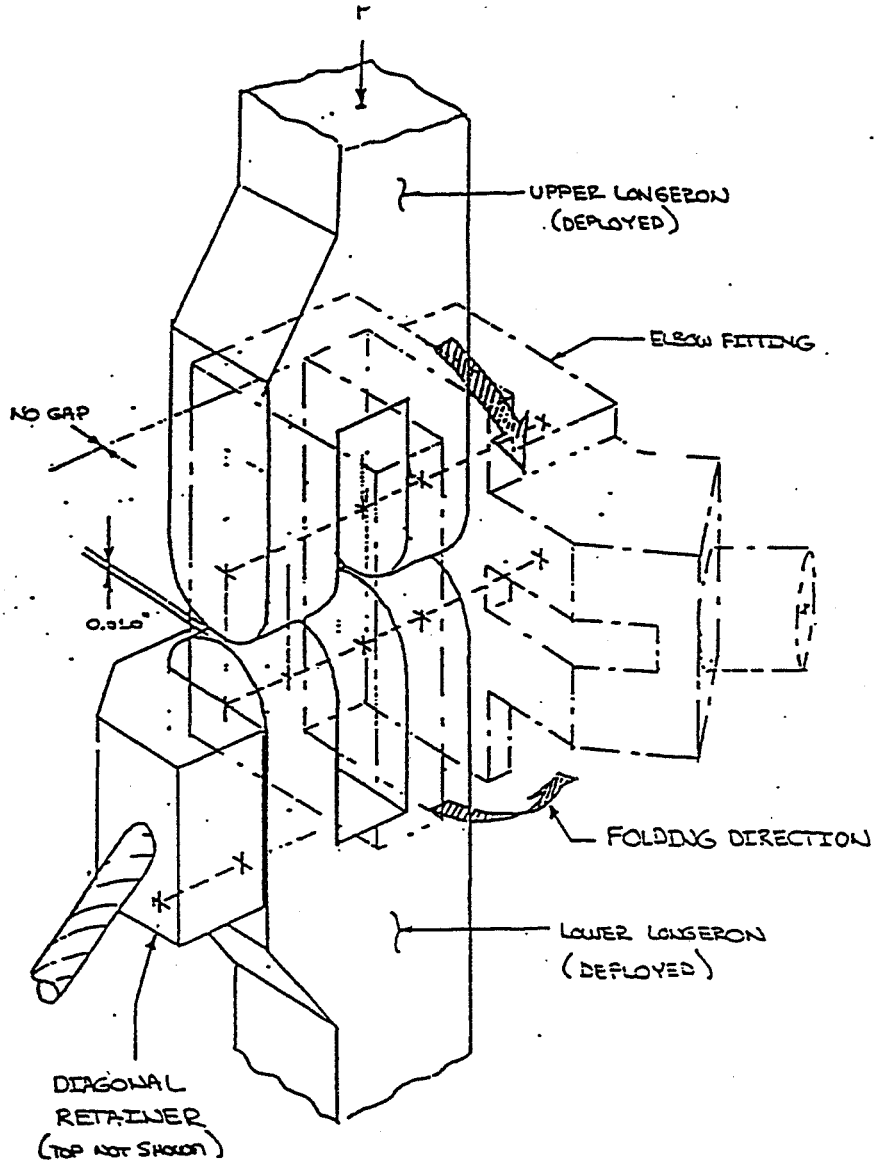

Figure 7 - Elbow Fitting

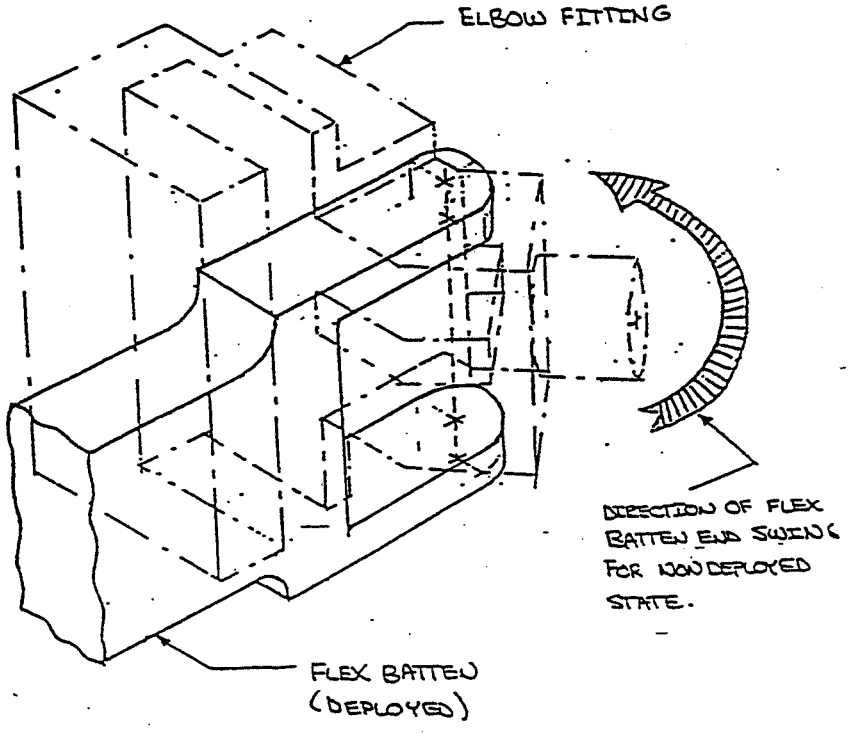

Figure 8 - Flexed Batten Forked End

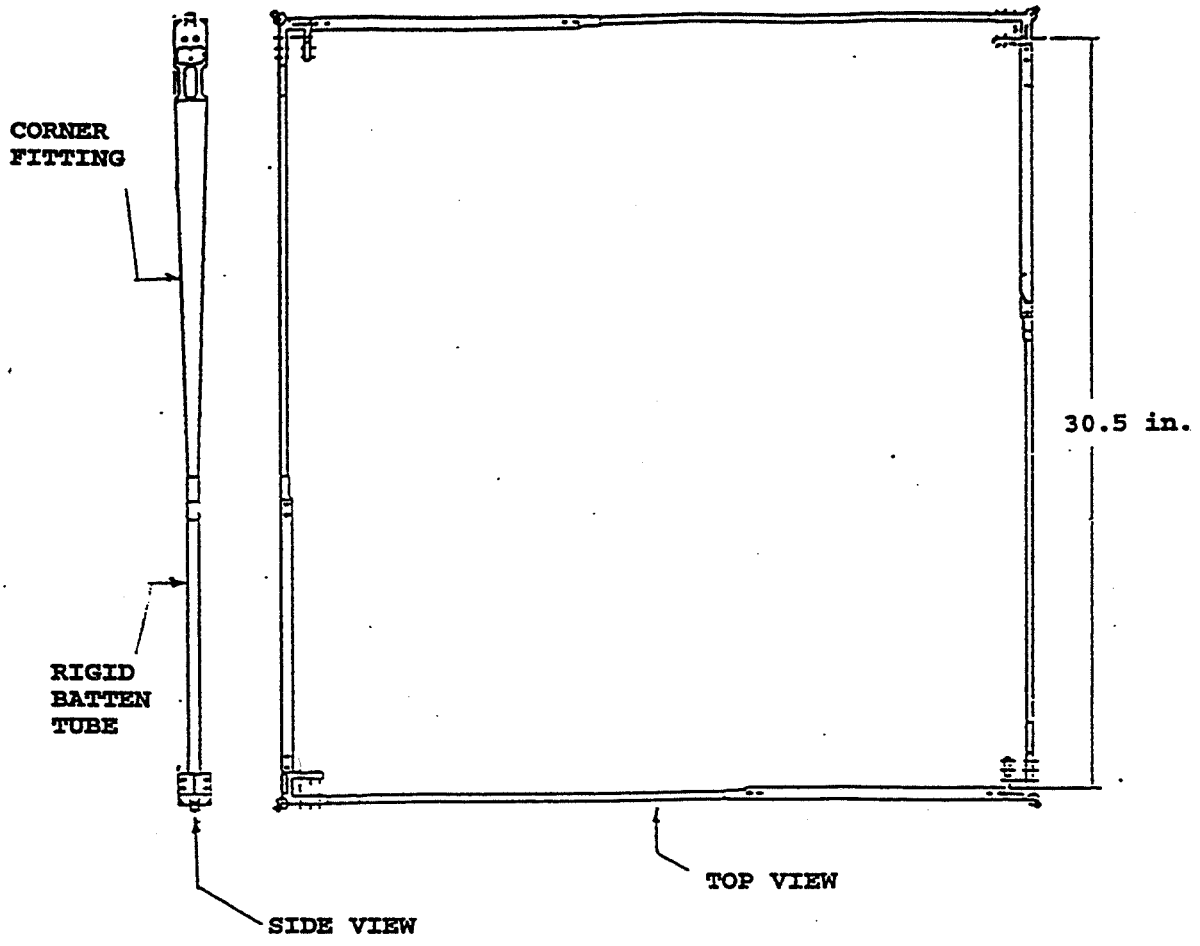

Figure 9 - Rigid Batten Frame

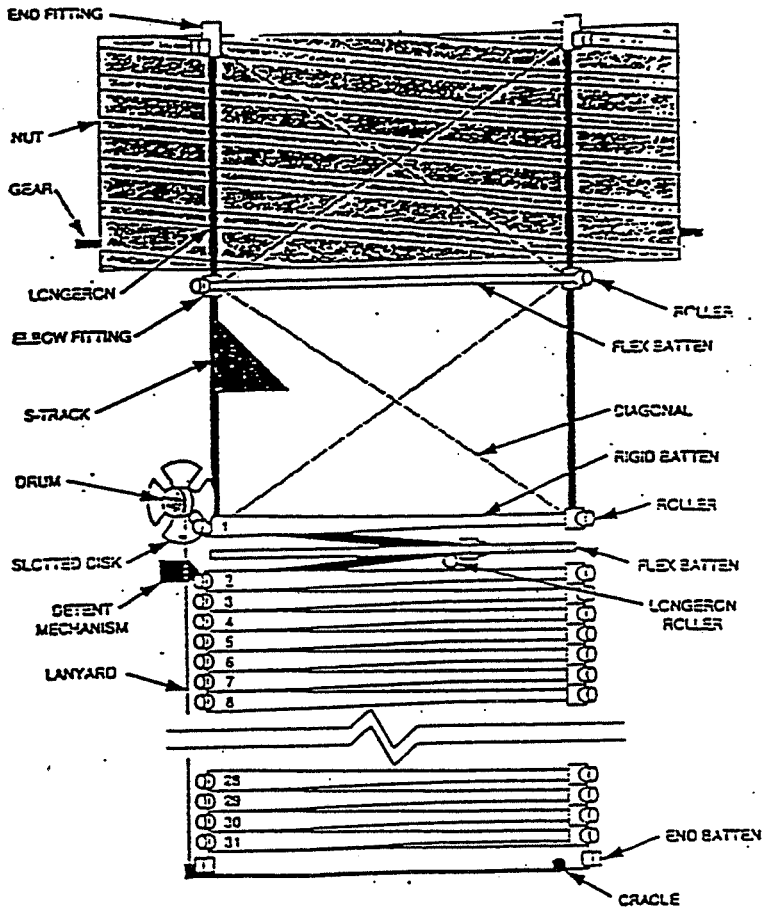

Figure 10 - Stowed FASTMast Position

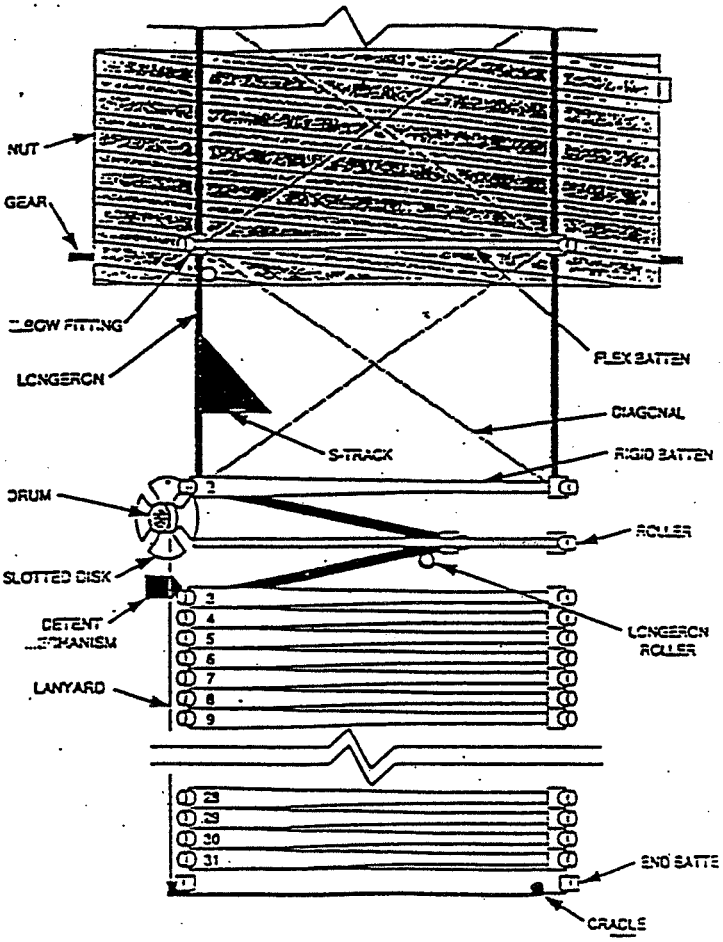

Figure 11 - Initiation of Bay-One Deployment

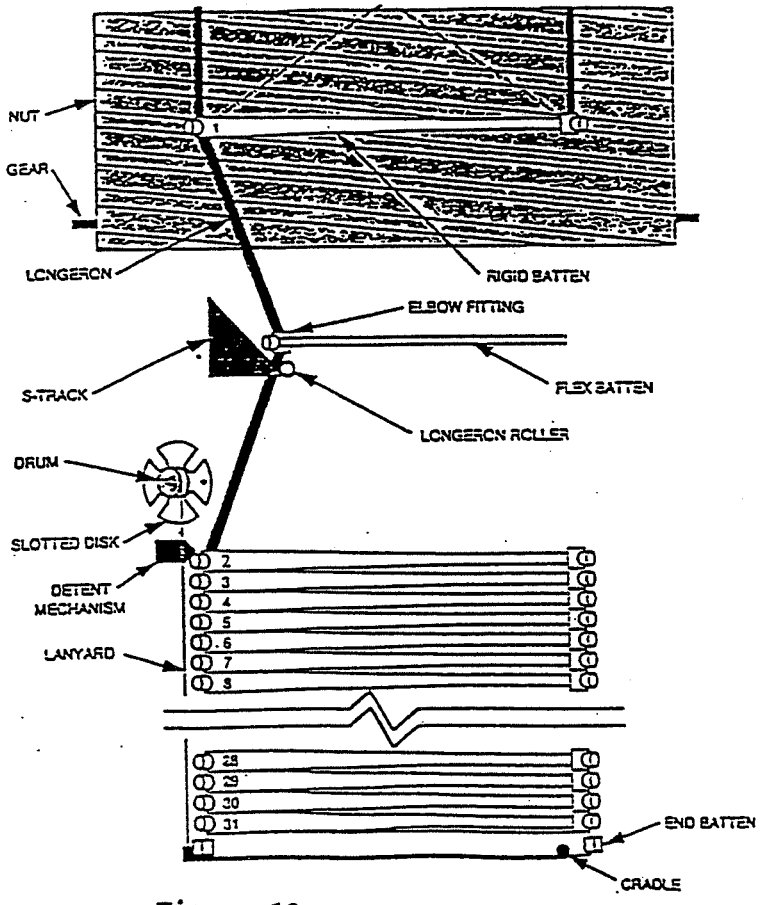

Figure 12 - Bay-One Deployment

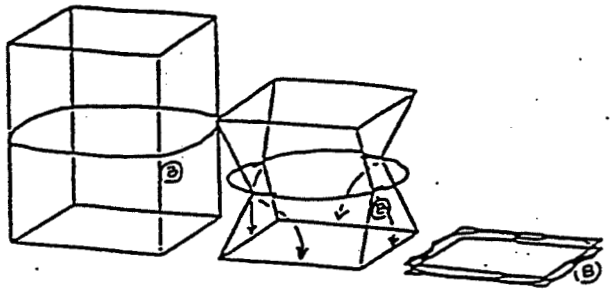

LONGERON MOVEMENT

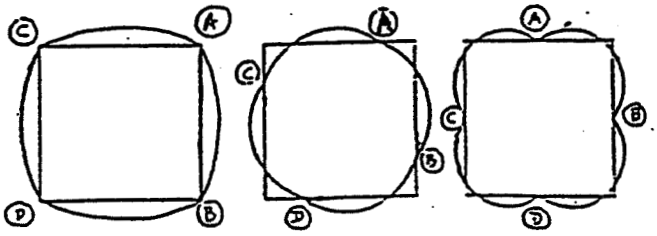

FLEX BATTEN MOVEMENT

Figure 13 - FASTMast Kinematics

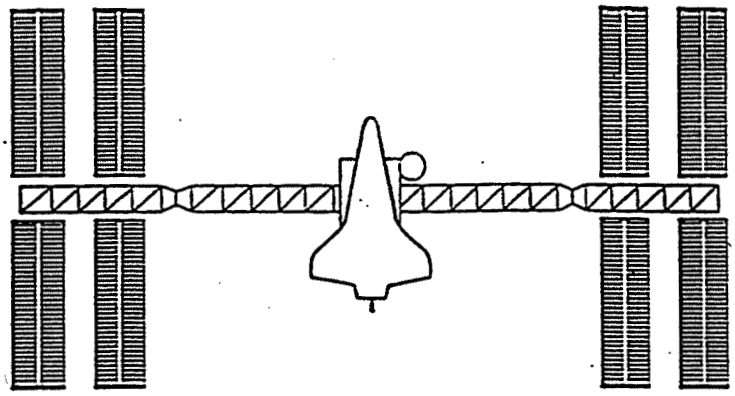

BUILD COMPLETE

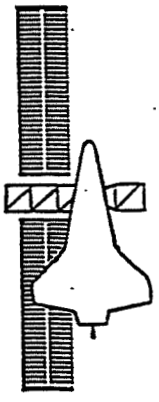

MISSION-BUILD TWO (MB-2)

Figure 14 - Shuttle/Space Station Size Comparison

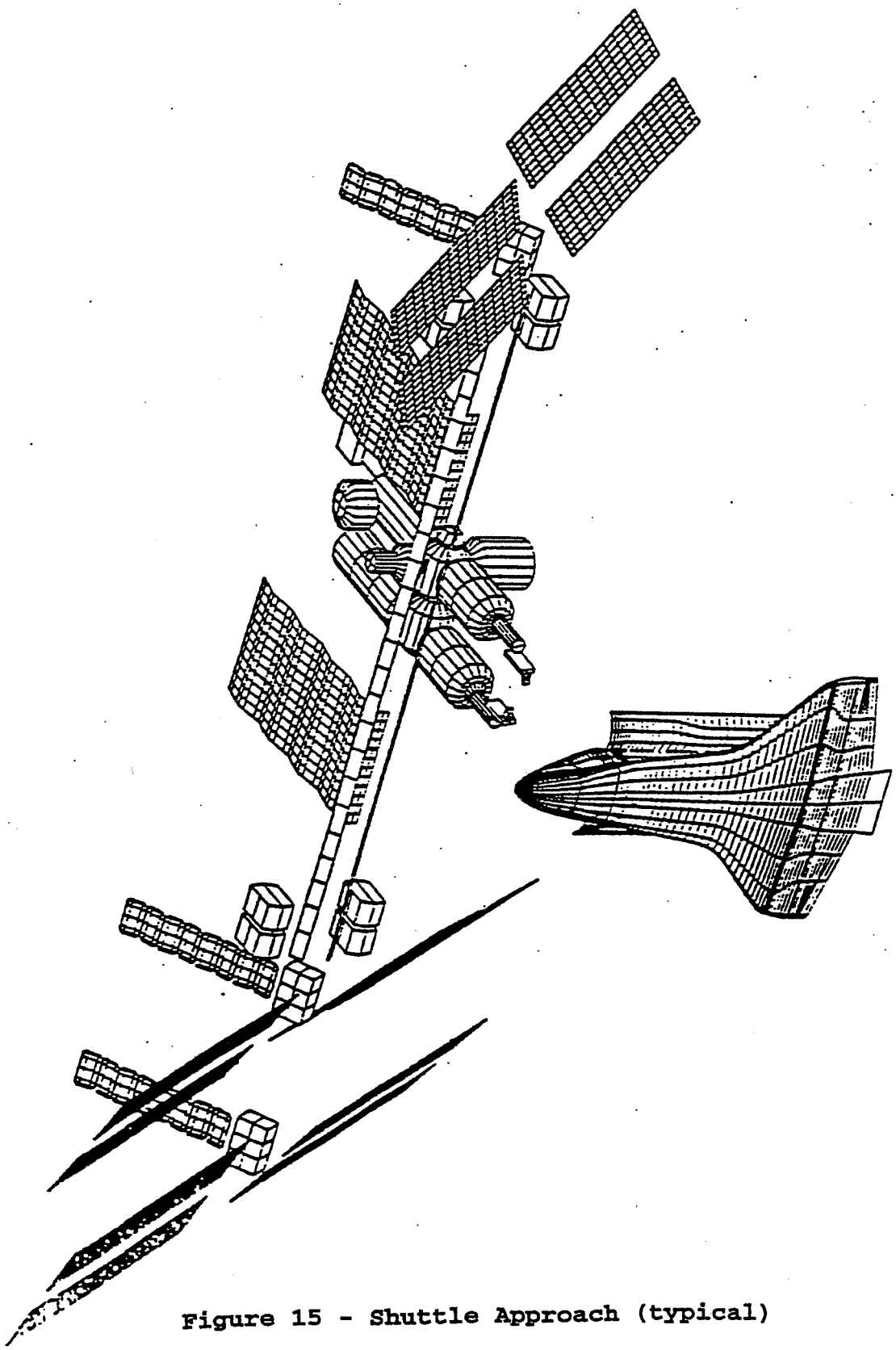

Figure 15 - Shuttle Approach (typical)

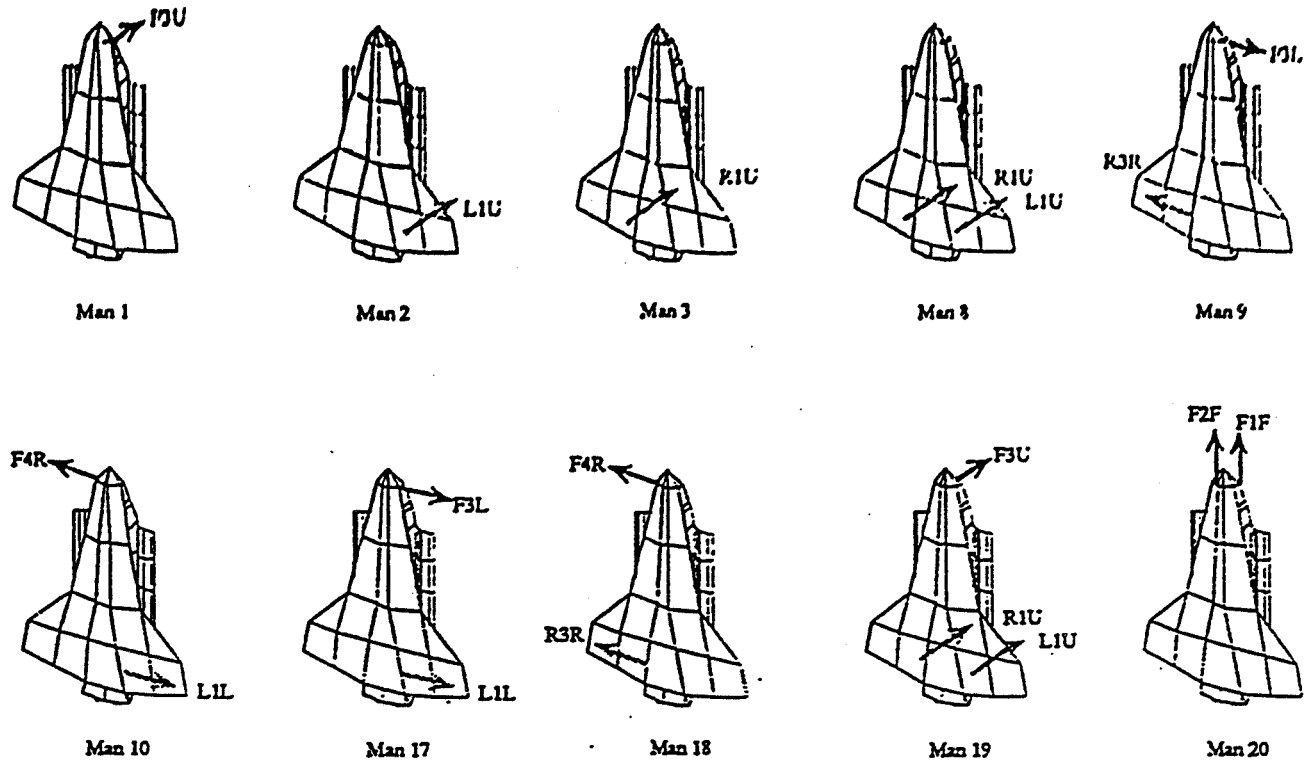

Figure 16 - Shuttle Thruster Firing Directions

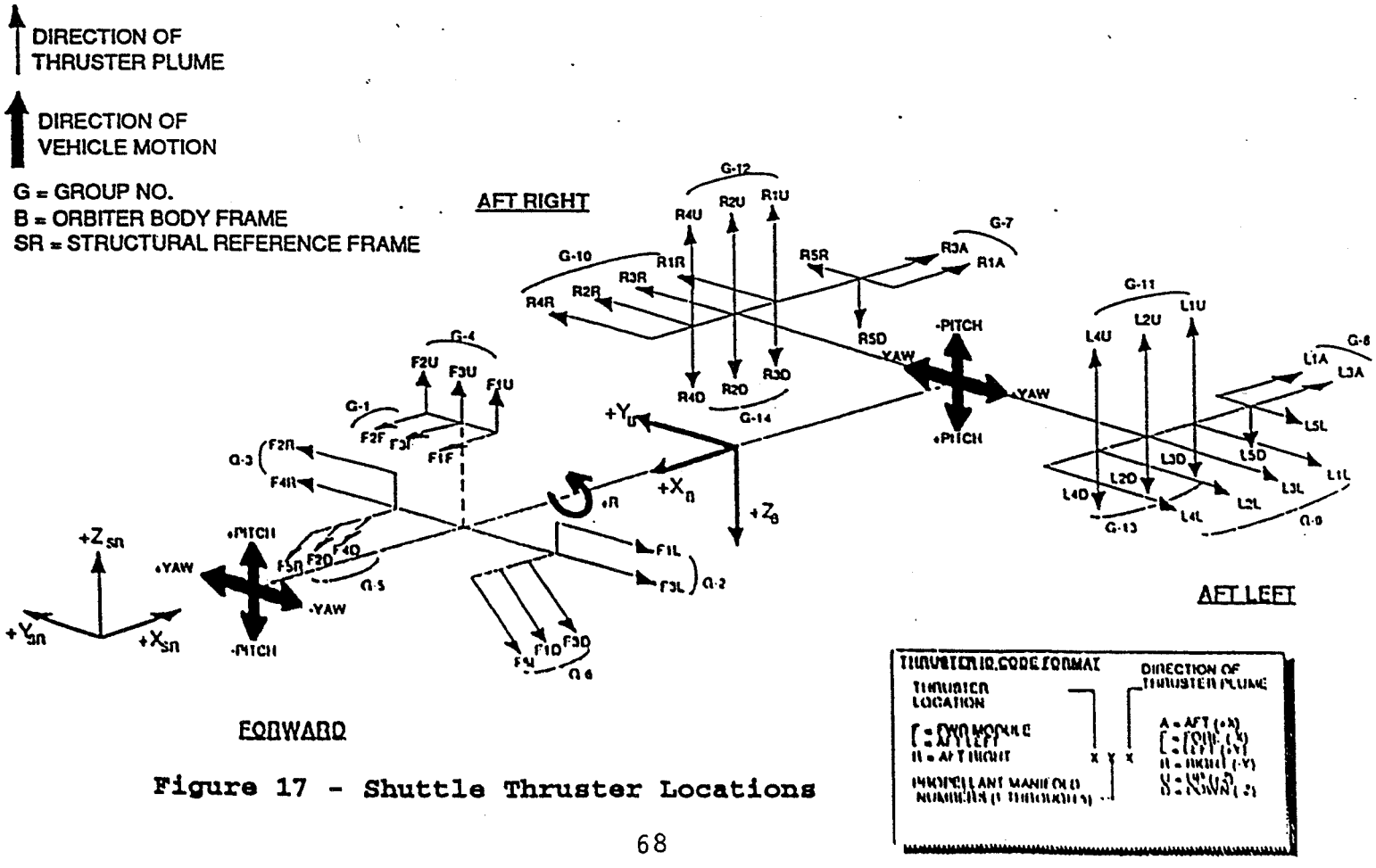

Figure 17 - Shuttle Thruster Locations

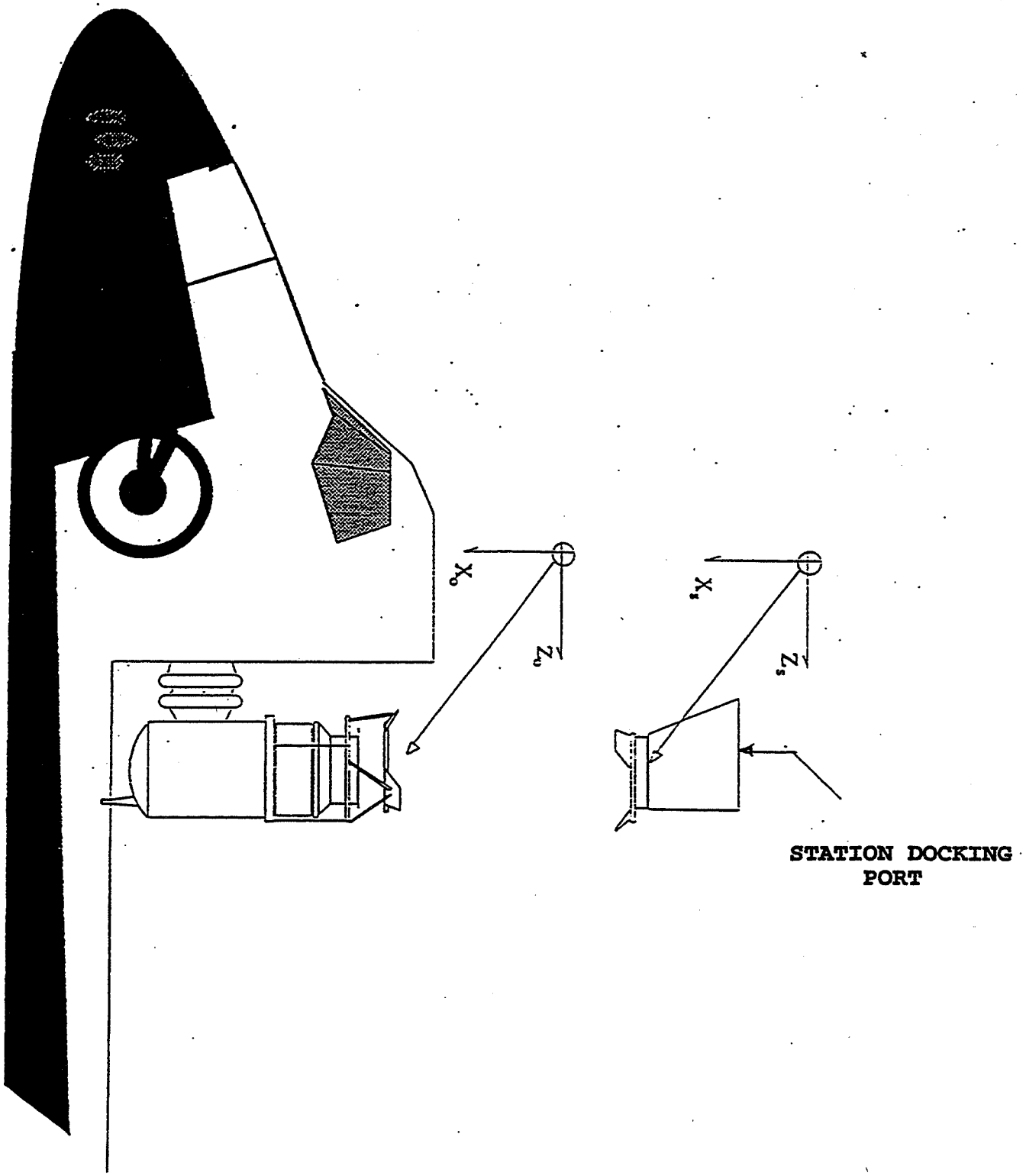

Figure 18 - Shuttle/Station Docking Mechanisms

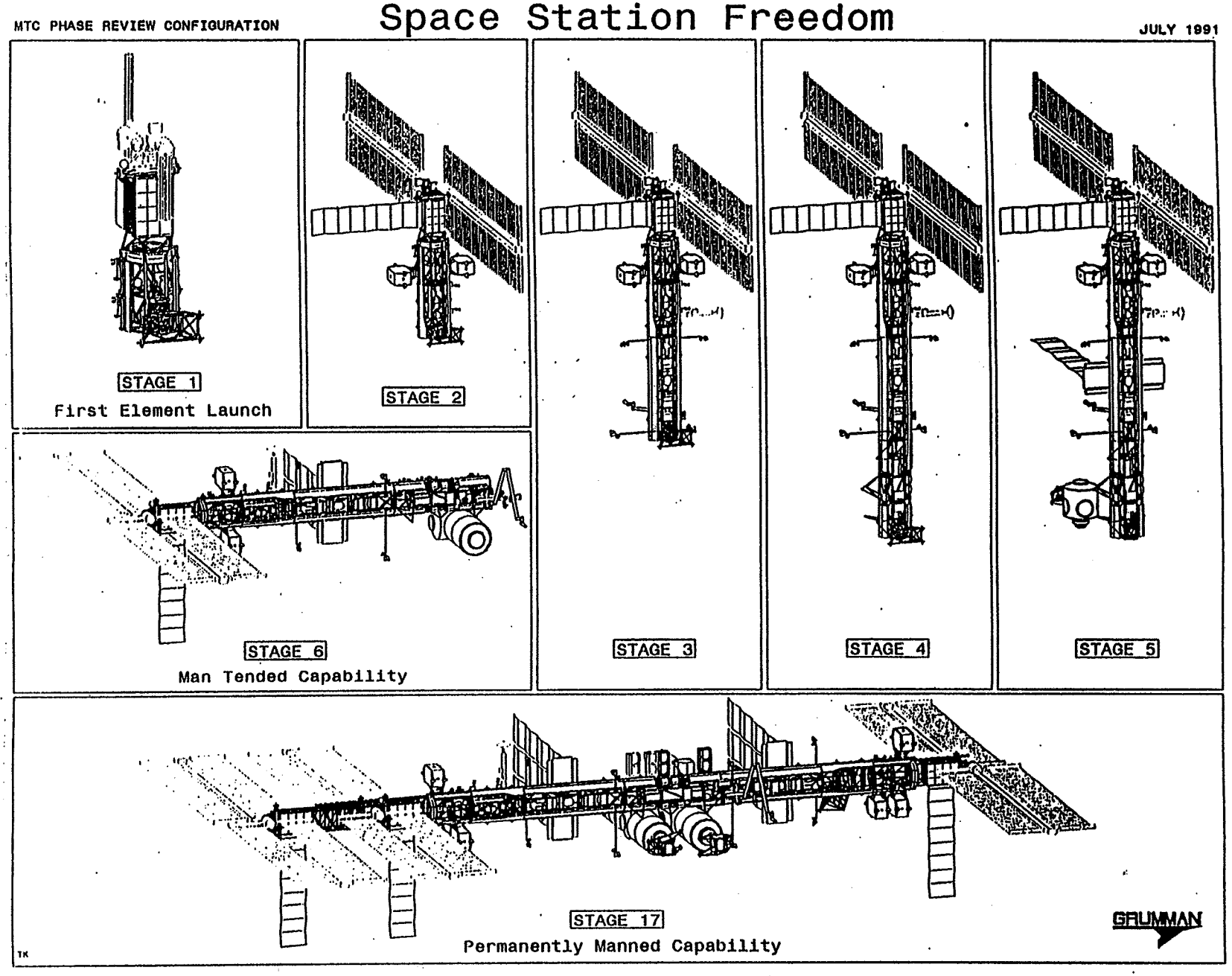

Figure 19 - Space Station Build Sequence

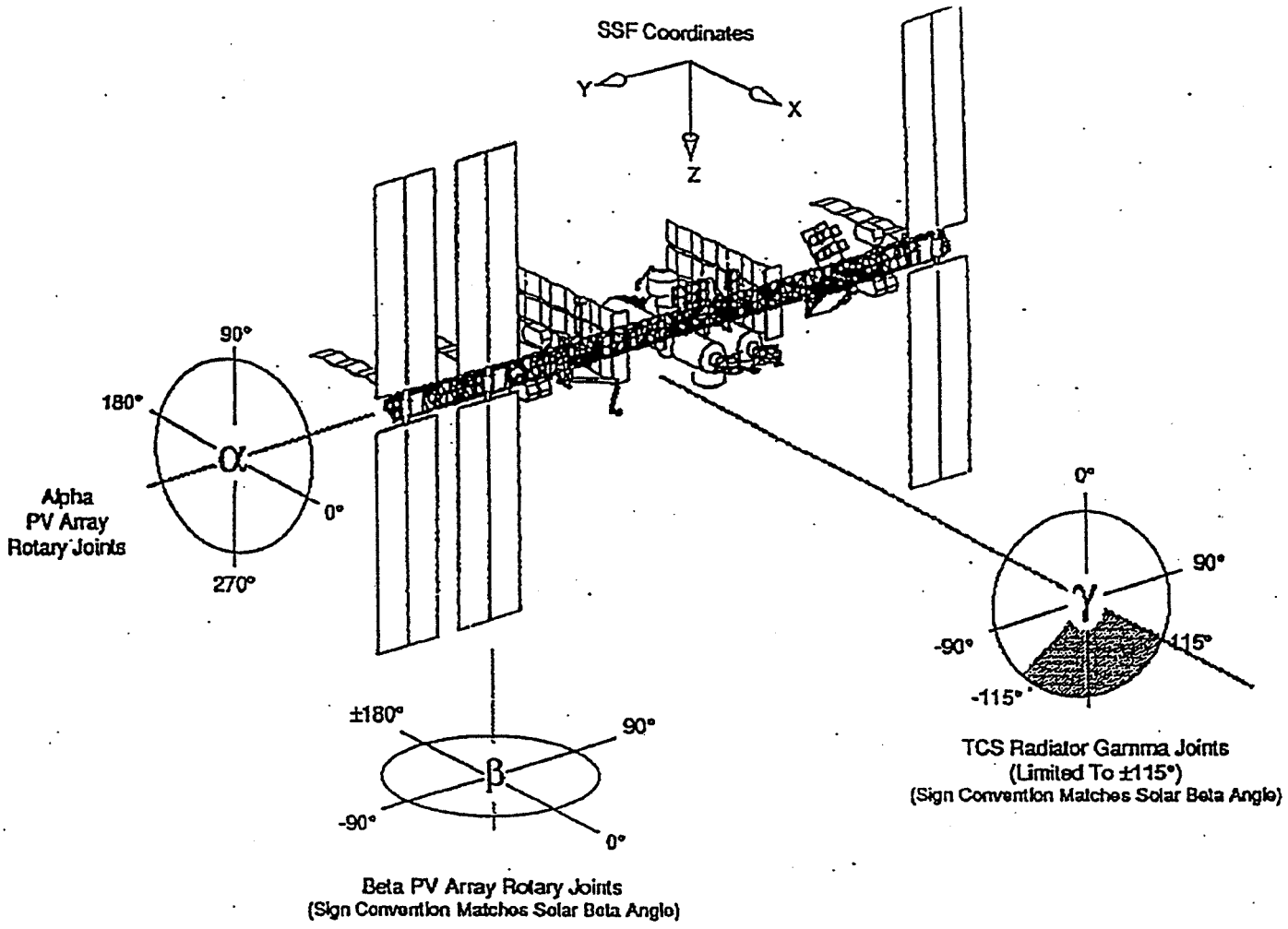

Figure 20 - Space Station Coordinate System

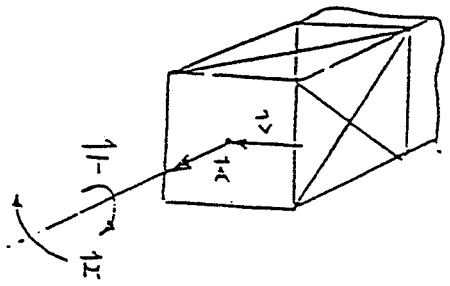

Figure 21 - FASTMast Loading (general)

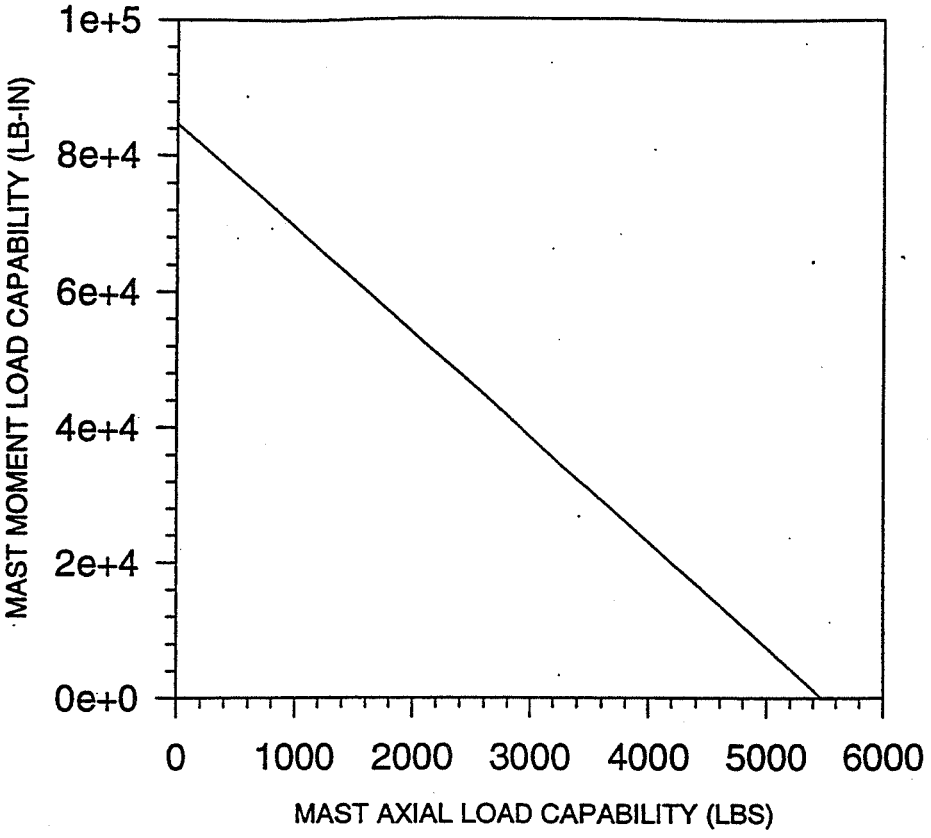

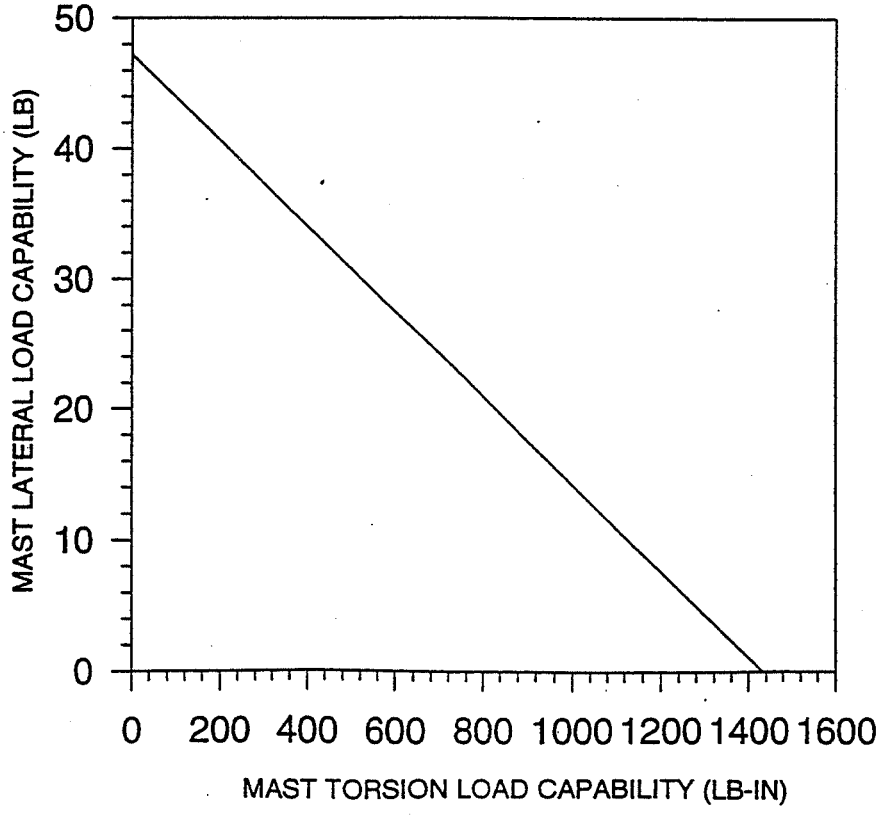

Figure 22 - FASTMast Design Load Curves

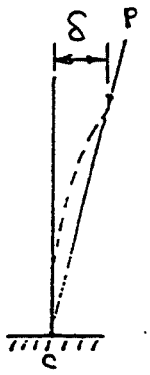

Figure 23 - Follower Force Action

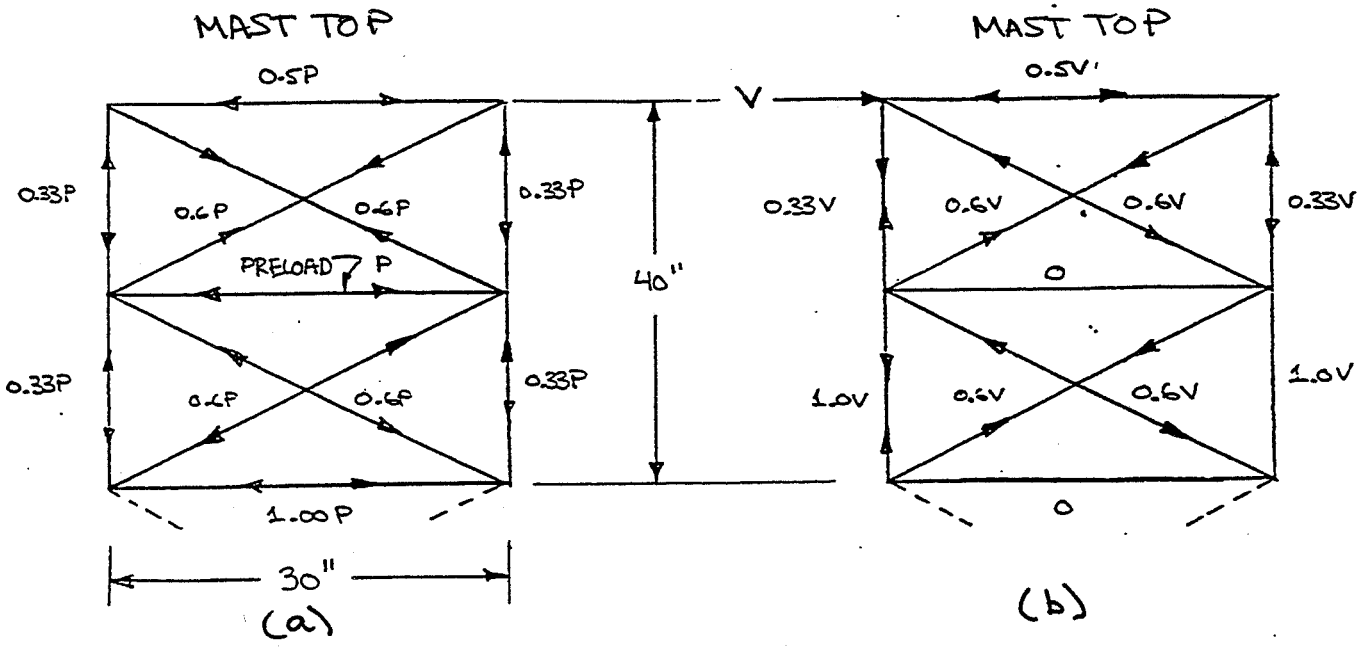

Figure 24 - FASTMast Reaction to Preload and Shear Load

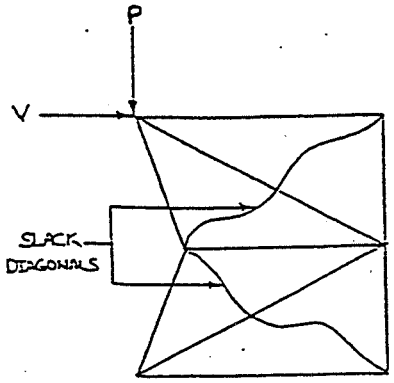

Figure 25 - Loss of Diagonal Tension

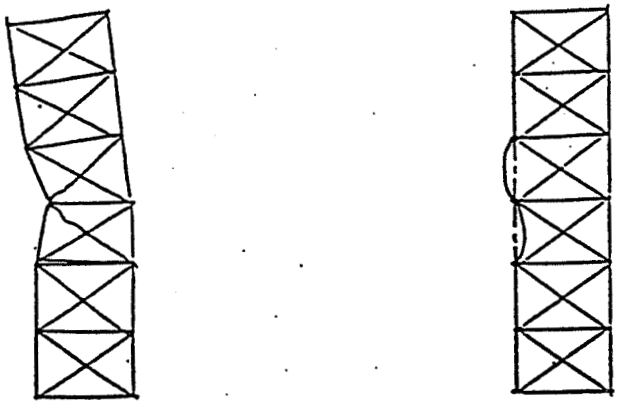

FOLDING FAILURE MODE
(NONLINEAR)

EULER BUCKLING OF LONGERON
(LINEAR)

Figure 26 - FASTMast Failure Modes

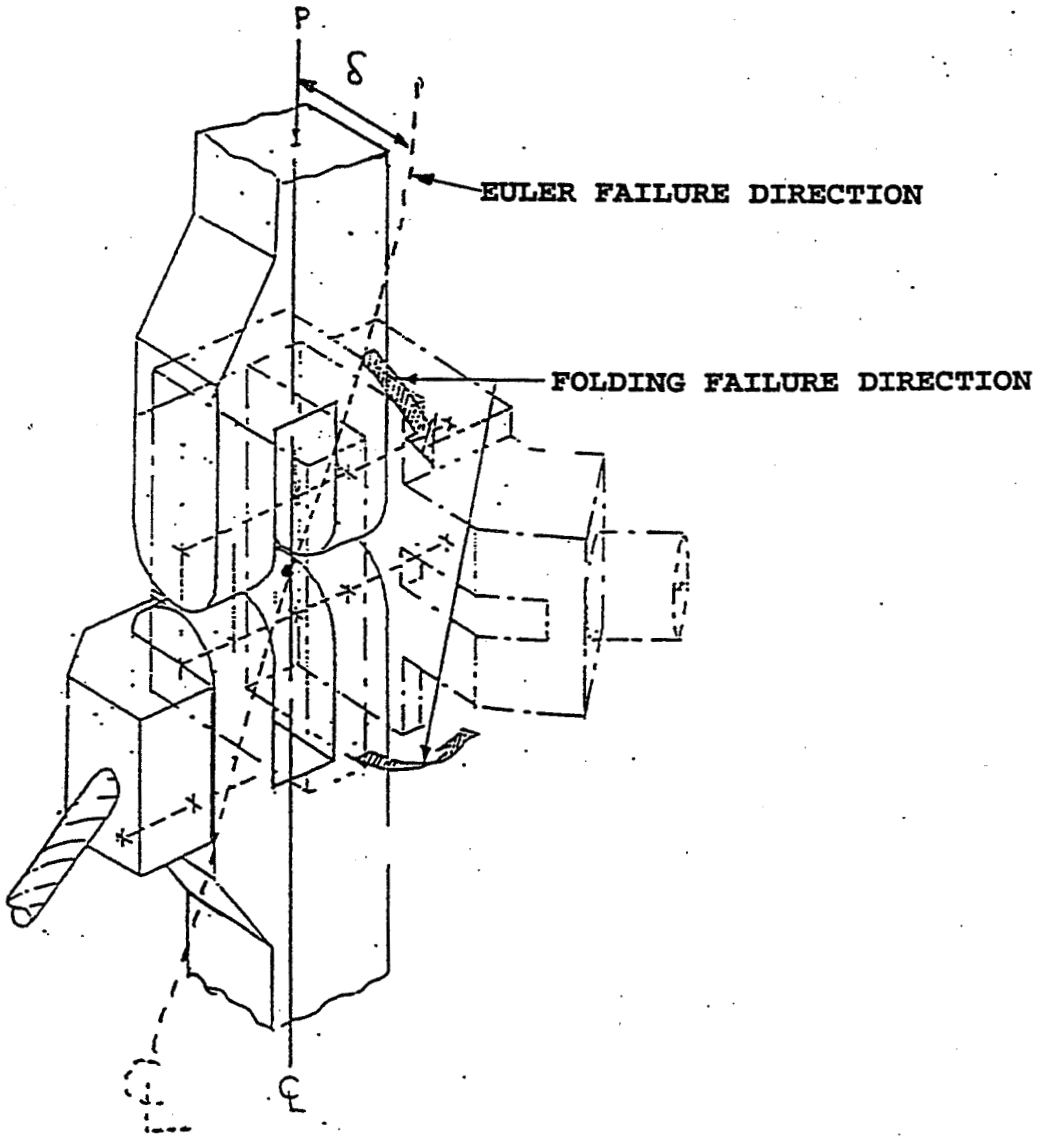

Figure 27 - Elbow Joint at Instability

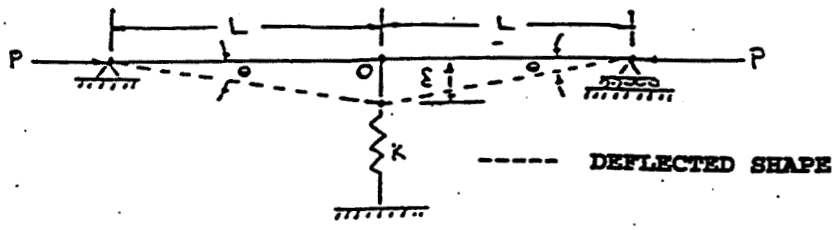

Figure 28 - Longeron/Flex Batten Failure Mode for Global Mode (one-bay)

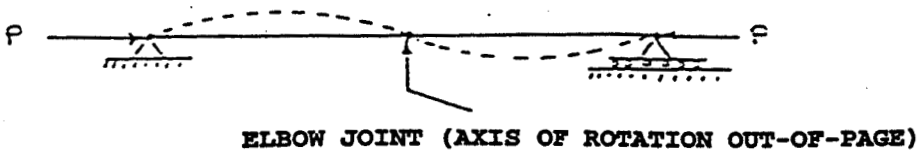

Figure 29 - Longeron/Flex Batten Failure Mode for Local Mode (one-bay)

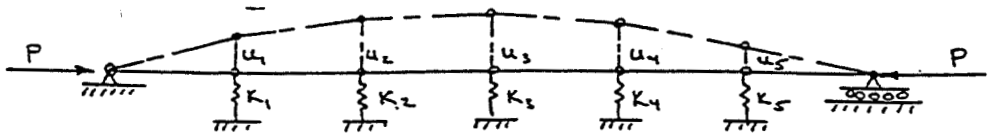

Figure 30 - Longeron/Flex Batten Failure Mode for Global Mode (three-bay)

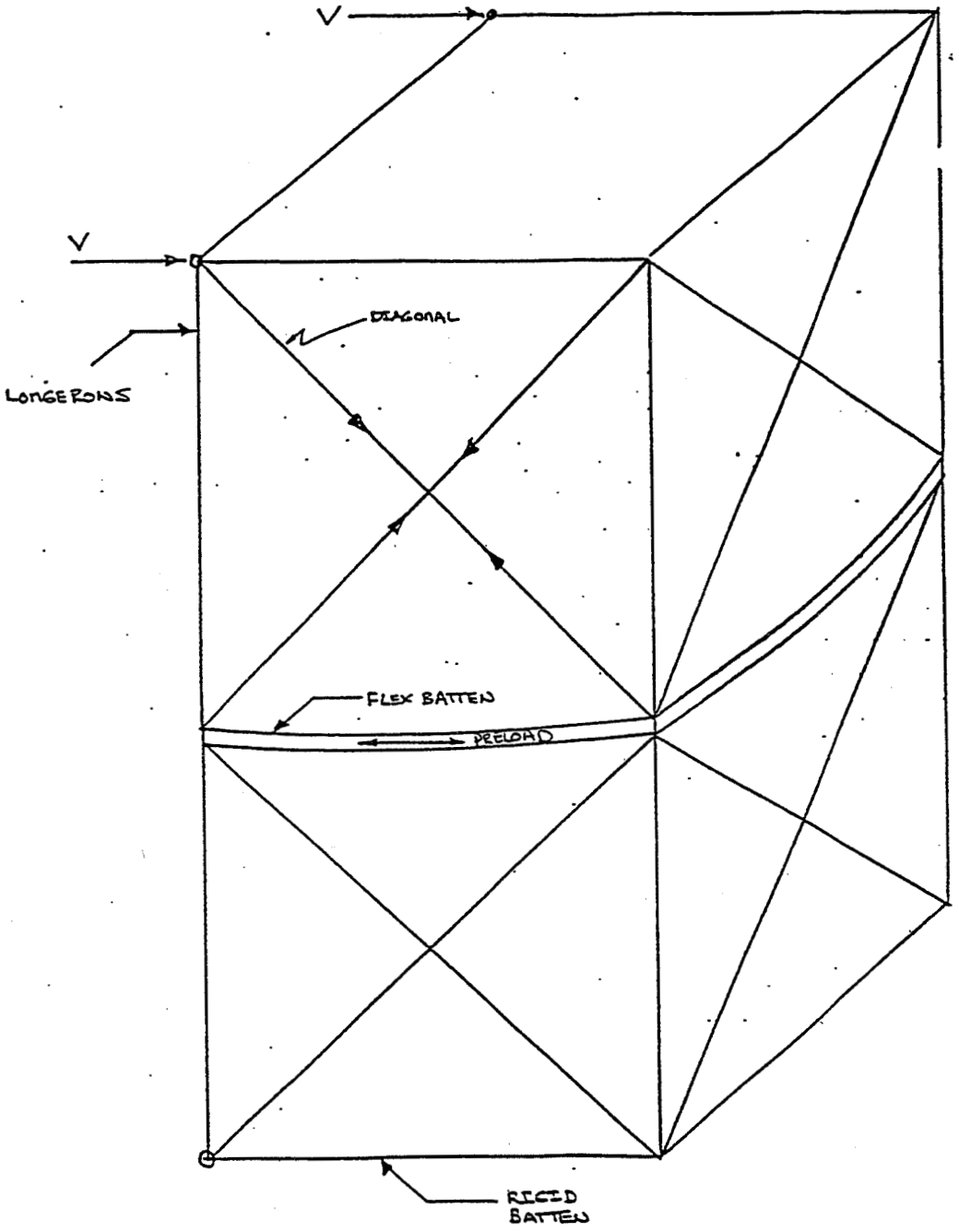

Figure 31 - Lateral Load V Applied at Top of Space Truss

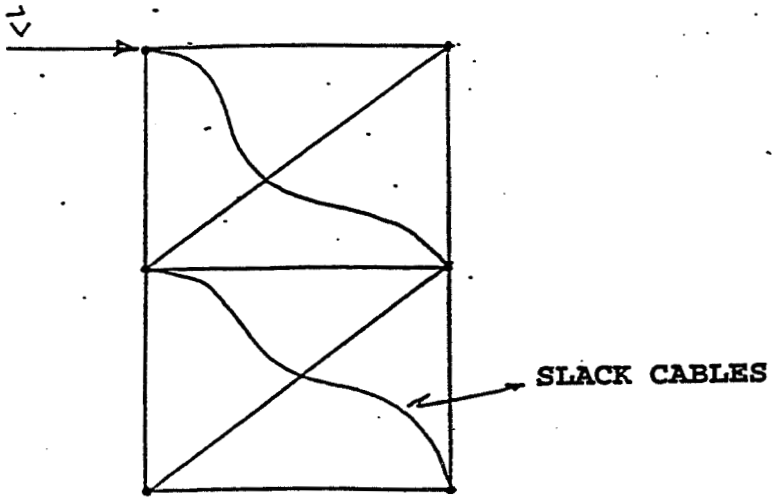

Figure 32 - Diagonal Action Due to Lateral Load V

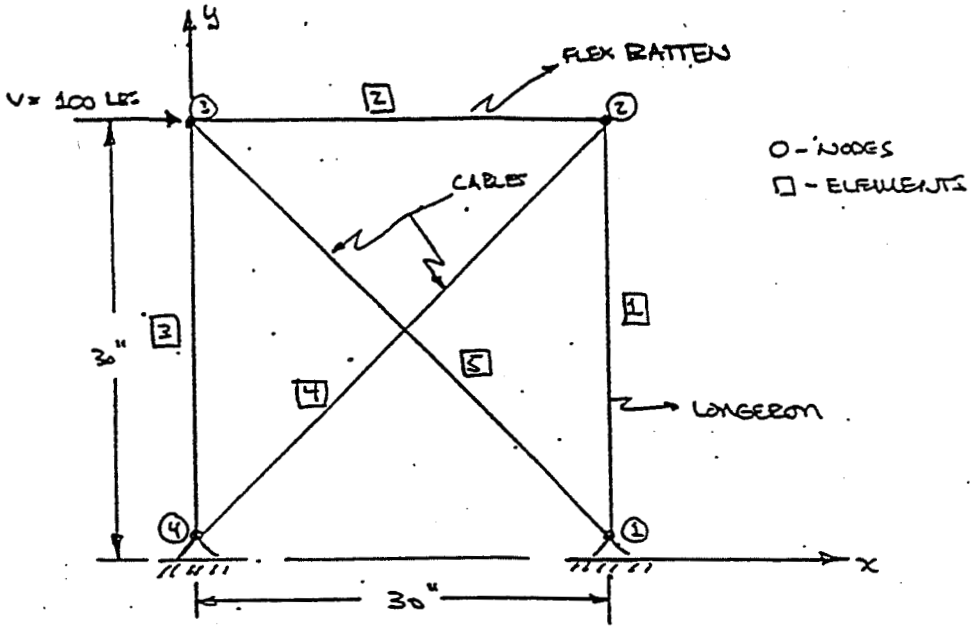

Figure 33 - Planar Truss Model

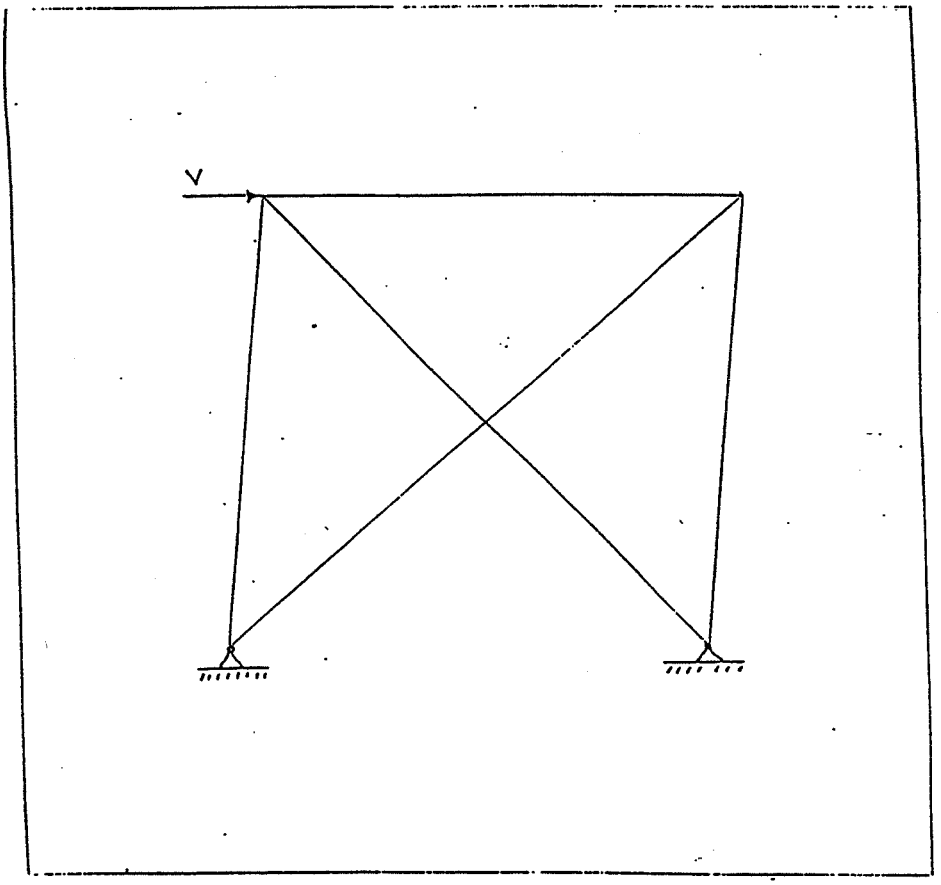

Figure 34 - Deformed Shape of Planar Truss

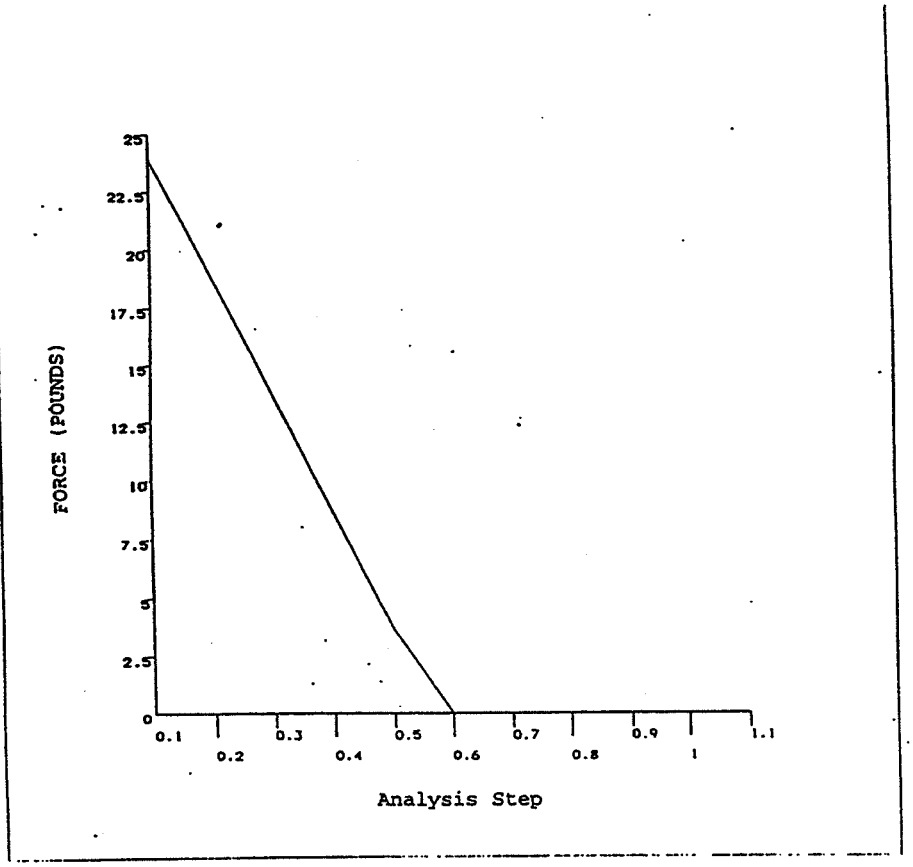

Figure 35 - Element Five Internal Load Versus Load-Step (x-direction)

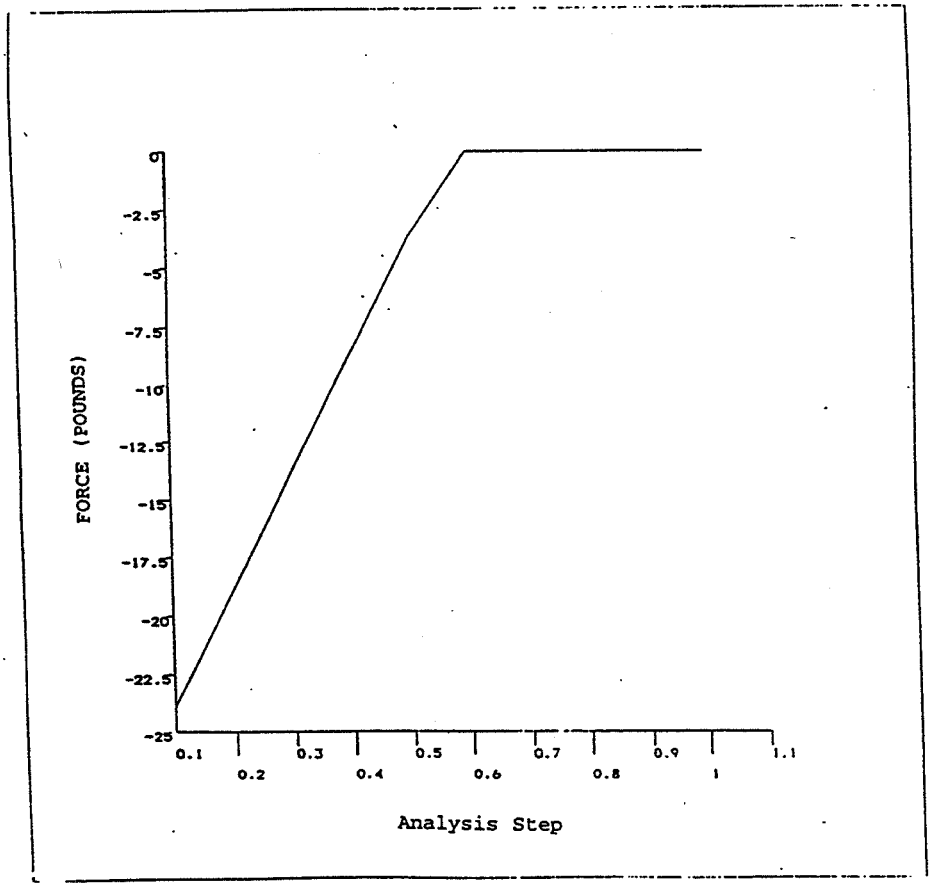

Figure 36 - Element Five Internal Load Versus Load-Step (y-direction)

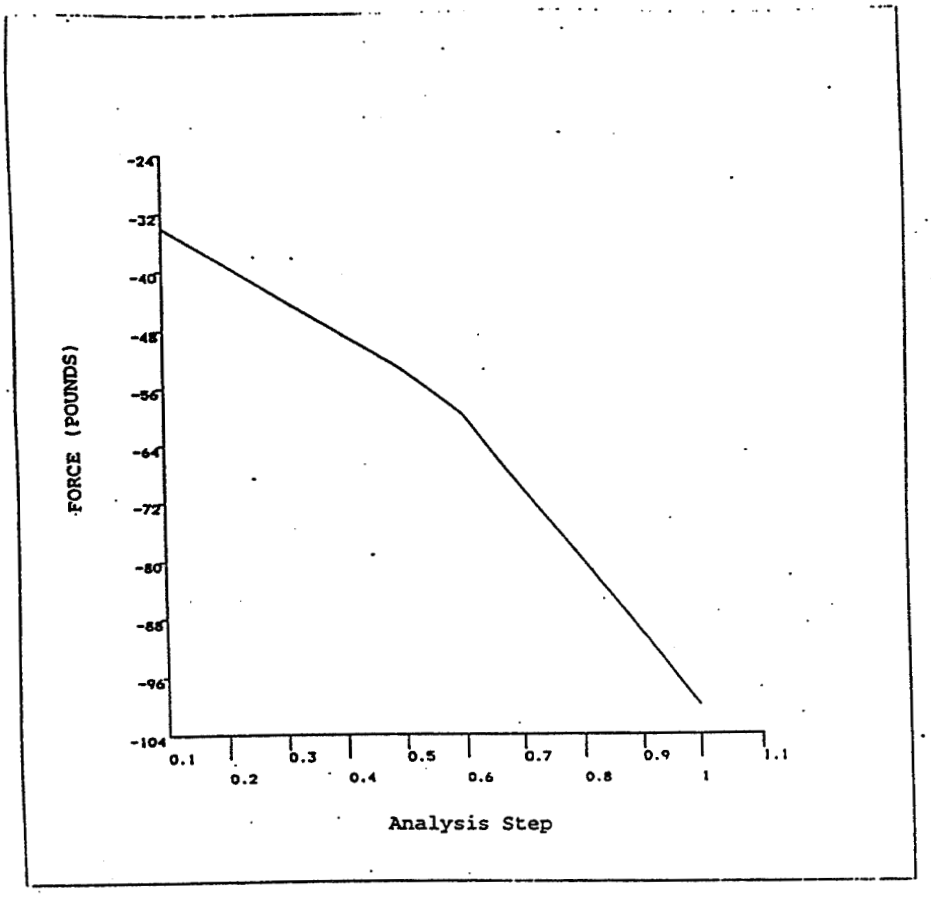

Figure 37 - Element Four Internal Load Versus Load-Step (x-direction)

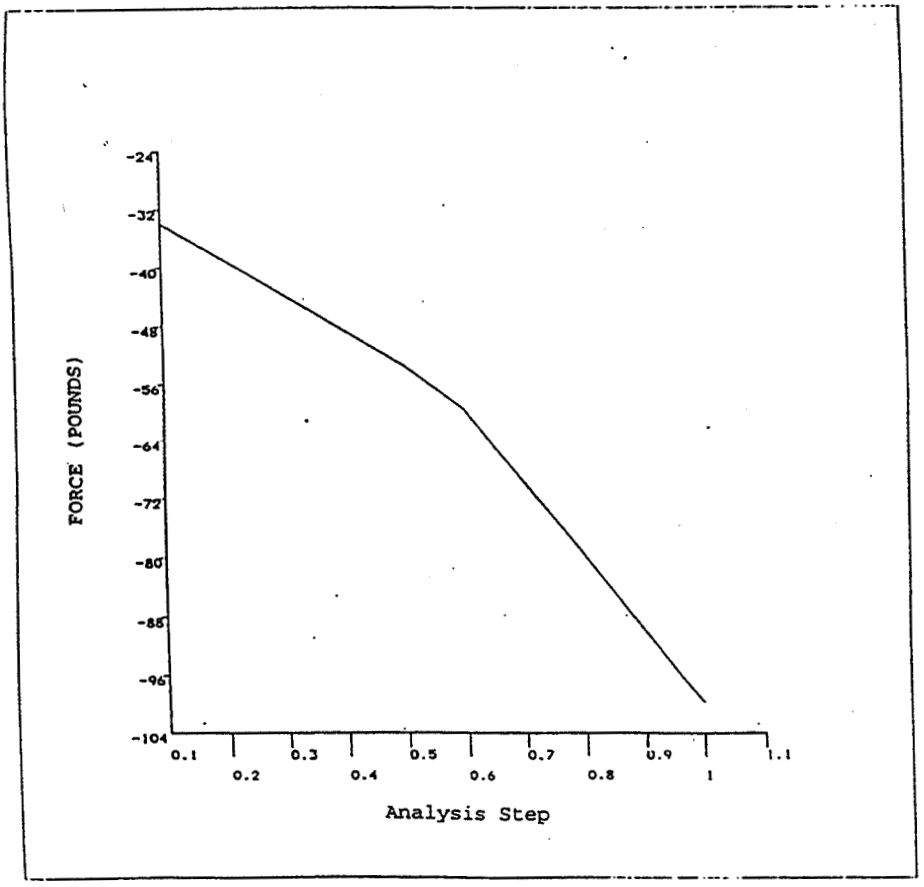

Figure 38 - Element Four Internal Load Versus Load-Step (y-direction)

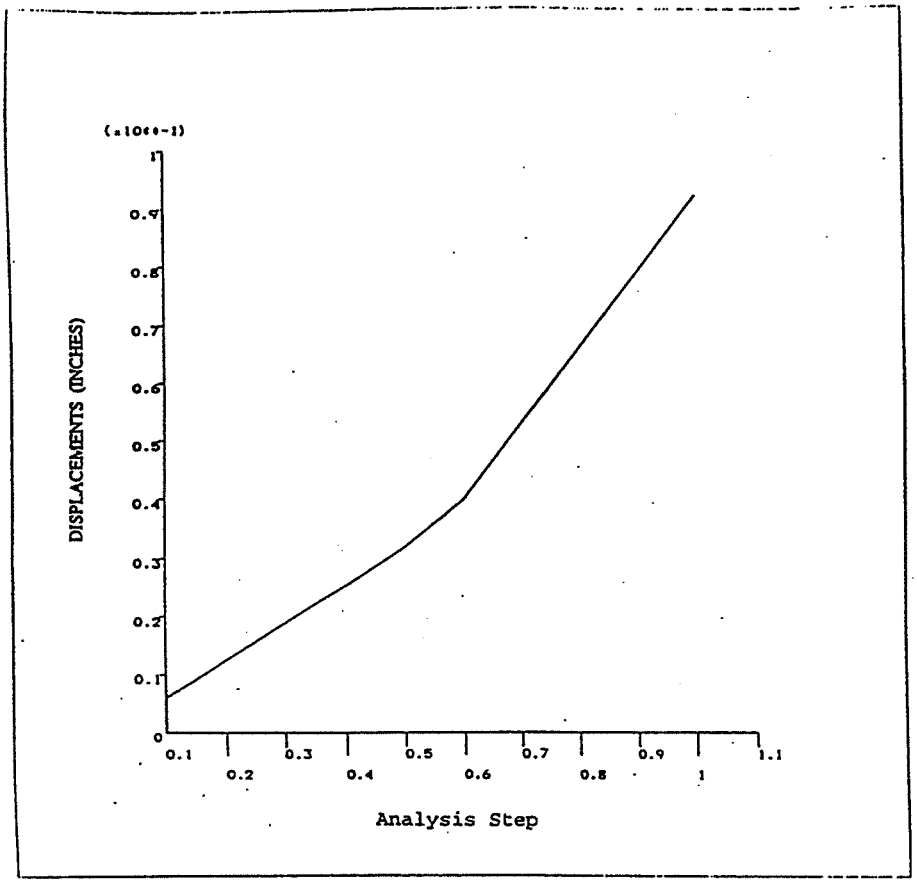

Figure 39 - Node Three x-Displacement

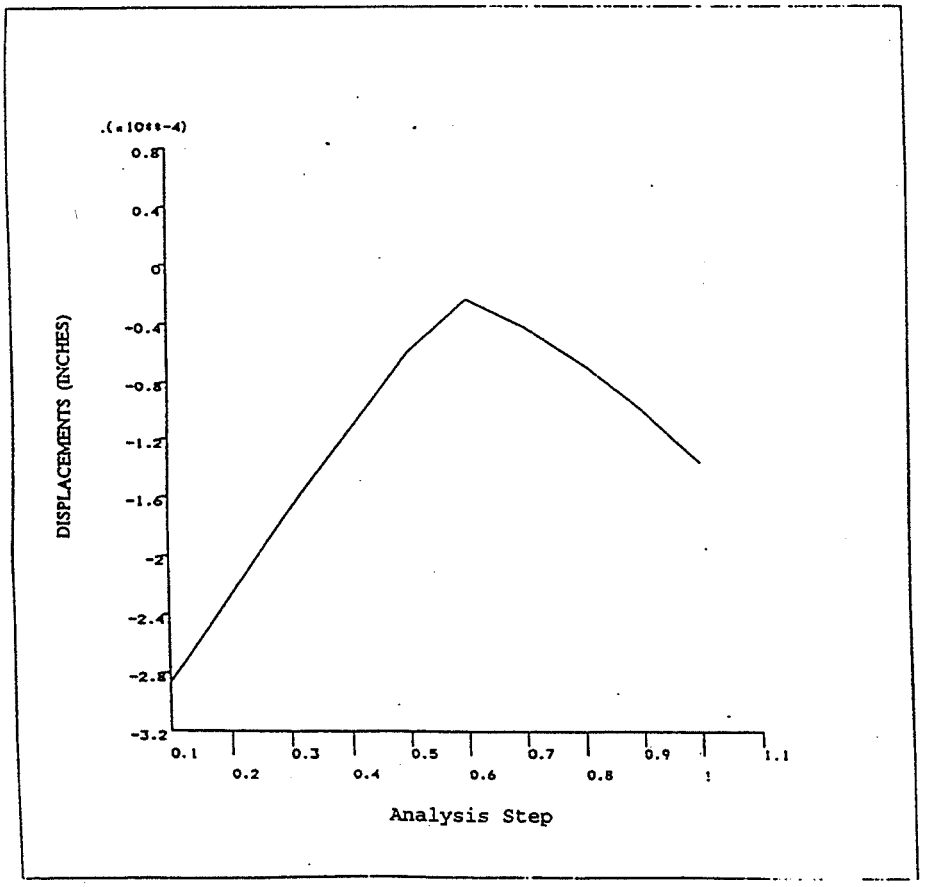

Figure 40 - Node Three y-Displacement

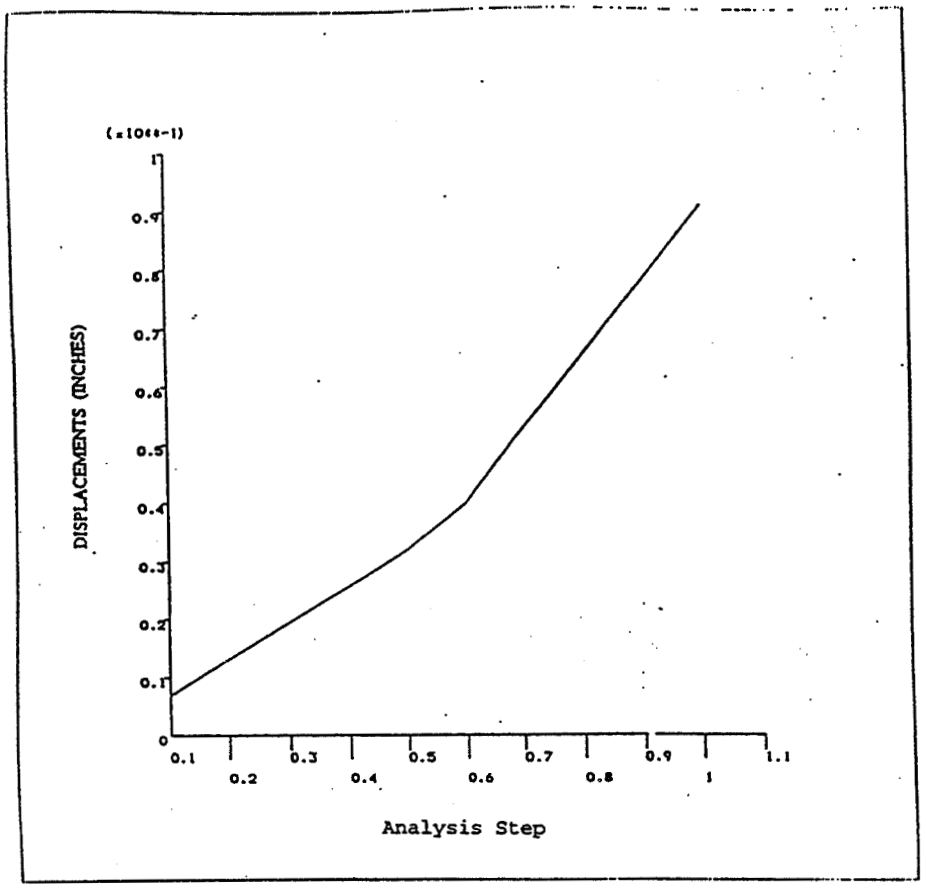

Figure 41 - Node Two x-Displacement

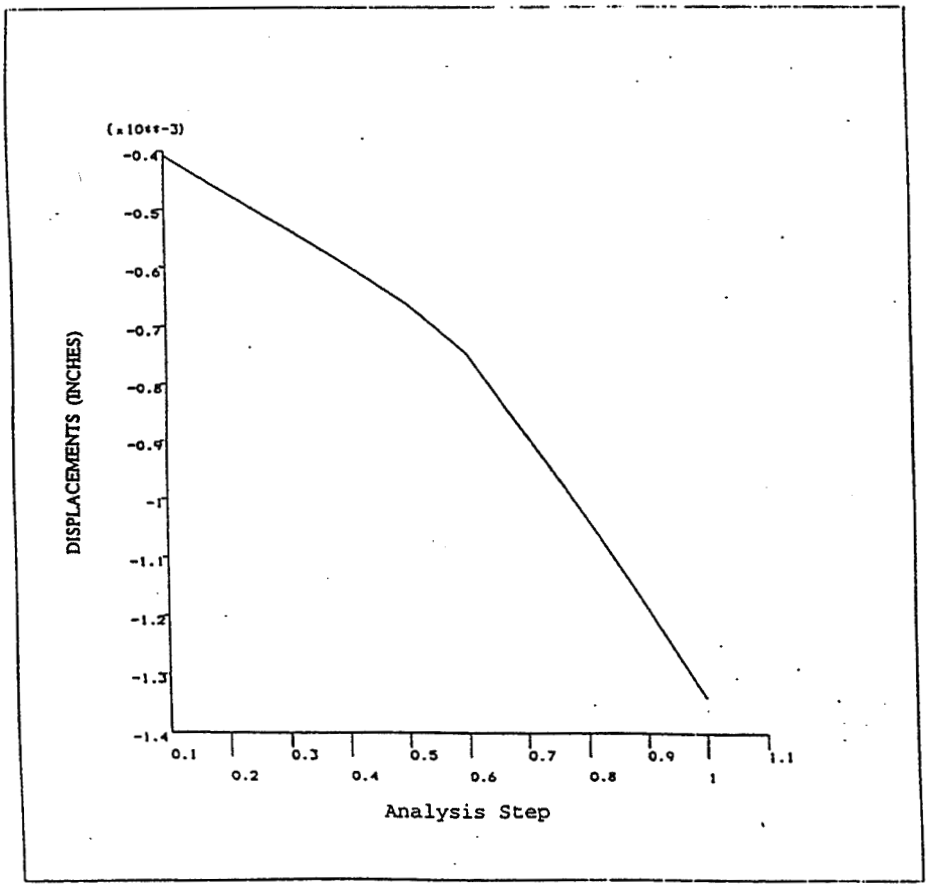

Figure 42 - Node Two y-Displacement

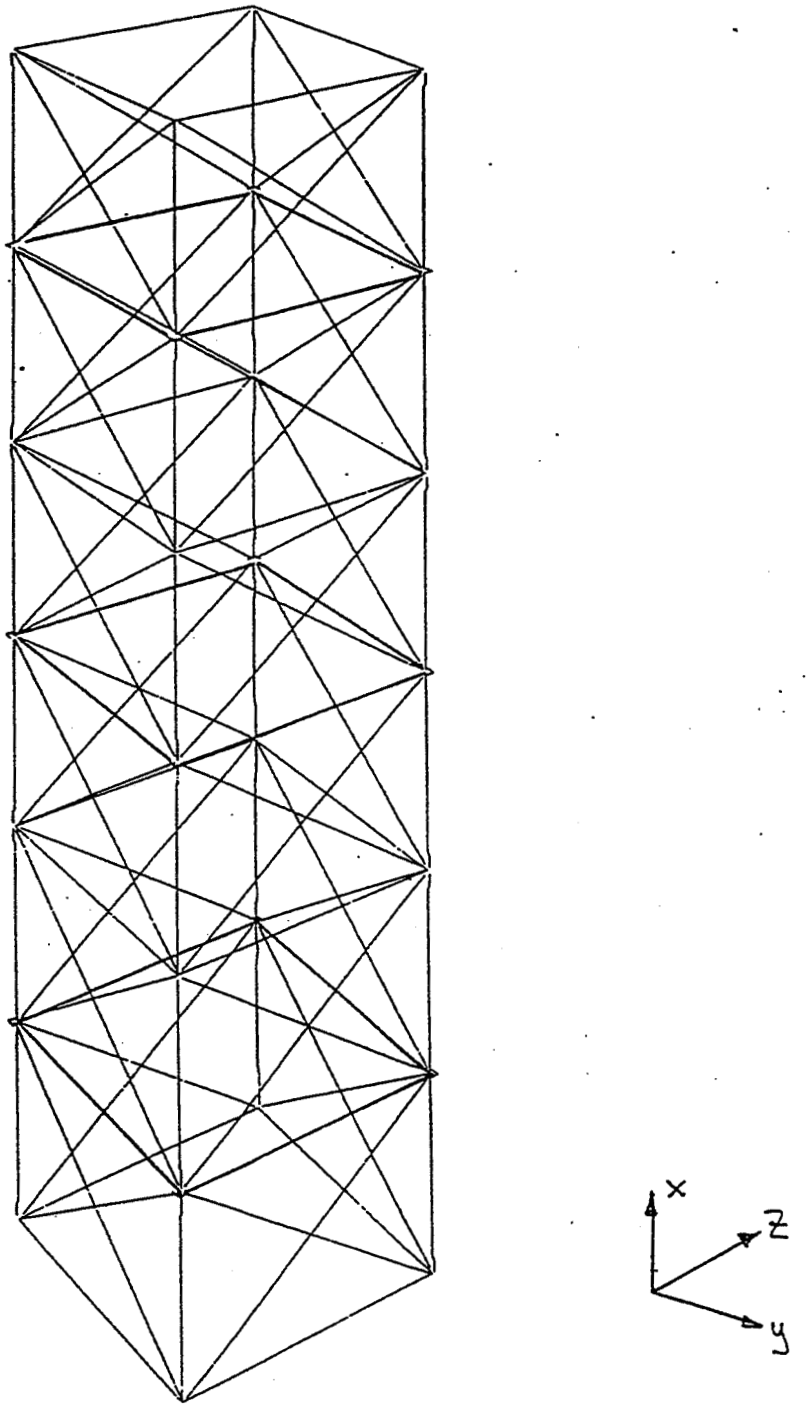

Figure 43 - NASTRAN Finite Element Model

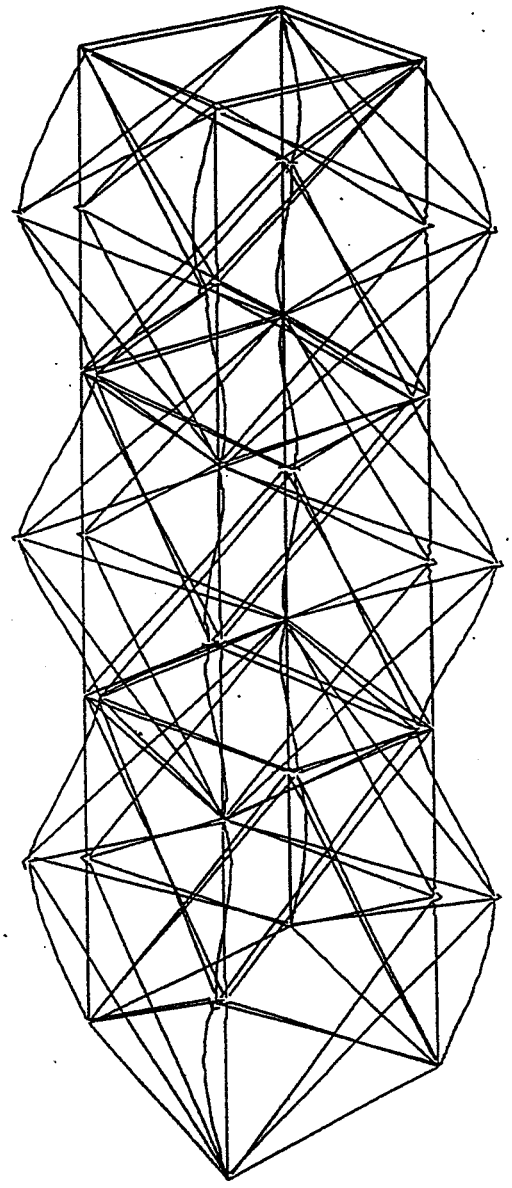

Figure 44 - NASTRAN Finite Element Model with Preload

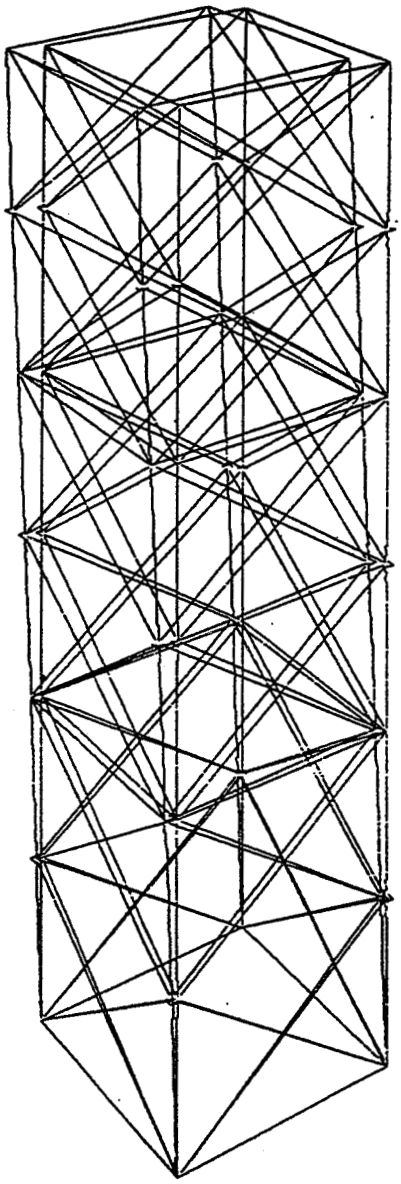

Figure 45 - Deflected Shape of NASTRAN Model Due to 100 lb Lateral Load at Mast Top

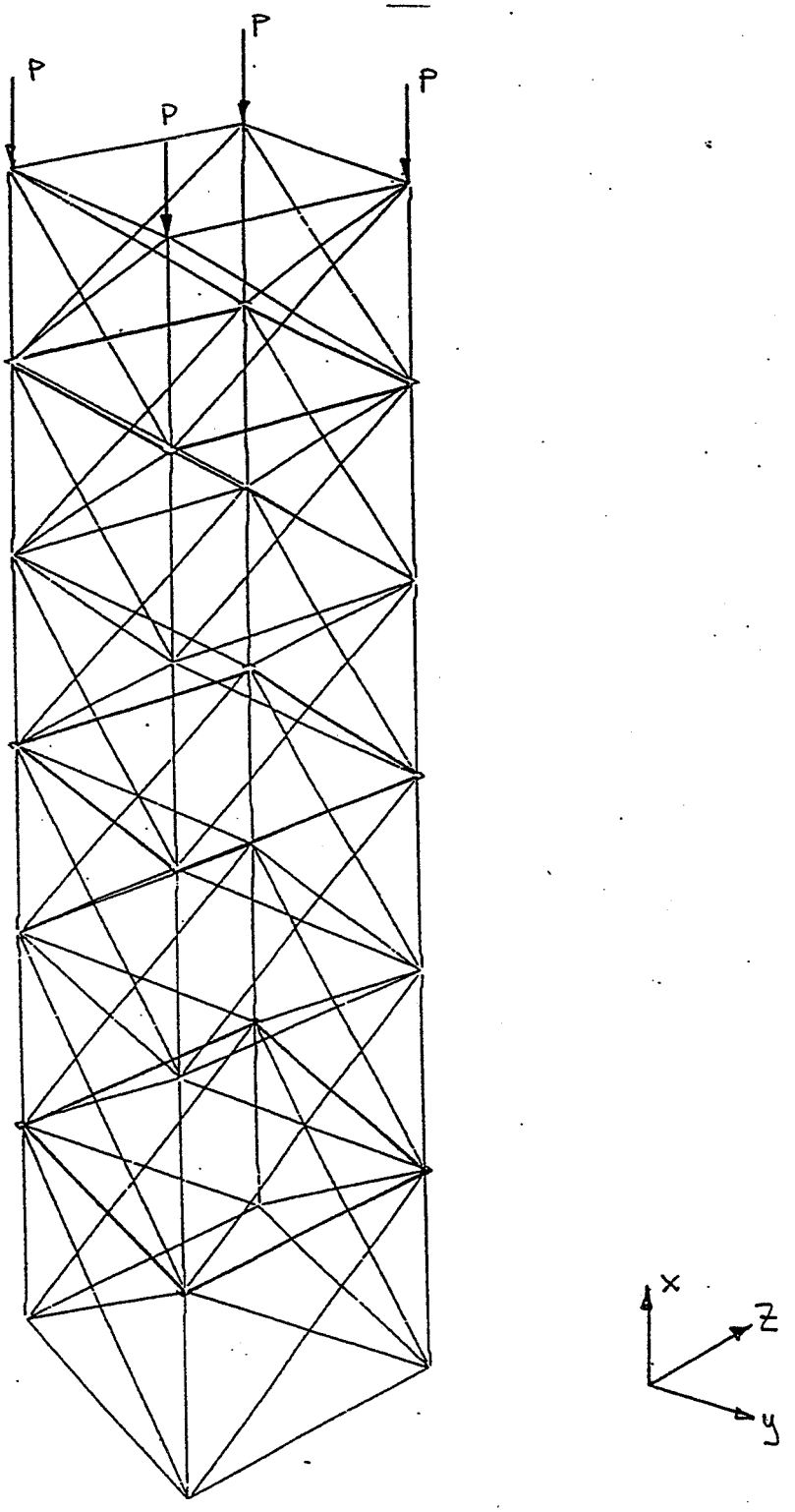

Figure 46 - Axial Load for Linear Buckling Analysis

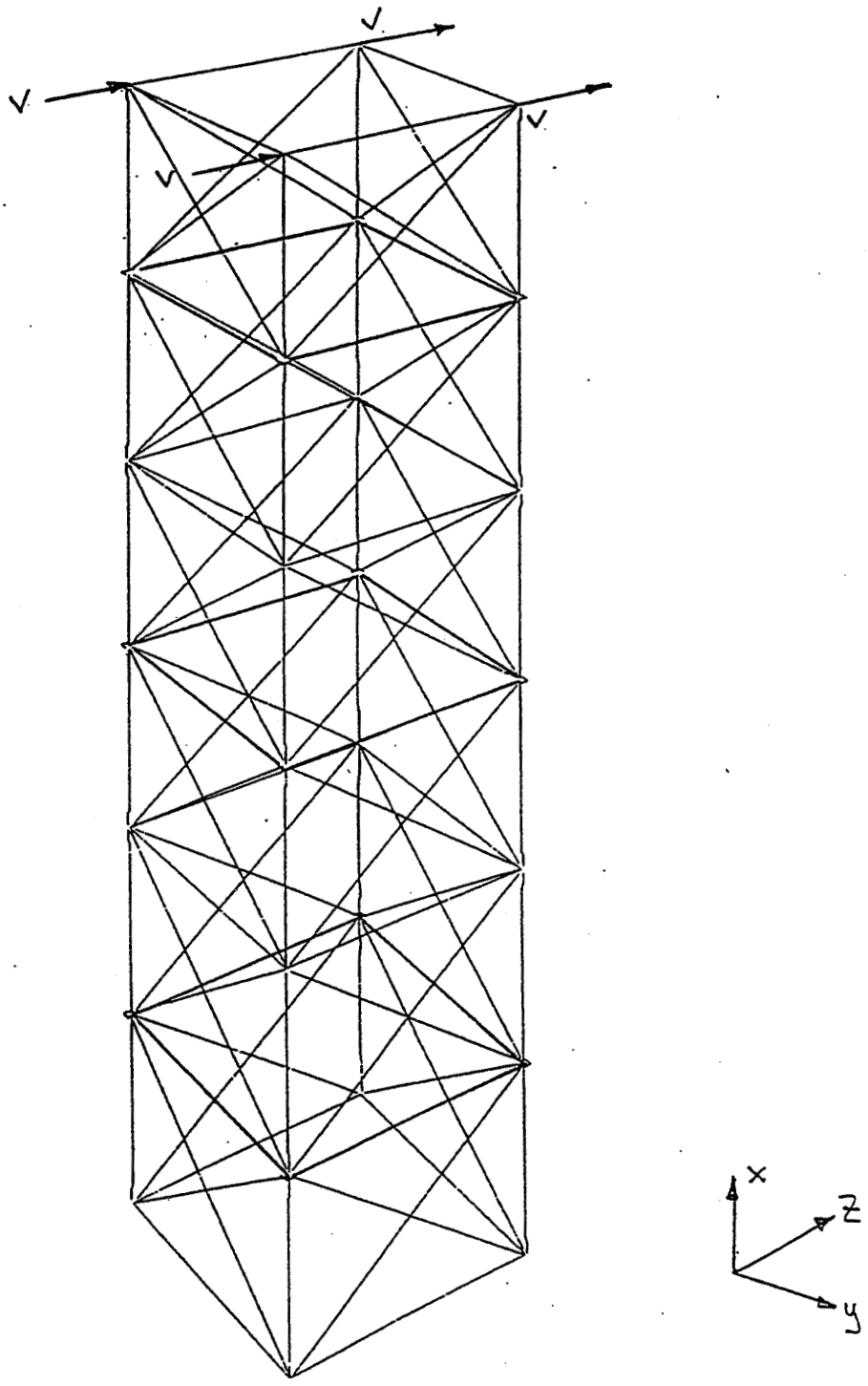

Figure 47 - Lateral Load for Linear Buckling Analysis

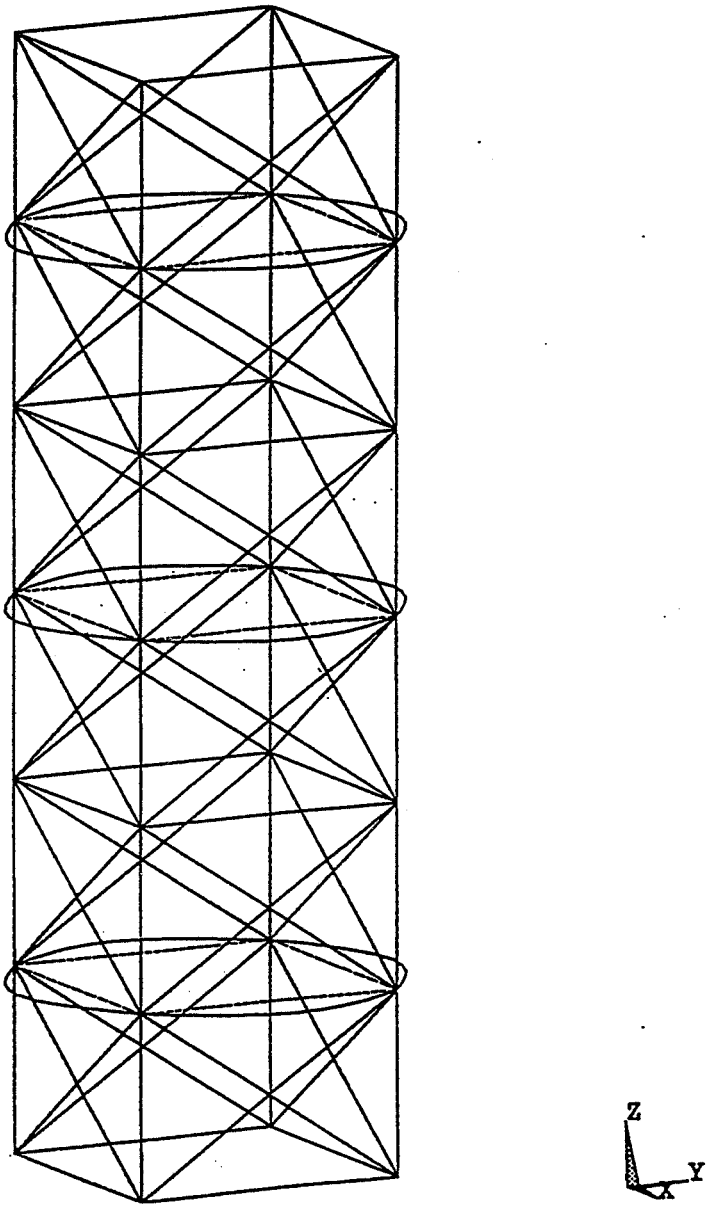

Figure 48 - ANSYS Finite Element Model with Preload

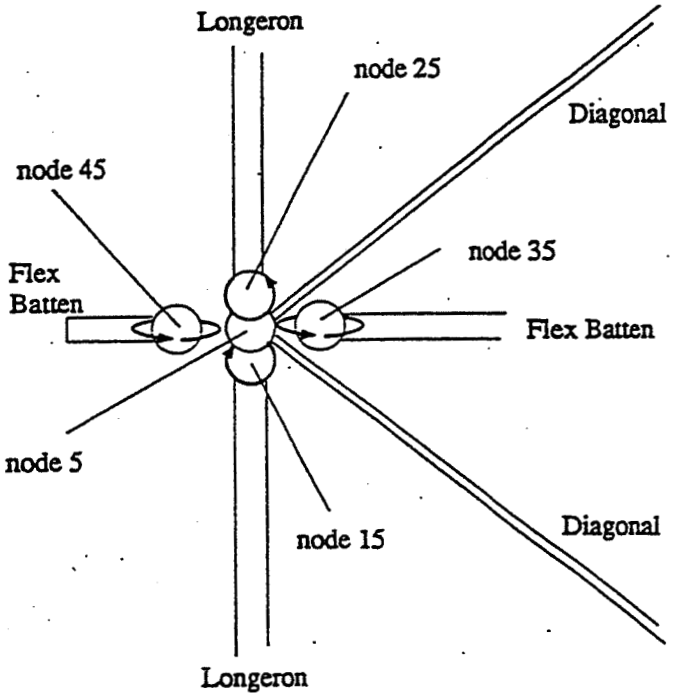

Figure 49 - ANSYS Model Hinge Joint

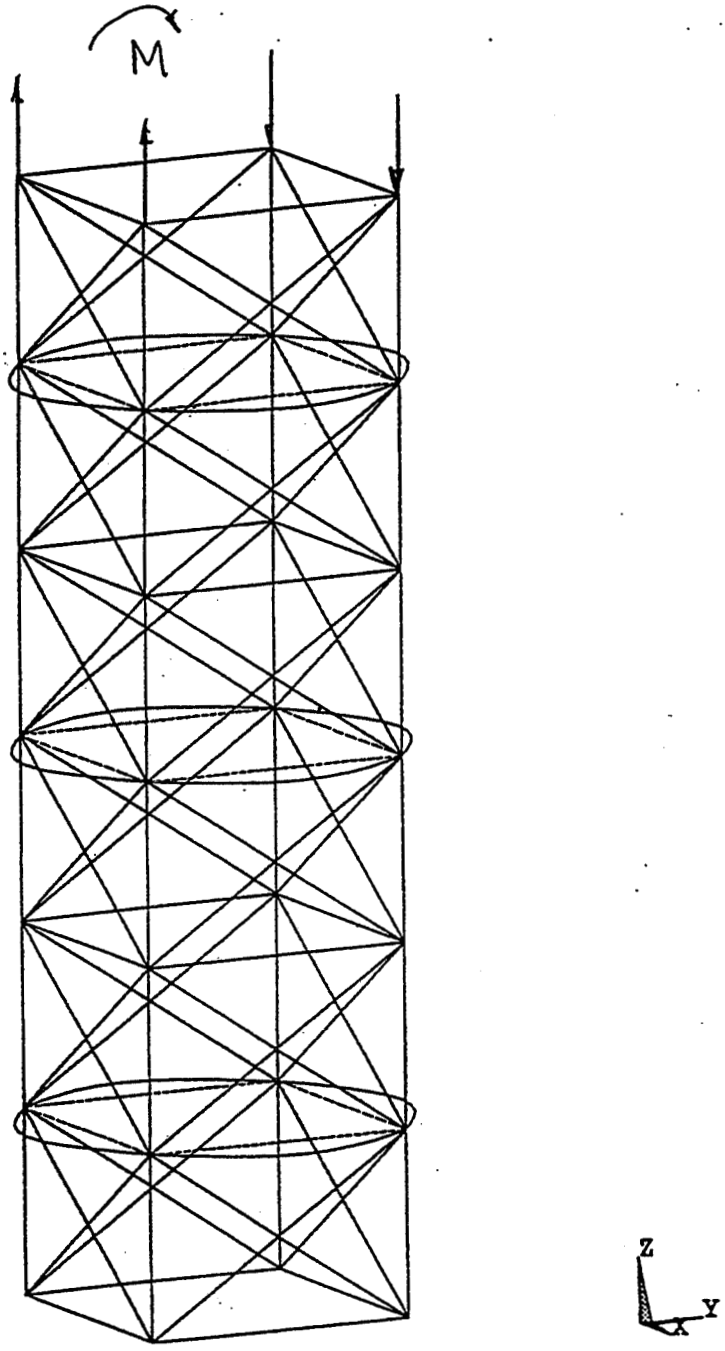

Figure 50 - Moment Load for Large Displacement Analysis

C-2

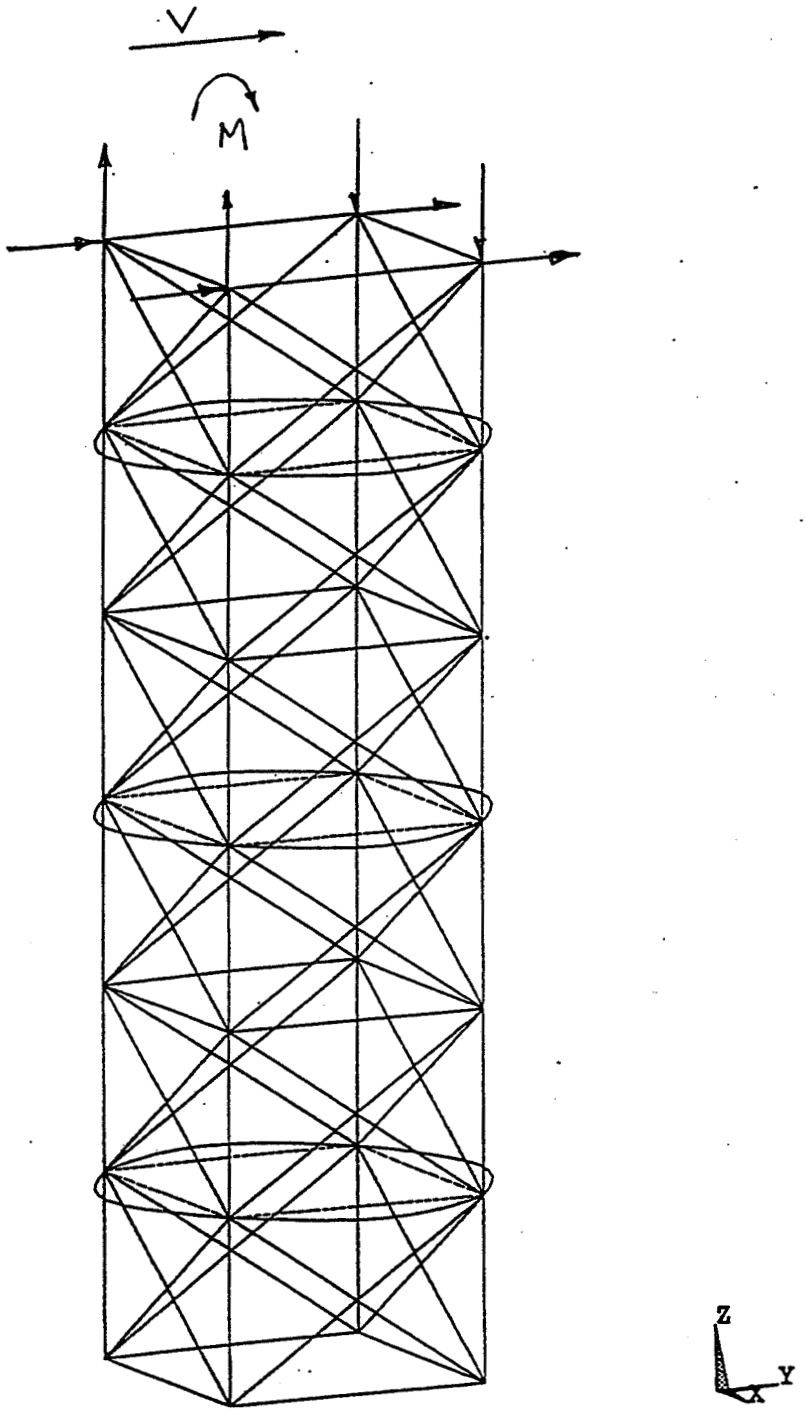

Figure 51 - Combined Loading for Large Displacement Analysis

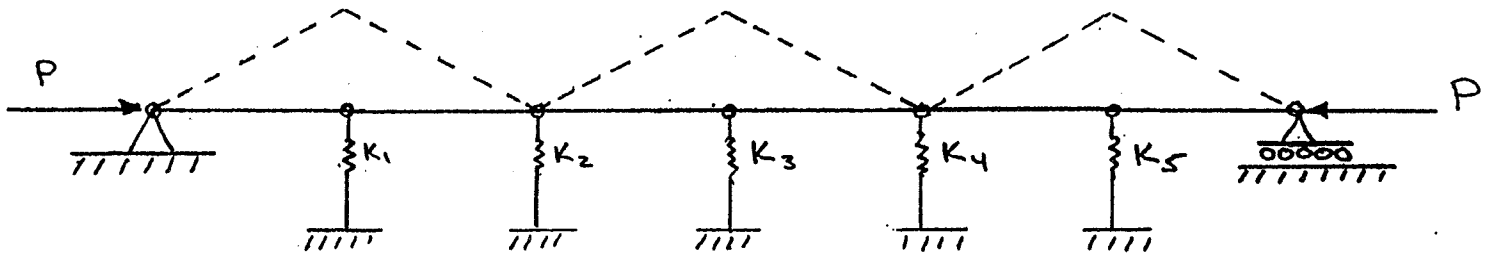

Figure 52 - Failure Mode for One-Dimensional Global Failure mode for a Three-Bay Longeron System

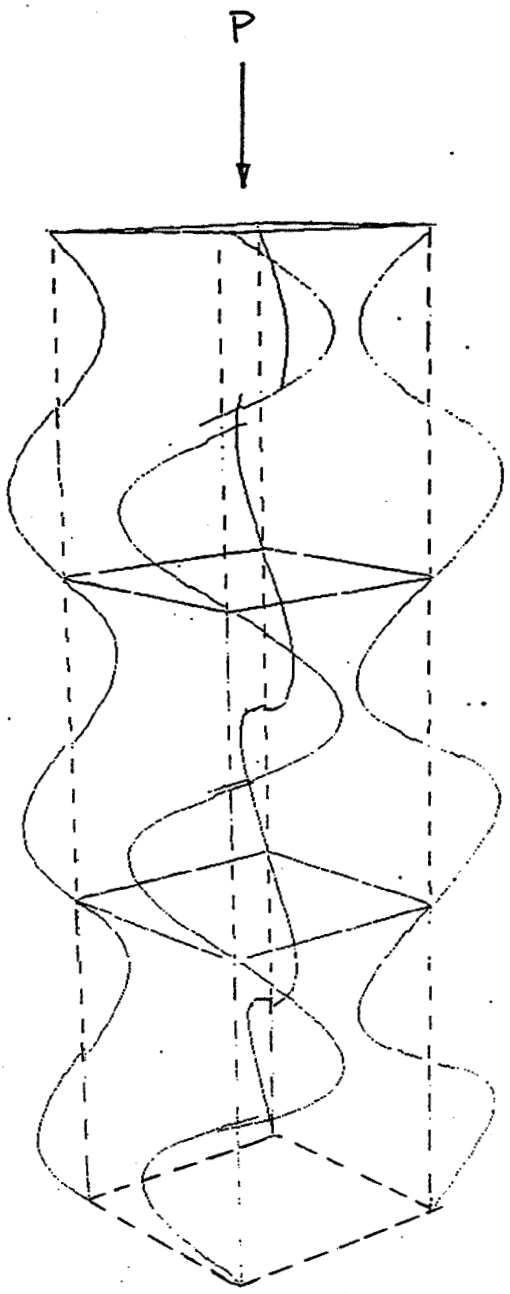

Figure 53 - Failure Mode for Linear Buckling Due to Axial Column Load

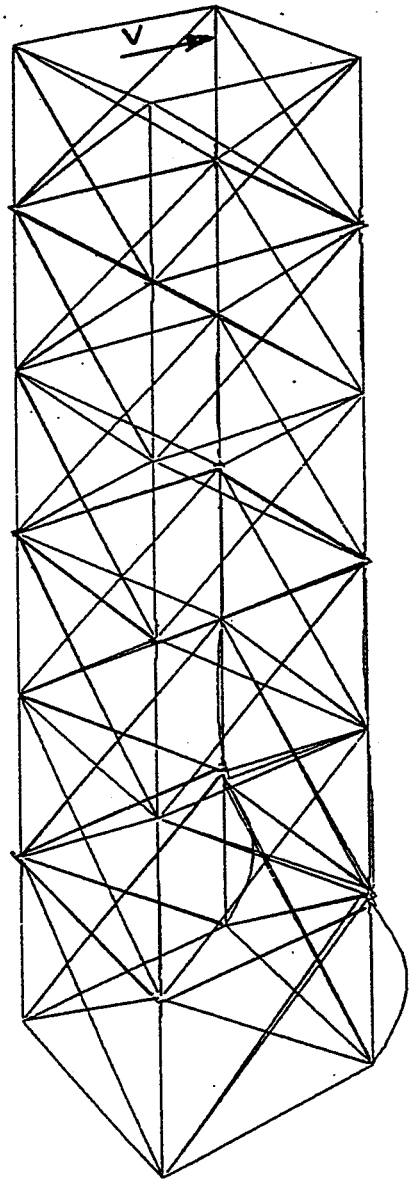

Figure 54 - Failure Mode for Linear Buckling Due to Lateral Load

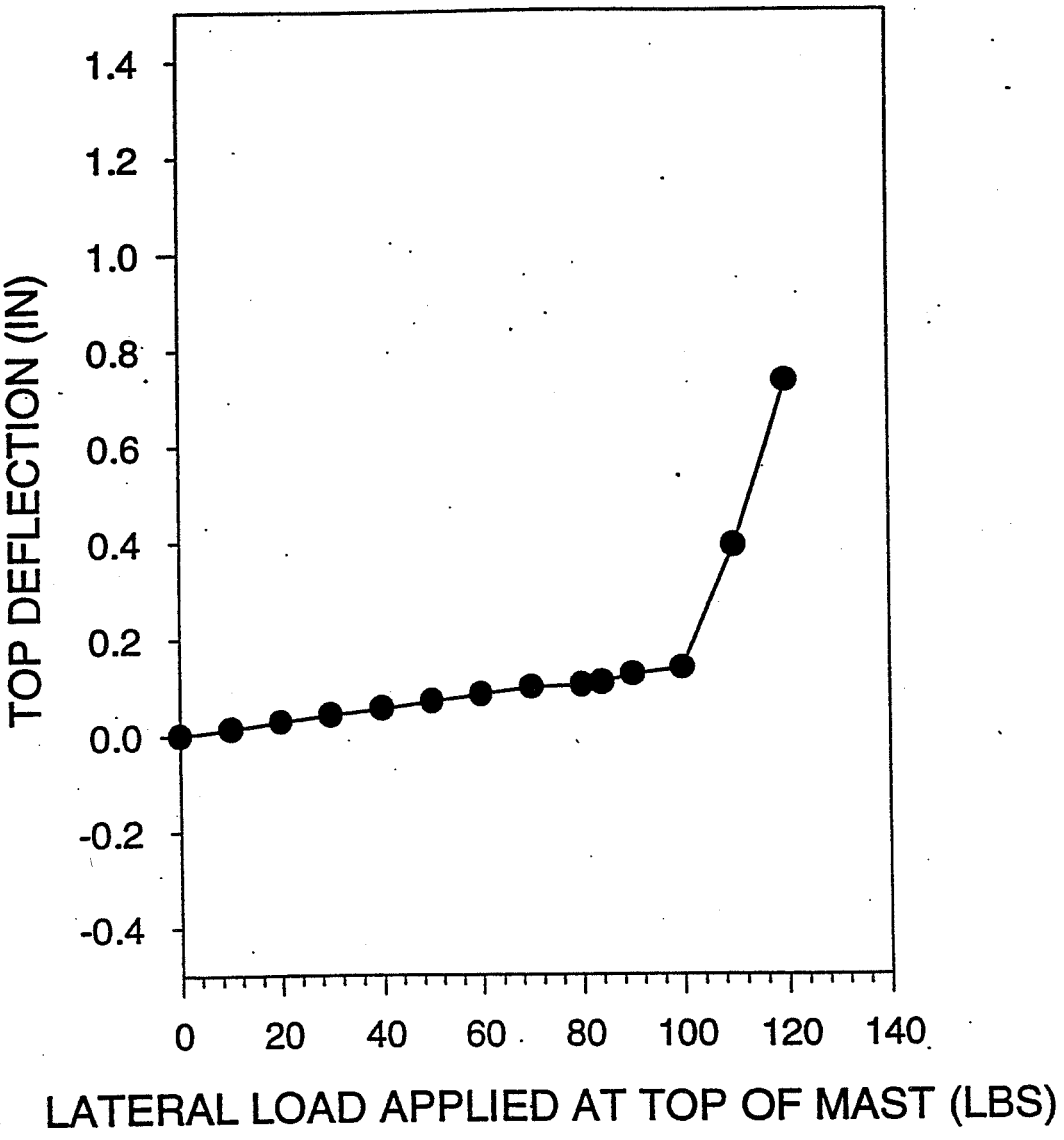

Figure 55 - Lateral Deflection Versus Lateral Load V Applied at Mast Top

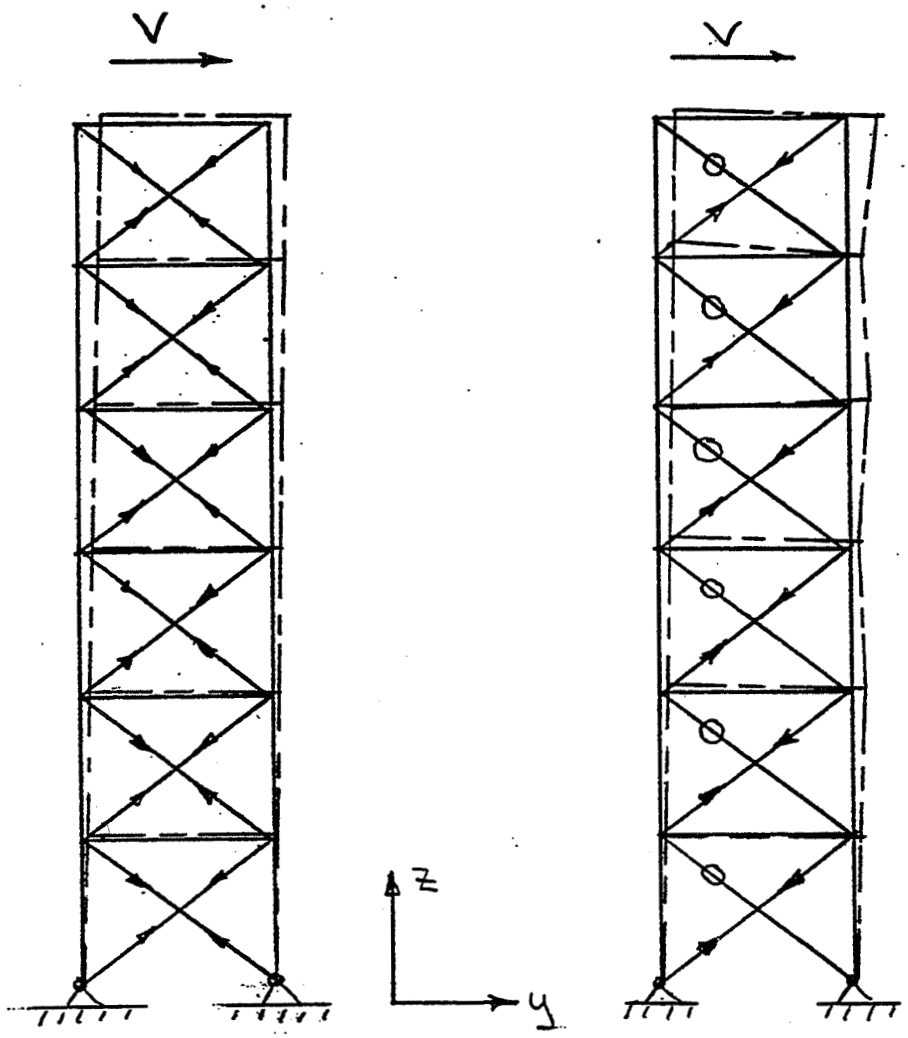

Figure 56 - Diagonal Preload Under Influence of Lateral Load V Applied at Mast Top

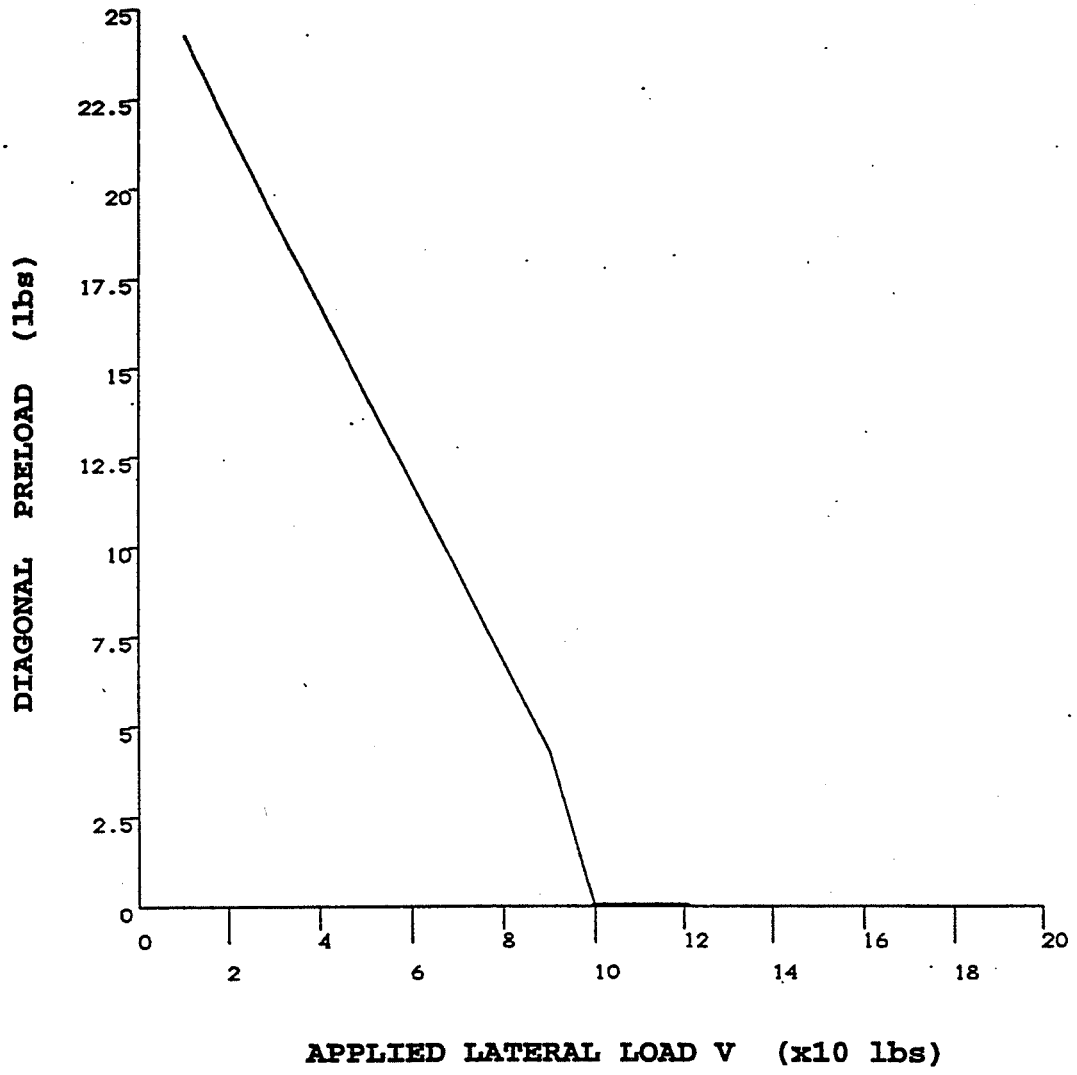

Figure 57 - Diagonal Preload Versus Lateral Load V Applied at Mast Top (typical)

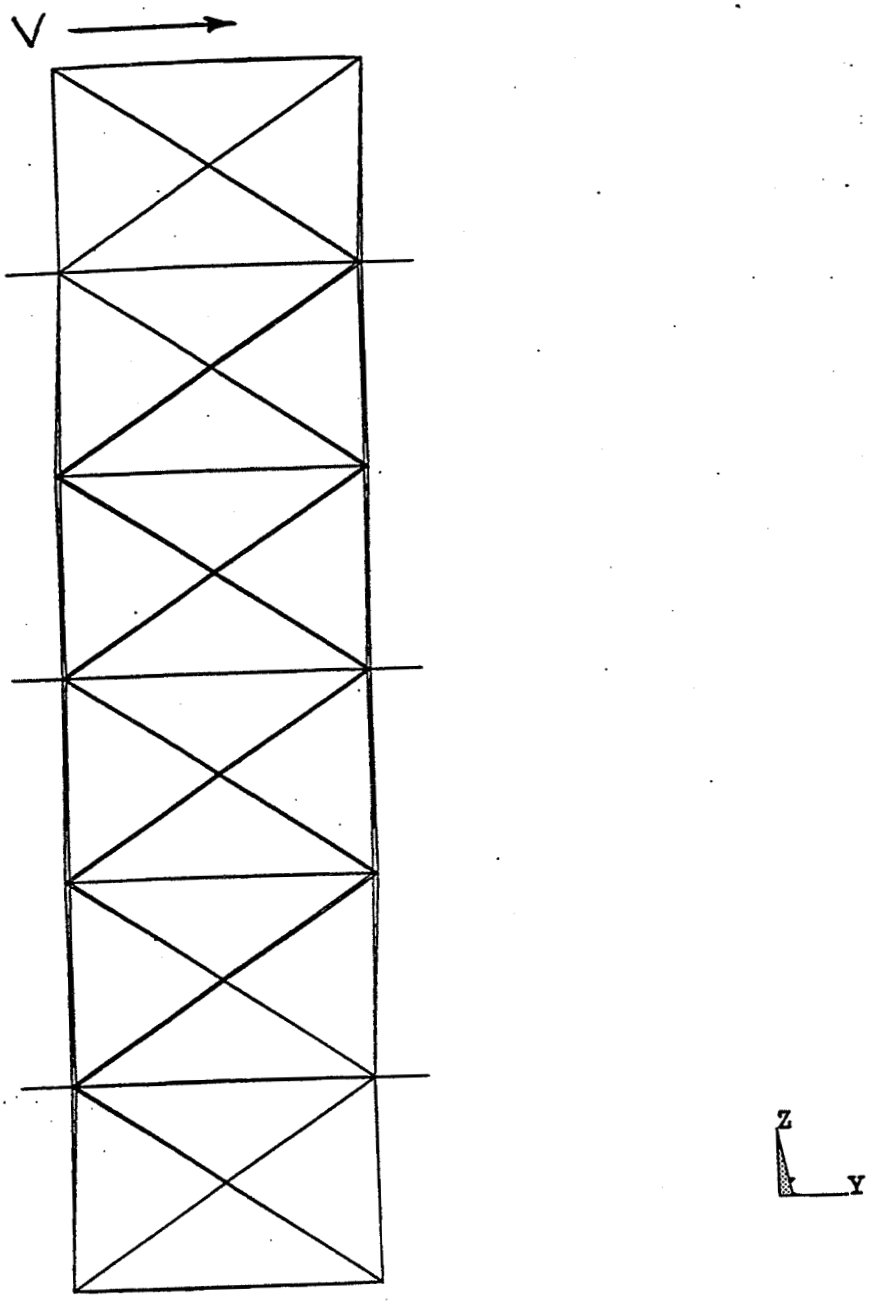

Figure 58 - Deformed Shape Due to Lateral Load V Applied at Mast Top

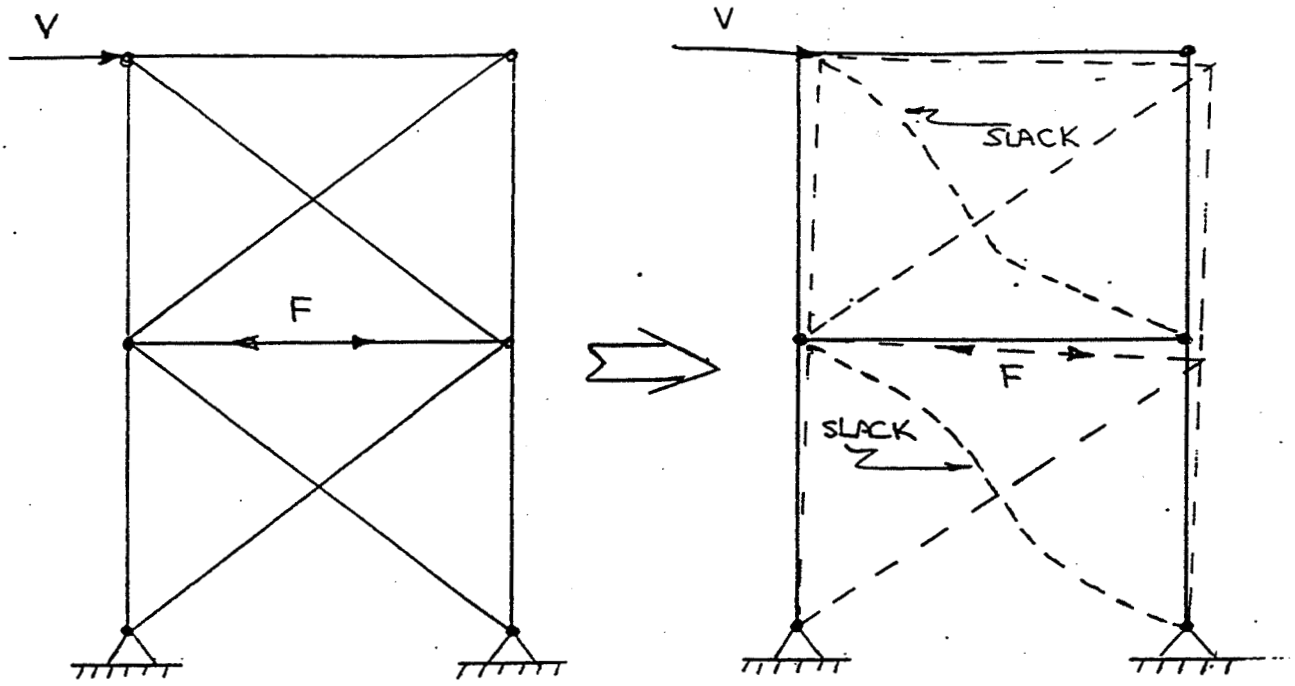

(a) All diagonals effective (b) Two diagonals effective

Figure 59 - Planar Truss for Stiffness Degradation Discussion

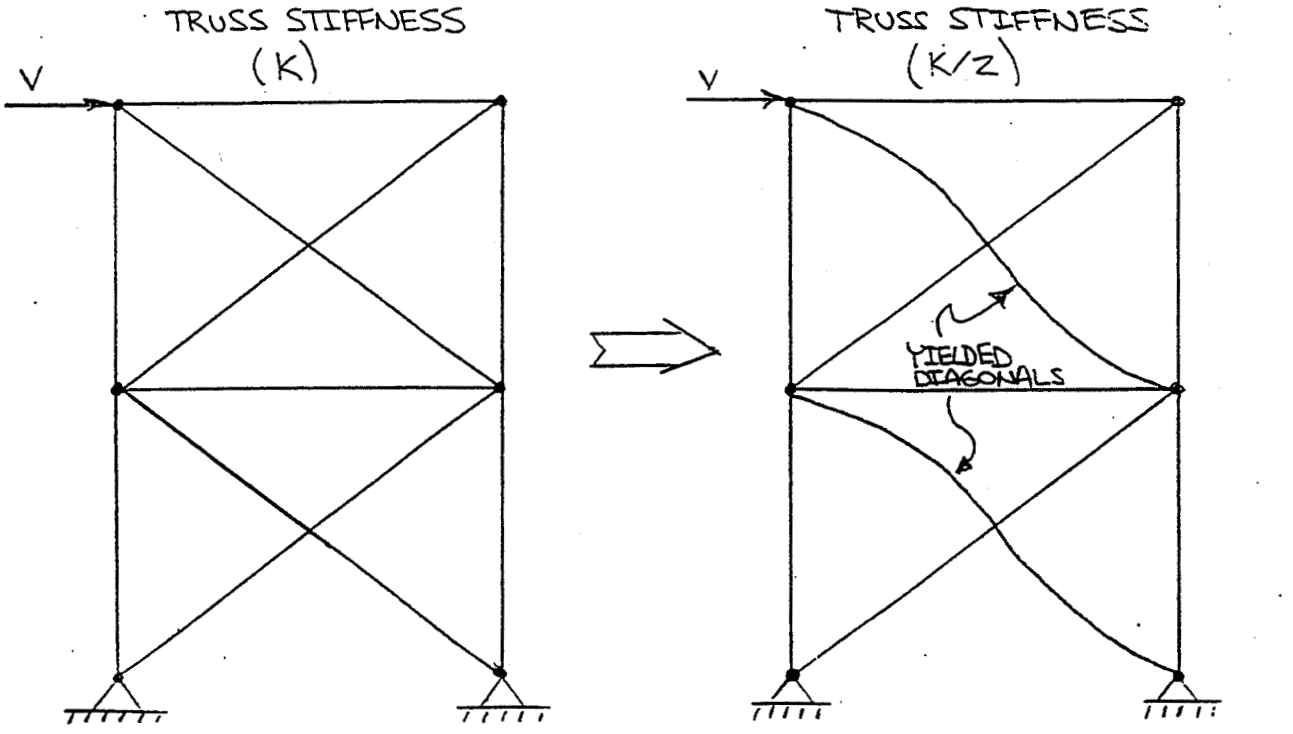

(a) All diagonals effective (b) Two diagonals effective

Figure 60 - Planar Truss Containing No Flexible Batten Element

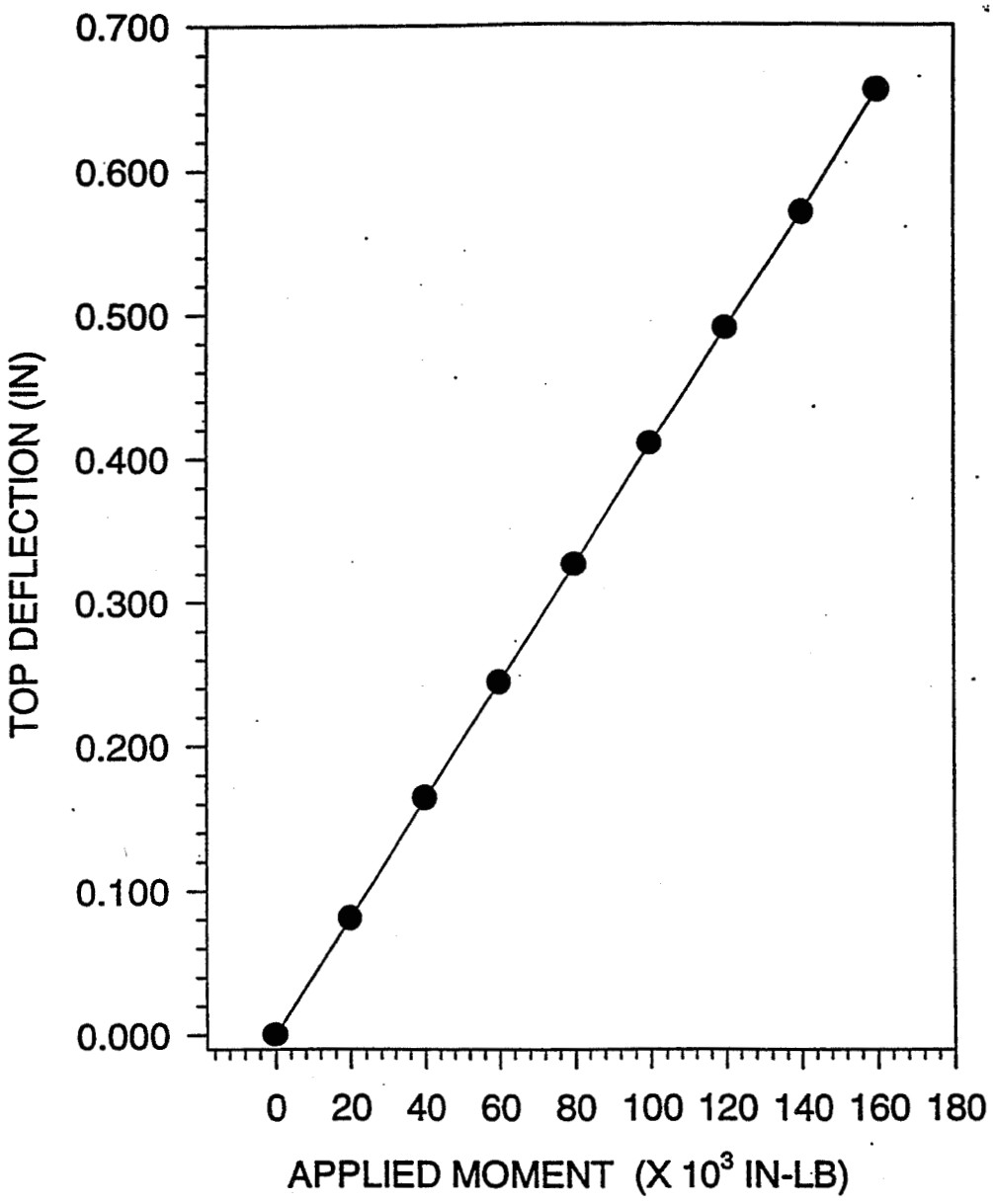

Figure 61 - Lateral Deflection Versus Moment Load M Applied at Mast Top

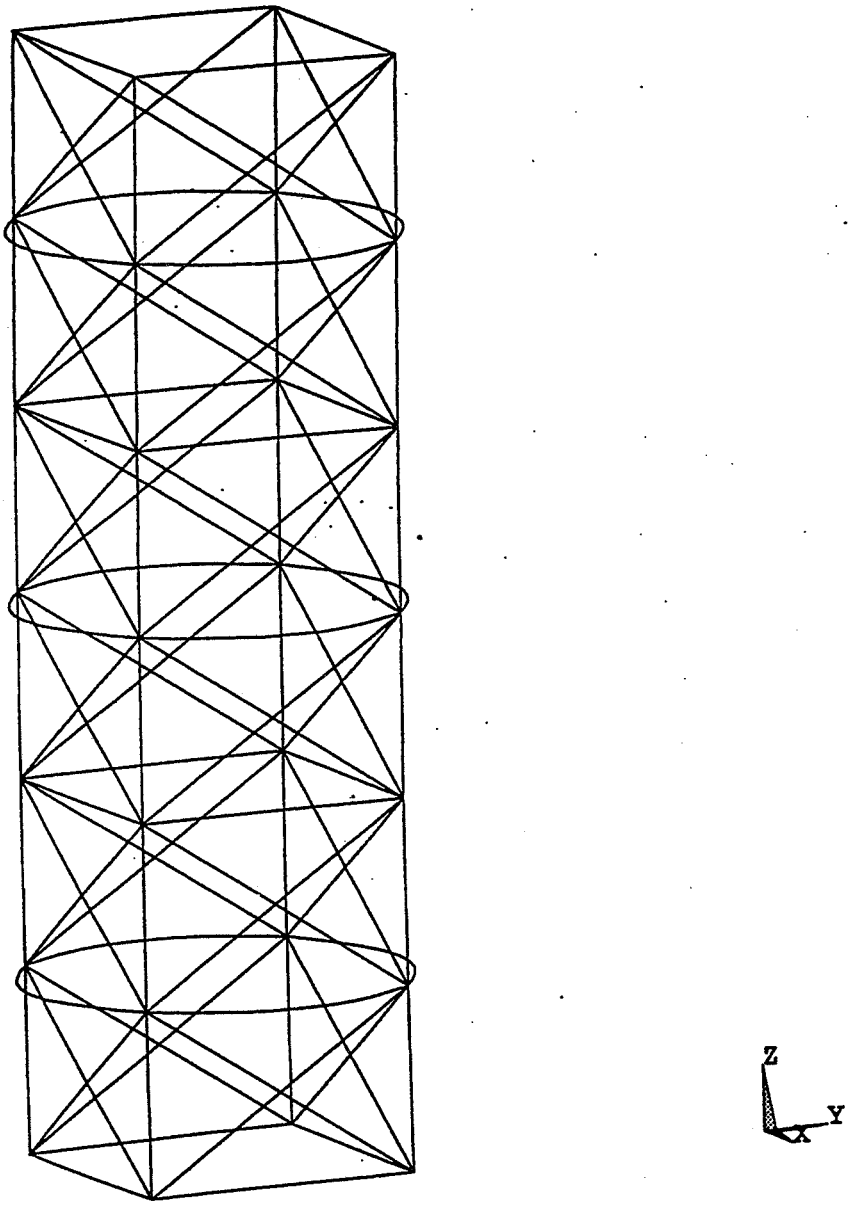

Figure 62 - Deformed Shape Due to Moment Load M Applied at Mast Top

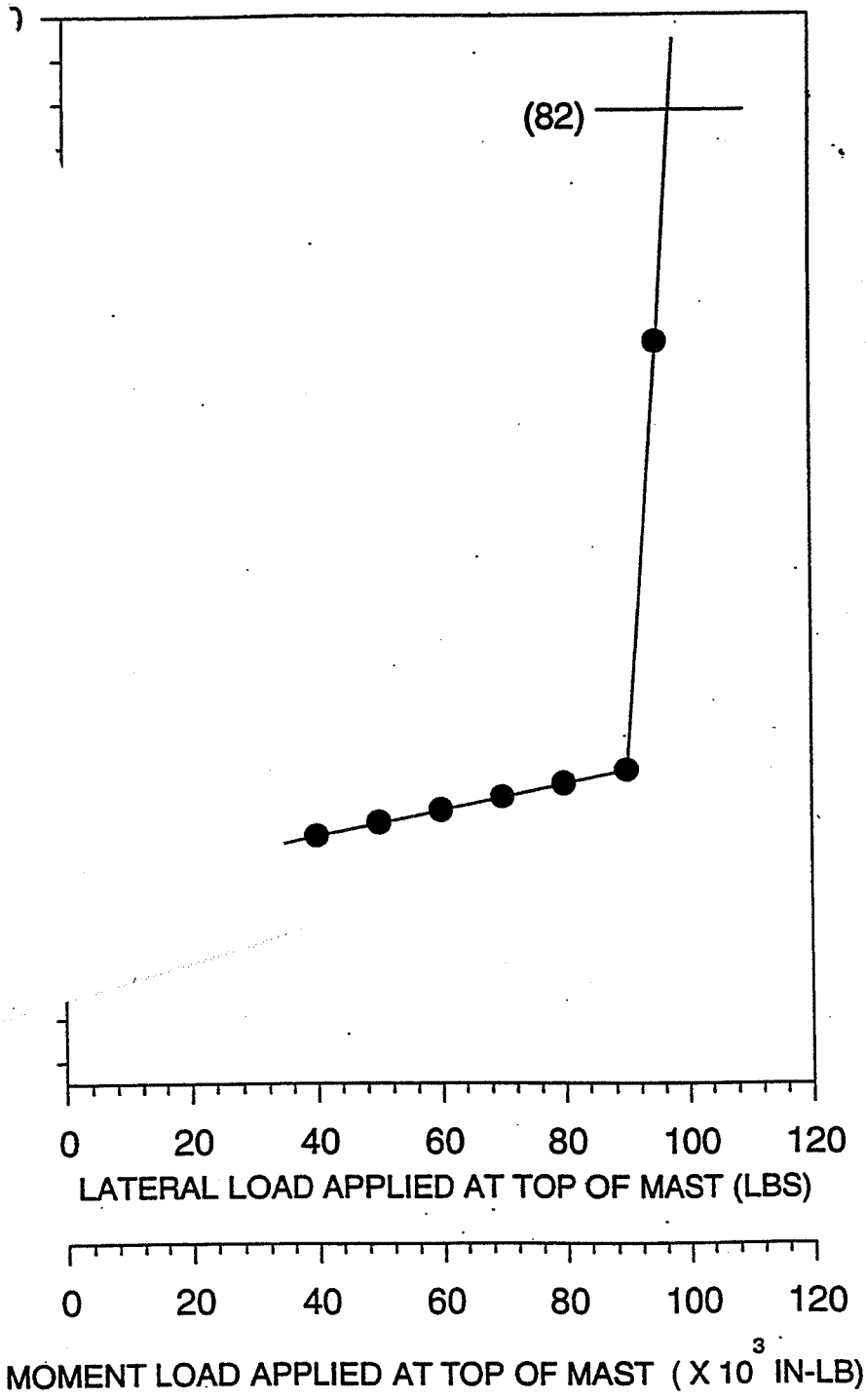

Figure 63 - Lateral Deflection Versus Loads M and V Applied at Mast Top

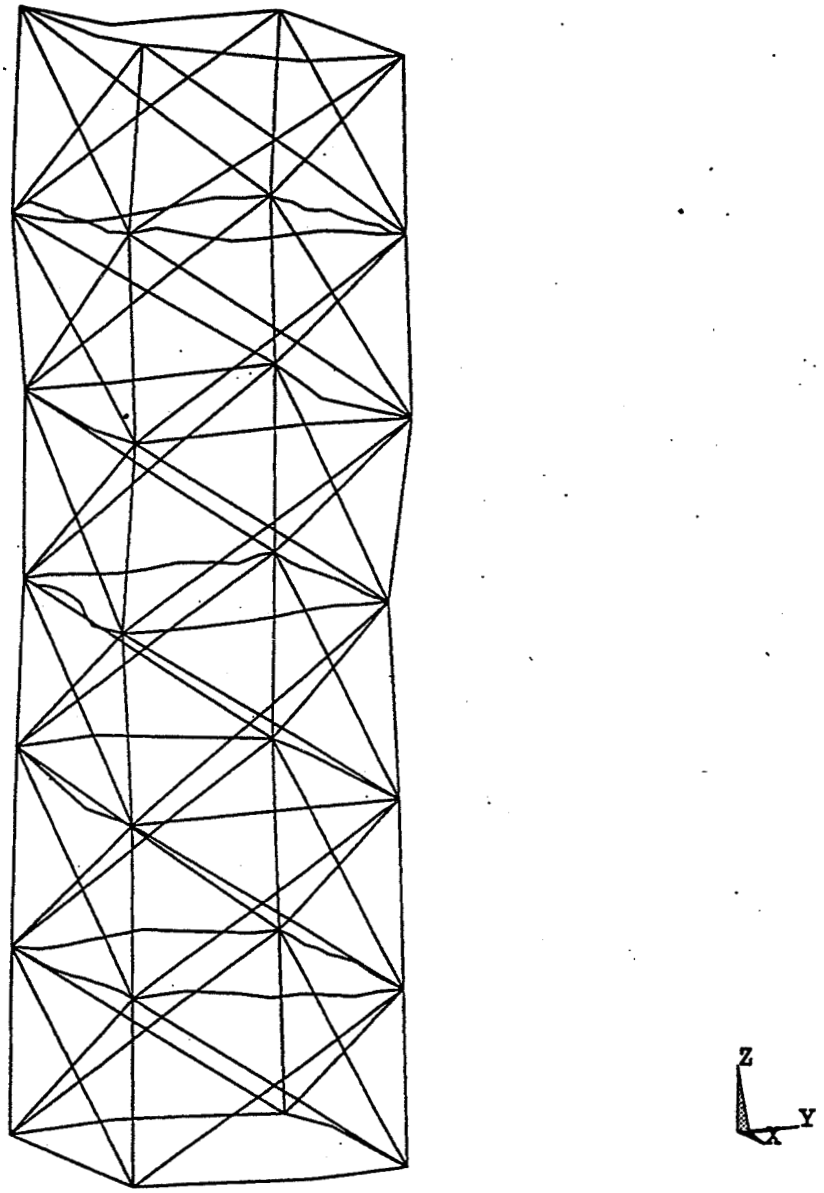

Figure 64 - Deformed Shape Due to Combined Loads M and V Applied at Mast Top (isometric)

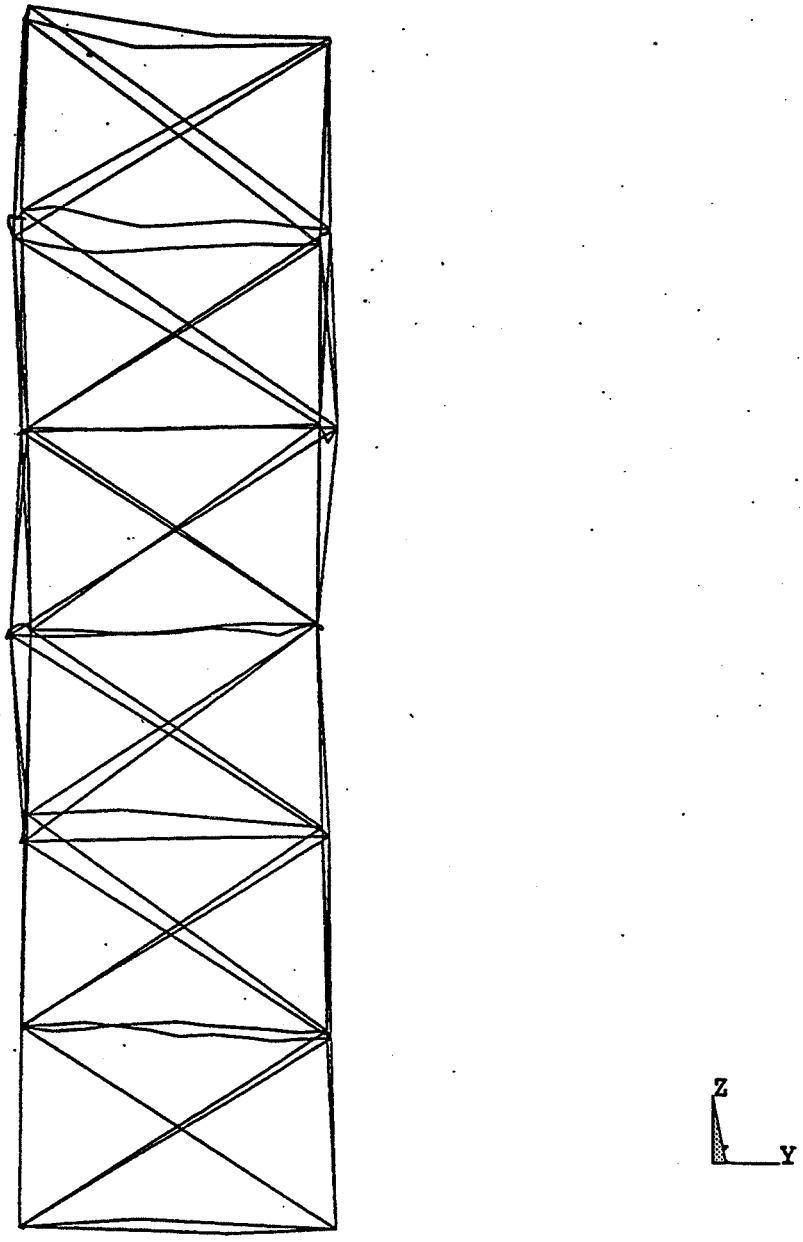

Figure 65 - Deformed Shape Due to Combined Loads M and V Applied at Mast Top (side view)

Mast Element	Material	Length	Area	Young's Modulus	Movement of Inertia I_{yy}[1]	Movement of Inertia I_{zz}[2]
		IN	IN^2	LB/IN^2	IN^4	IN^4
Tapered Longeron	Aluminum 6061-T6	19.750000	0.348100	10×10^6	0.010100	0.010100
Straight Longeron	Aluminum 6061-T6	19.750000	0.250000	10×10^6	0.005210	0.005210
Rigid Batten	Aluminum 6061-T6	19.300000	0.063900[3] 0.036200[4]	10×10^6	0.017400[3] 0.001440[4]	0.000436[3] 0.000316[4]
Batten Tube	Aluminum 6061-T6	11.200000	0.051110	10×10^6	0.001390	0.001390
Flex Batten	Fiberglass	31.750000	0.103000	8×10^6	0.001210	0.000591
Diagonal	Stainless Steel	36.000000	0.002318	29×10^6	———	———

1. Element y-axis oriented such that with x-axis along length of element right-hand rule is satisfied
2. Element z-axis vertical to cross-section
3. Wide end of tapered section
4. Narrow end of tapered section

Table 1 - Engineering Properties of Principal FASTMast Components

Structural Element	Material	Young's Modulus	Poisson's Ratio	Area	Moment of Inertia	Coefficient of Thermal Expansion
		LB/IN^2		IN^2	IN^4	$IN/IN\cdot F^o$
Longeron	Al-6061	$10X10^6$	0.33000	0.25000	0.00521	0.0
Flex Batten	Fiberglass	$8X10^6$	0.33000	0.10300	0.00121	$1.0X10^{-6}$
Diagonal	Stainless Steel	$30X10^6$	0.33000	0.00231	N/A	0.0

Table 2 - Properties for Two-Dimensional Nonlinear Planar Truss Study

MODEL	CRITICAL LOAD (LB.)	
	LOCAL FAILURE MODE	GLOBAL FAILURE MODE
1-BAY	2492.00	4000.00
3-BAY	2492.00	4000.00

Table 3 - One-Dimensional Linear Stability Analysis Results

LOAD TYPE	CRITICAL LOAD		MAXIMUM LONGERON AXIAL LOAD AT INSTABILITY	
	LINEAR	NONLINEAR	LINEAR	NONLINEAR
AXIAL	1915.25 lb.	----------	1910.12 lb.	----------
TIP SHEAR	1298.28 lb.	No Failure	2375.42 lb.	No Failure
BENDING MOMENT	---------[1]	No Failure	----------	No Failure

1. Dashed line indicates load type was not analyzed

Table 4 - Three-Dimensional Independent Load Analysis

REPORT DOCUMENTATION PAGE

Form Approved
OMB No. 0704-0188

1. AGENCY USE ONLY (*Leave blank*)	2. REPORT DATE	3. REPORT TYPE AND DATES COVERED
	May 1995	Technical Memorandum

4. TITLE AND SUBTITLE

Static Stability of a Three-Dimensional Space Truss

5. FUNDING NUMBERS

WU-478-42-10

6. AUTHOR(S)

John F. Shaker

7. PERFORMING ORGANIZATION NAME(S) AND ADDRESS(ES)

National Aeronautics and Space Administration
Lewis Research Center
Cleveland, Ohio 44135-3191

8. PERFORMING ORGANIZATION REPORT NUMBER

E-9679

9. SPONSORING/MONITORING AGENCY NAME(S) AND ADDRESS(ES)

National Aeronautics and Space Administration
Washington, D.C. 20546-0001

10. SPONSORING/MONITORING AGENCY REPORT NUMBER

NASA TM-106944

11. SUPPLEMENTARY NOTES

This report was submitted as a thesis in partial fulfillment of the requirements for the degree Master of Science to Case Western Reserve University, Cleveland, Ohio, April 1994. Responsible person, John F. Shaker, organization code 4310, (216) 433-5542.

12a. DISTRIBUTION/AVAILABILITY STATEMENT

Unclassified - Unlimited
Subject Categories 01, 18, and 39

This publication is available from the NASA Center for Aerospace Information, (301) 621-0390.

12b. DISTRIBUTION CODE

13. ABSTRACT (*Maximum 200 words*)

In order to deploy large flexible space structures it is necessary to develop support systems that are strong and lightweight. The most recent example of this aerospace design need is vividly evident in the Space Station solar array assembly. In order to accommodate both weight limitations and strength performance criteria, ABLE Engineering has developed the Folding Articulating Square Truss (FASTMast) support structure. The FASTMast is a space truss/mechanism hybrid that can provide system support while adhering to stringent packaging demands. However, due to its slender nature and anticipated loading, stability characterization is a critical part of the design process. Furthermore, the dire consequences surely to result from a catastrophic instability quickly provide the motivation for careful examination of this problem. The fundamental components of the Space Station solar array system are the (1) solar array blanket system, (2) FASTMast support structure, and (3) mast canister assembly. The FASTMast once fully deployed from the canister will provide support to the solar array blankets. A unique feature of this structure is that the system responds linearly within a certain range of operating loads and nonlinearly when that range is exceeded. The source of nonlinear behavior in this case is due to a changing stiffness state resulting from an inability of diagonal members to resist applied loads. The principal objective of this study was to establish the failure modes involving instability of the FASTMast structure. Also of great interest during this effort was to establish a reliable analytical approach capable of effectively predicting critical values at which the mast becomes unstable. Due to the dual nature of structural response inherent to this problem, both linear and nonlinear analyses are required to characterize the mast in terms of stability. The approach employed herein is one that can be considered systematic in nature. The analysis begins with one and two-dimensional failure models of the system and its important components. From knowledge gained through preliminary analyses a foundation is developed for three-dimensional analyses of the FASTMast structure. The three-dimensional finite element (FE) analysis presented here involves a FASTMast system one-tenth the size of the actual flight unit. Although this study does not yield failure analysis results that apply directly to the flight article, it does establish a method by which the full-scale mast can be evaluated.

14. SUBJECT TERMS	15. NUMBER OF PAGES
Nonlinear; Stability; FASTMast; Truss; Space station	114
	16. PRICE CODE: A06

17. SECURITY CLASSIFICATION OF REPORT	18. SECURITY CLASSIFICATION OF THIS PAGE	19. SECURITY CLASSIFICATION OF ABSTRACT	20. LIMITATION OF ABSTRACT
Unclassified	Unclassified	Unclassified	

National Aeronautics and
Space Administration

Lewis Research Center
21000 Brookpark Rd.
Cleveland, OH 44135-3191